C. 1

SOLIDS CIRCULATION RATE MEASUREMENT IN A CIRCULATING FLUIDIZED BED

by

JAMES J. BURKELL

B.A.Sc., The University of British Columbia, 1984

A THESIS SUBMITTED IN PARTIAL FULFILLMENT OF
THE REQUIREMENTS FOR THE DEGREE OF
MASTER OF APPLIED SCIENCE

in

FACULTY OF GRADUATE STUDIES
(Department of Chemical Engineering)

We accept this as conforming
to the required standard

THE UNIVERSITY OF BRITISH COLUMBIA
APRIL, 1986

In presenting this thesis in partial fulfilment of the requirements for an advanced degree at the University of British Columbia, I agree that the Library shall make it freely available for reference and study. I further agree that permission for extensive copying of this thesis for scholarly purposes may be granted by the head of my department or by his or her representatives. It is understood that copying or publication of this thesis for financial gain shall not be allowed without my written permission.

Department of Chemical Engineering

The University of British Columbia
2075 Wesbrook Place
Vancouver, Canada
V6T 1W5

Date April 22, 1986

Abstract

This thesis documents the investigation of three methods of determining solids fluxes in a circulating fluidized bed (CFB). An impact flowmeter used the force of the recirculating particles striking a pan which spanned the diameter of the return column to measure solids circulation rates. A modified orifice, with a conical entrance section, used the additional pressure differential resulting from solids flowing counter-currently to gas to determine solids fluxes. The third method used the velocities of particles travelling through the vertical section of an L-valve to determine solids circulation rates.

The results obtained in this work show that the impact flowmeter and the method utilizing L-valve particle velocities are viable methods of measuring solids fluxes in a CFB. However, further research is required before these methods can be confidently used. The modified orifice, as studied, was not sensitive enough to sense solids circulation. However, the meter may offer potential if studied with co-current gas solids flow.

TABLE OF CONTENTS

TABLE OF CONTENTS - CONTINUED

TABLE OF CONTENTS - CONTINUED

LIST OF TABLES

LIST OF FIGURES

LIST OF FIGURES - CONTINUED

LIST OF FIGURES - CONTINUED

LIST OF FIGURES - CONTINUED

LIST OF FIGURES - CONTINUED

Acknowledgement

I would like to express my gratitude to the following individuals:

Dr. J.R. Grace for his guidance, support and suggestions during the course of this study.

Clive Brereton for his instruction and assistance in the operation of the CFB unit.

Robert Soszynski for his demonstration in the operation of the IBM XT computer and the Tecmar Programmable datalogging board and for the use of his data logging program.

Dr. B. Bowen for the use of his plotting subroutines.

Frank Laytner for his assistance in drawing the figures.

I would also like to thank the staff of the Chemical Engineering Stores and Workshops for their invaluable assistance in the design, acquisition and construction of my equipment.

Finally, I would like to thank all the others who have assisted me in my work and endured my presence these past years.

1.1 Introduction

Fluidized beds continue to be used in industry as an effective means of contacting a fluid, usually a gas, with particulate solids. Fluidized bed units, generally operated in the bubbling or turbulent fluidization regimes, have successfully performed as:

- roasters
- catalytic cracking/regeneration units
- chemical reactors for the production of acrylonitrile, phthalic anhydride and other products involving highly exothermic organo-chemical reactions
- combustors for coal, biomass, refuse
- gasifiers for coal and biomass
- heat exchangers and constant temperature baths
- driers

This incomplete list of proven applications continues to grow with the ever-increasing understanding and knowledge of fluidized bed behaviour.

Some of the advantages of fluidized beds over alternate contacting methods, such as rotary kilns and packed moving beds, are: (Cohen et al., 1984; Fitzgerald et al., 1984; Grace and Matsen, 1980; Sneyd, 1984)

- compact design
- nearly isothermal bed conditions
- simple gas/solids introduction and removal relative to packed beds
- high gas/solids heat and mass transfer rates
- good solids mixing within the bed

- efficient heat addition and removal
- improved combustor performance resulting from:
    a) direct removal and reduction of atmospheric pollutants
    b) high heat transfer coefficients resulting in compact boiler designs

However, fluidized beds have several disadvantages as well:

- increased particle attrition and elutriation relative to packed beds
- gas short circuiting of the solids when operating in the bubbling regime
- high erosion rates of the bed vessel and heat exchange surfaces
- non-uniform solids residence time
- gas backmixing
- difficulties in scaling-up equipment

To overcome these problems and to better understand their behaviour, fluidized beds have been the subject of considerable industrial and academic research. This research has concentrated on the achievement of a basic understanding of fluidized bed behaviour and the development of empirical and semi-empirical design correlations, thus enabling design and scale-up of units to be more reliable.

Until recently, the study of fluidized beds focussed on the particulate, bubbling and slugging fluidization regimes. However, recent years have seen increased interest in the turbulent and fast fluidization regimes, both for practical applications and in fundamental research.

The fast fluidization regime, lying between the turbulent fluidization and pneumatic transport regimes, is characterized by a solids suspension of

voidage 0.8 to 0.995 which lacks a discernible bed surface. There is a substantial net upflow of solids with fluxes of the order of 5 to 200 kg/m^2s. Examination of the flow reveals that individual particles travel upward with the gas, while "clusters" or "strands" of particles move up and down in co- and counter-current flow relative to the gas, principally near the wall of the containing vessel.

The fast bed column is usually built as part of a closed loop, with an adjacent column to return the particles to the bottom of the upflow section. Entrained solids carried out of the fast bed are separated by cyclones and collected in the solids return standpipe. A butterfly valve in the solids return section of the loop is frequently used to determine solids circulation rates. This arrangement, shown in Figure 1.1, has been called a Circulating Fluidized Bed (CFB).

Previous studies, (Cohen et al., 1984; Engstrom, 1980; Jones, 1983; Roeck, 1982; Yerushalmi et al., 1976; Yerushalmi and Cankurt, 1978), have shown that CFB's offer most of the benefits of other fluidized bed contactors as well as additional advantages in terms of:

- compact design (reduced cross-sectional area)
- simple solids introduction
- higher gas throughput
- little gas backmixing
- intimate gas/solids contacting
- ability to handle cohesive solids
- high slip velocities
- enhanced gas-to-solids heat and mass transfer

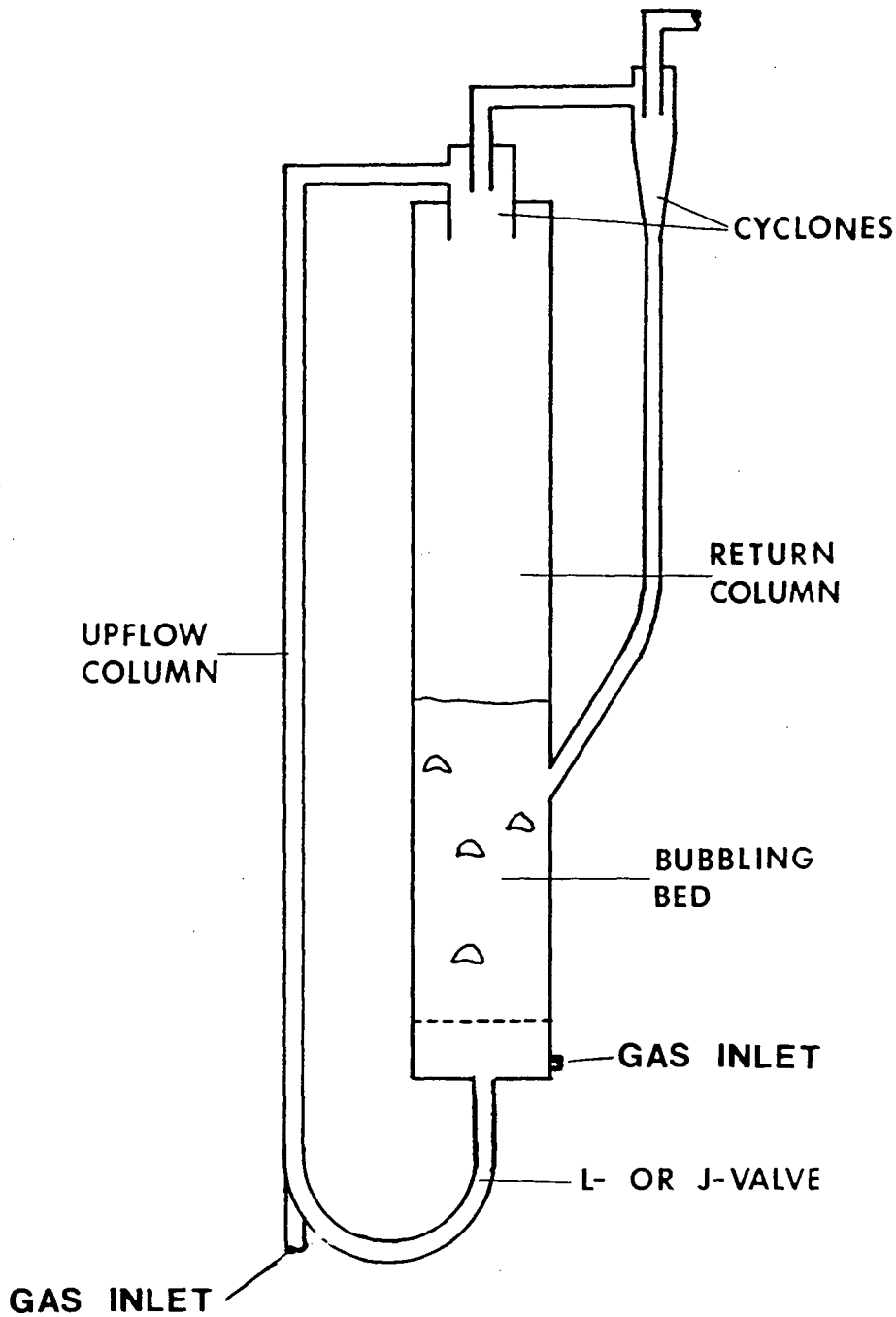

Figure 1.1 A conventional circulating fluidized bed

- improved combustor performance resulting from;
    a) flexibility in fuel material
    b) controlled turndown and load following
    c) enhanced sulphur capture
    d) improved combustion efficiency
    e) fewer number of feedpoints required
    f) reduced NO_x emission levels

However, CFB's have been shown to suffer the disadvantages of: (Cohen et al., 1984; Yerushalmi et al., 1976)

- limitations on particle size
- greater heat transfer surface requirements
- difficult gas/solids separation
- scale-up uncertainties
- accelerated equipment erosion

Interest in CFB's has resulted in extensive reseach in both the industrial and academic communities. This research has been directed towards a fundamental understanding of the behaviour and dynamics of CFB systems to be applied in the design and development of these units. Current areas of interest include the study of:

- gas-to-particle heat and mass transfer rates and mechanisms
- bed heat addition and removal
- bed hydrodynamics
- erosion of CFB's and their auxiliary equipment
- particle attrition and elutriation
- CFB operating characteristics, e.g. solids holdup, turndown, load following

- the applicability of CFB's as chemical reactors
- combustion and gasification processes

To study these phenomena it is necessary to measure such fundamental variables as:

- local solids density
- solids throughput or flux
- gas and solids velocities and flow patterns
- gas composition as a function of position
- chemical conversion of gaseous and solid reactants
- heat and mass transfer coefficients
- combustion efficiencies
- temperature profiles
- pollutant emissions

This project addressed the problem of solids flux measurement, an important parameter when studying any aspect of a CFB's operation. In both research and industrial applications of a CFB, an accurate, continuous method of measuring solids circulation rate is desired. Ideally the method would be non-interfering and suitable for high temperature and possibly high pressure operation.

The particular aims of this study were:

1) To develop one or more flowmeters to continuously measure solid circulation rates in CFB's.
2) To test the flowmeter(s) at different CFB operating conditons, i.e different solids circulation and gas flow rates.

3) To study the effect of flowmeter geometry on solids circulation rate measurement.

4) To determine the effect of closure of a butterfly valve, located in the return loop, on solids flux.

5) To investigate the response of the solids circulation to a change in solids feedrate to the fast bed.

6) To study the relationship between the L-valve particle velocity and solids flux.

Two distinct methods of measuring solids circulation rates were developed and investigated: An impact flowmeter used the force of the recirculating solids striking a pan in the return column; an orifice modified with a conical entrance section utilized the additional pressure drop resulting from the presence of solids flowing counter-currently through an upwards moving gas stream.

1.2 Previous Studies and Methods

Previous methods of measuring CFB solids circulation rates have presented problems due to the nature of their operation and restricted applicability.

One method used to measure solids flux involved blocking the solids circulation loop and observing the accumulation of solids above, or depletion below, the blockage, as a function of time. A butterfly valve, located in the solids return column of the circulation loop, has been used to stop the solids circulation, Figure 1.2 (Yerushalmi et al., 1978; Bierl et al., 1980). In another study, a slide valve was used to stop solids circulation, Figure 1.3 (Fusey et al., 1985). In both these methods, circulation rates were estimated by monitoring the change in pressure drop,

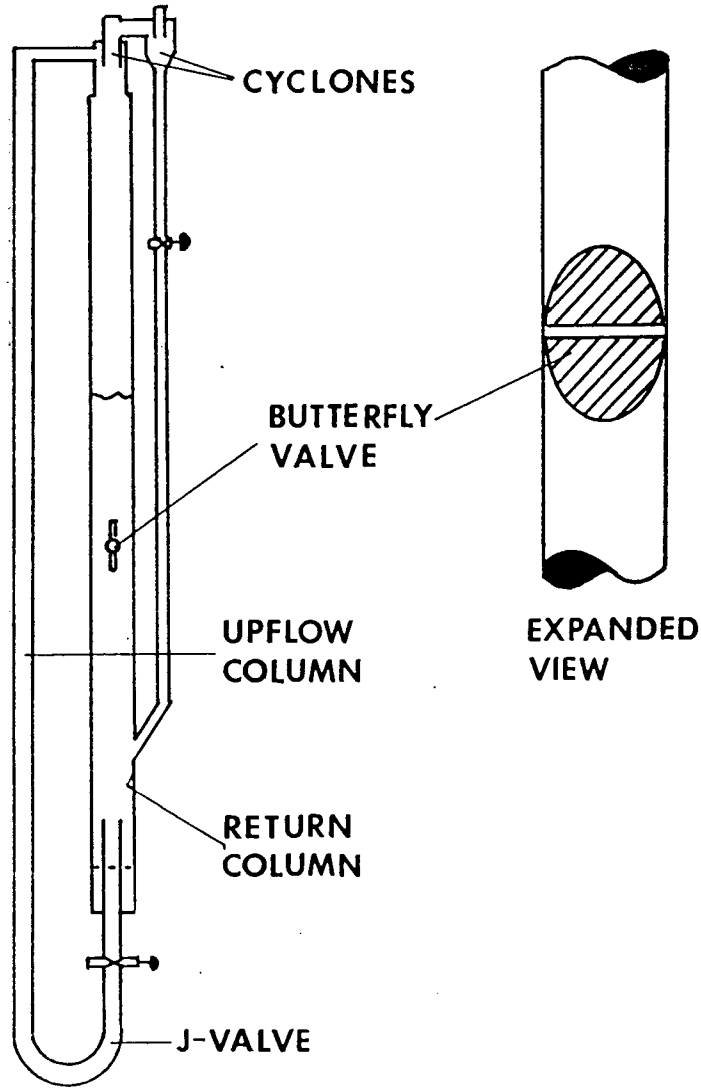

Figure 1.2 City College's circulating bed facility (Yerushalmi et al., 1978)

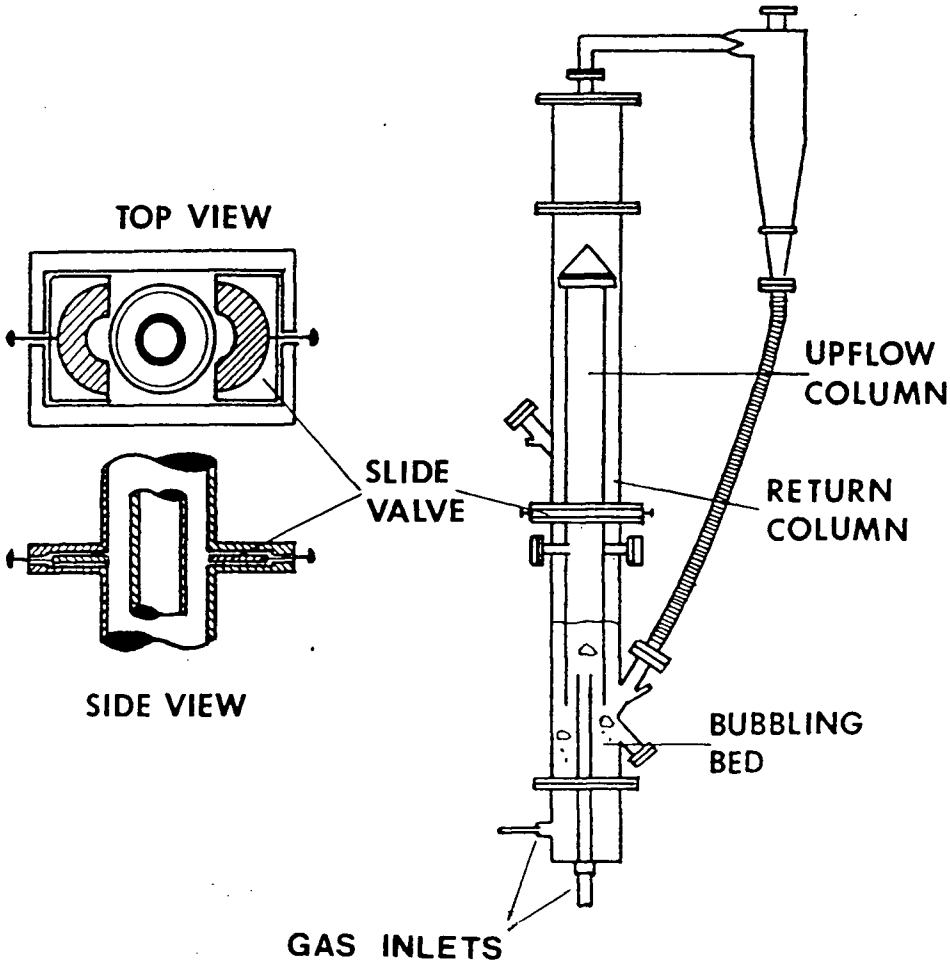

Figure 1.3 U.B.C.'s concentric circulating bed (Fusey et al., 1985)

across the valve and the accumulating solids, with time. The valves, constructed to be permeable to gas but impermeable to solids, allowed gas to continue to flow slowly up through the standpipe while the solids circulation was blocked. The upwards flowing gas maintained the solids accumulating on the valve in a fluidized state, thus ensuring even solids distribution on the valve and enabling solids flux to be calculated from the rate of change of pressure drop across the valve and solids.

The use of a valve to determine solids circulation rates has four basic limitations: Closing of the valve creates an additional pressure drop in the system which perturbs the pressure balance of the CFB unit and might significantly affect the operation of the equipment. Dumping of the accumulated solids at the end of the measurement may affect the CFB unit. A porous butterfly or slide valve may be very difficult to maintain in a high temperature reactor. The method does not provide a continuous measure of solids circulation rates.

A second method used to determine solids circulation rates involved observing the movement of identifiable particles passing through a transparent non-mechanical L- or J-valve or loop seal as they returned to the base of the upflow section of the CFB (Goldblatt, 1985).

By assuming uniform solids velocity in the valve and assigning a bulk density to the solids flowing through the valve, the solids circulation rate may be estimated. However, if a velocity profile exists, or the assumed bulk density is not representative of the actual bulk density in the L-valve, the solids circulation rate may be poorly estimated. This problem may be overcome by calibrating the valve for the particular solid being used. Calibration would involve measuring the solids, e.g. via a

butterfly valve, and relating it to the corresponding solids velocity in the valve.

To use these methods, tracer particles must be observed as they move through the L- or J-valve or loop seal. This is easily accomplished when working with ambient temperature, laboratory scale CFB's, since such units may be constructed from transparent materials. However, this approach may not be suitable for high temperature and/or large CFB's, since materials of construction requirements and the need to observe solids movement through the valve may be in conflict. Furthermore, it would be difficult to incorporate this flow measurement technique into a system where automatic measurement of solids circulation rates is required.

A third method, which has not yet been applied to solids flux measurement but may offer promise, is isokinetic sampling, involving withdrawal of fluid and solids from a flowing stream at velocities equal to the local stream velocities. This technique minimizes the effect of the sampling procedure on the stream flow behaviour and provides a sample more representative of the flowing stream. Isokinetic sampling has been used to take gas and solids samples from spouted and fluidized beds to determine gas and solids conversions, flow patterns and velocities, and solids loadings (Base, 1976; van Breugel, 1969/70). Isokinetic probes have been successfully used in situations involving co-current gas/solids flow. In these cases, a hot wire anemometer has often been employed to measure the fluid stream velocities used in determining the sampling rates. Previous work, (van Breugel, 1969/70), has shown that isokinetic probes may be used to sample a dense gas-solids stream. However, caution must be exercised to avoid plugging of the probes by solids.

By assuming a uniform solids distribution and velocity profile in the solids return column, the solids circulation rate can be calculated using a single probe and sampling point. However, if the solids flowrate varies with position and/or time, it would be necessary to use a number of sampling points and/or probes to measure the solids flux accurately. Further problems may arise in determining the sampling rate, since the gas and solids flow counter-currently at different velocities. In addition, the broad particle size distribution in CFB's, typically varying from micron to millimeter size, may lead to complications in determining the sampling rate.

2.0 Experimental Apparatus and Procedures

2.1 Circulating Bed System

The CFB unit used in this study is shown in Figure 2.1. The circulating bed system consisted of two parallel columns, a 0.152 m ID fast bed column and a 0.330 m ID return standpipe, with the latter also acting as a solids storage vessel. Solids, fed by a non-mechanical L-valve, entered the bottom of the fast bed column and were entrained by the upward flowing gas. This resulted in a net flux of solids upward and out of the fast bed column. Entrained solids exiting the fast bed were separated from the carrier gas by a primary cyclone, followed by a secondary cyclone and two tertiary cyclones which could be arranged in parallel or series. Separated solids were returned to the bubbling bed of the return solids standpipe, while the carrier gas was exhausted to atmosphere. Particles flowed from the bottom of the return vessel downward through the L-valve to the fast bed, thus closing the circulation loop.

2.1.1 Fast Fluidization Column and Air Supply System

The fast bed column, constructed of 0.152 m ID transparent acrylic tubing of wall thickness 6.4 mm, permitted visual observation to be made concurrently with physical measurements. The column, of height 9.14 m, was assembled from a series of shorter flanged sections, varying in length from 0.46 m to 1.37 m. Seals between sections were provided by 0.191 m ID, 3.18 mm diameter butadiene O-rings. A 0.156 m diameter multi-orifice distributor at the bottom of the fast bed column provided primary air introduction and distribution. The distributor, designed to have 19% free

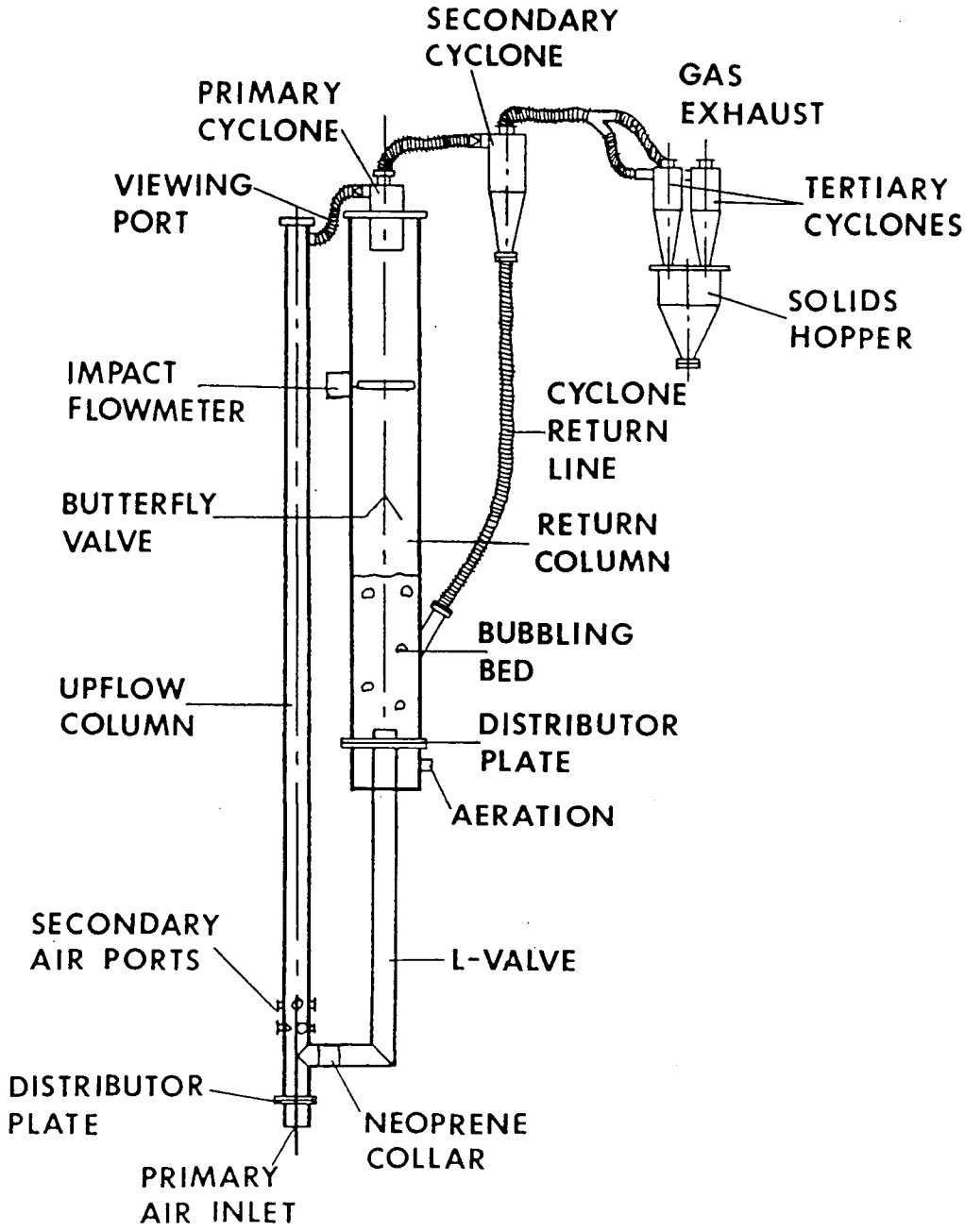

Figure 2.1 The circulating bed equipment

area, consisted of 200 mesh stainless steel screen sandwiched between two 12.7 mm thick Dural Aluminum distributor plates. The screen prevented backflow of solids into the windbox and piping. The upper and lower distributor plates were drilled with aligned 6.4 mm and 7.9 mm diameter holes respectively, on a 12.7 mm square pitch. The distributor was held in place by the windbox which was bolted to the bottom of the upflow column. Solids entered the vessel from the L-valve through a 0.152 m ID circular side inlet located 0.152 m above the distributor. The top of the vessel was closed with a 12.7 mm thick blind flange. Gas and entrained solids left the upflow vessel through a 0.102 m ID side outlet located 0.152 m below the top of the column.

Primary air to the fast bed was provided using either a 0.03 m^3/s, 200 kPag compressor or a 0.15 m^3/s, 50 kPag Sutorbuilt blower, model 7HV. The compressor did not have sufficient capacity to provide gas velocities capable of maintaining the bed in the fast fluidization regime, but was useful for operating the bed in the particulate, bubbling or turbulent fluidization regimes. The blower, on the other hand, was capable of providing superficial gas velocities up to 8.0 m/s, which was sufficient for sustaining the particulate material used in this study in the fast fluidization regime. Secondary air, could also be supplied by the blower.

Compressor airflow was metered by a rotameter and regulated with a 25.4 mm globe valve. Blower airflow to the fast bed column was measured with an orifice meter centrally located in a 2.24 m straight run of 76.2 mm ID copper tube. Four orifices, with orifice-to-tube diameter ratios of 0.08, 0.17, 0.41 and 0.67, were available for use in the orifice meter. Orifice meter pressure differentials were measured by a water manometer, while pressures upstream of the meter were measured with a mercury manometer. Regulation of the blower airflow was by two valves. A 76.2 mm gate valve, downstream of the orifice meter, was used for coarse flow adjustment. A 76.2 mm globe valve, tied in upstream of the orifice meter, provided fine flow adjustment by bleeding air from the blower discharge.

The fast bed column was equipped with wall ports at 0.457 m intervals, starting 0.152 m above the distributor. These ports were used to insert capacitance and gas and solids sampling probes, up to 6.4 mm in diameter, and to take pressure measurements along the length of the column.

2.1.2 L-Valve

Solids returned to the bottom of the fast bed through the non-mechanical L-valve shown in Figure 2.2. L-valves generally consist of a tall, vertical section of pipe connected at 90° to a shorter pipe, in an "L" configuration. Solids movement through the valve was adjusted by varying the point and degree of aeration of solids in the valve (Knowlton, 1977).

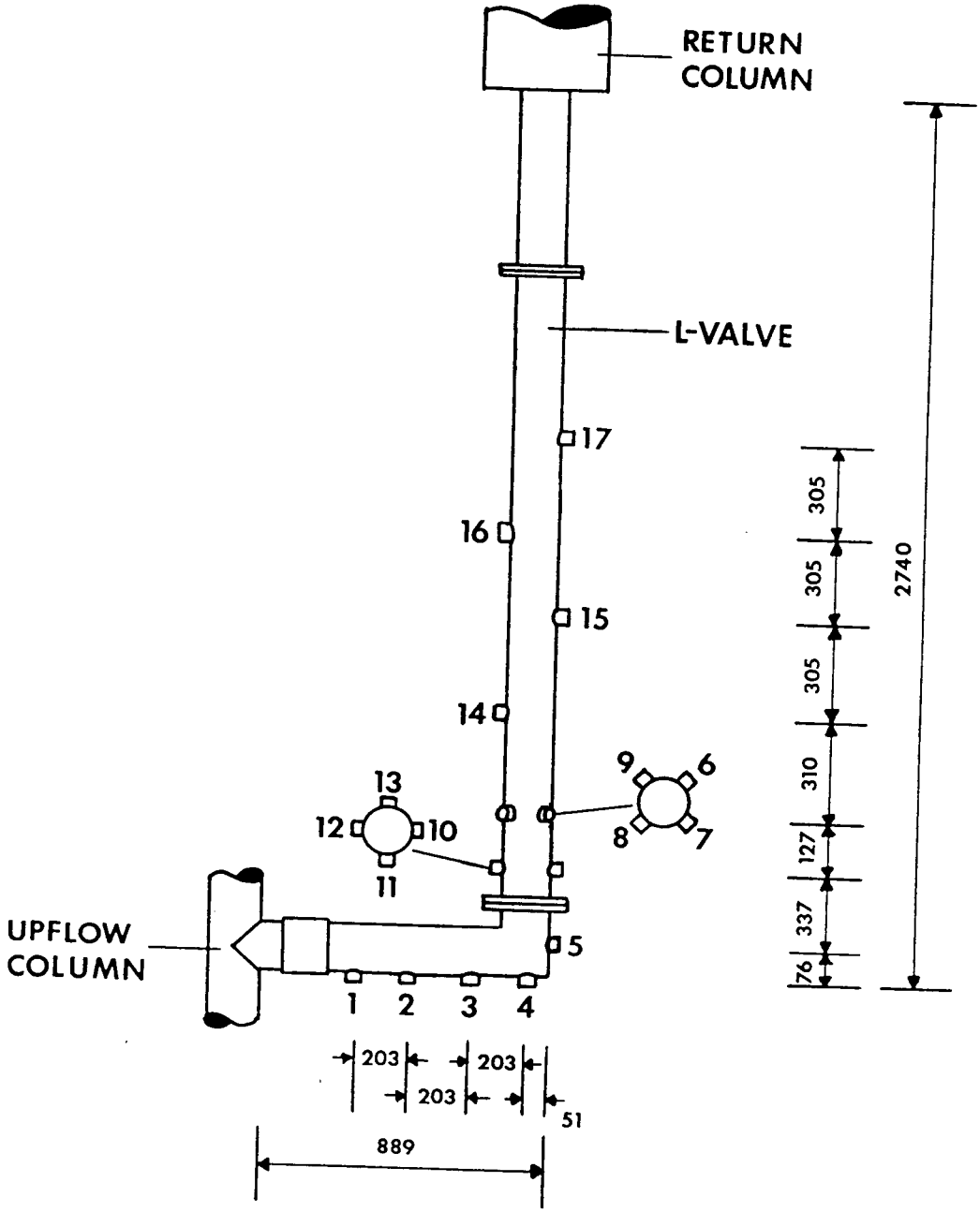

Figure 2.2 The L-Valve. Numbers refer to aeration taps. All dimensions shown are in mm.

The L-valve used in this study had vertical and horizontal sections of length 2.74 m and 0.89 m respectively. The upper portion of the vertical leg entered the bubbling bed of the return vessel from below through the windbox, Figure 2.1. Solids fed to the top of the L-valve, by the bubbling bed, flowed downward through the valve to the bottom of the upflow column. The horizontal leg of the valve was connected to the solids inlet section of the fast bed vessel by a flexible neoprene collar which permitted the sections to move independently of each other and compensated for misalignment and differential expansion in the system.

Aeration of the L-valve was provided using any combination of seventeen aeration ports shown in Figure 2.2. Eight aeration points at the base of the vertical section of the L-valve were evenly spaced around the circumference of the vertical section of the L-valve in sets of four at 0.20 m and 0.54 m above the base of the valve. The lower set was aligned with the horizontal leg, while the upper set was offset by 45° with respect to the horizontal leg. These ports were used to aerate the solids in the lower section of the vertical leg of the valve. Four ports located every 0.30 m on alternate sides of the vertical section, starting 0.85 m above the L-valve base in line with the horizontal leg, were used to aerate the solids in the upper portion of the vertical leg. Along the base of the L-valve, four ports were used to aerate the solids in the horizontal leg. The seventeenth aeration port was located on the vertical leg of the L-valve 0.076 m above its base, directly opposite the horizontal leg. Airflow to

to each aeration port was measured by a rotameter and regulated with a 6.4 mm needle valve.

Solids flowrate through the L-valve was adjusted by varying the air injection points and air injection rates in the L-valve. To provide a smooth flow of fine solids, dp < 100 μm, solids in the horizontal length of the valve were vigorously aerated, while solids in the upper portion of the vertical leg were thoroughly aerated to eliminate bridging. Circulation rate was adjusted by varying the aeration rate to the ports in the lower portion of the vertical section of the L-valve and the port opposite the horizontal leg. Higher circulation rates were obtained by increasing the flow of air to the horizontal leg aeration ports, but control of the circulation rate was still by the previously mentioned ports. For coarse solids, dp > 100 μm, aeration ports #6 and #7, Figure 2.2, were used to control and adjust solids circulation rates.

2.1.3 Cyclones

Solids entrained with the gas leaving the fast fluidization column were recovered in cyclones and recirculated to the solids return standpipe. Gas and solids exiting the fast bed, flowed through a 0.102 m ID flexible hose to the primary cyclone where the majority of the solids were separated. A 0.127 m OD plexiglass section with a 9.5 mm probe port permitted observations, sampling and measurements of the flow exiting the fast column; see Figure 2.1. Solids not separated by the primary cyclone were carried with the exhaust gas to the secondary cyclone through a 0.127 m ID flexible hose. The exhaust leaving the secondary cyclone flowed

through a 0.102 m ID flex hose to the tertiary cyclones and was then exhausted to atmosphere.

The primary cyclone, Figure 2.3, constructed from 0.203 m ID sch. 40 seamless mild steel pipe, was situated on top of the solids recirculation column, Figure 2.1. This cyclone did not have a conical bottom. Instead, the separated solids dropped directly from the cylindrical body of the cyclone to the freeboard of the solids return vessel.

The secondary cyclone, Figure 2.4, provided further solids separation. This cyclone was constructed from 0.203 m ID, sch. 40 seamless mild steel pipe, with the conical bottom formed from 6.4 mm mild steel plate. Solids separated by the secondary cyclone flowed to the return column through an aerated 63.5 mm ID flexible hose entering the vessel at a point 0.93 m above the distributor and below the bubbling bed surface.

The two 0.188 m ID Stairmand type high efficiency tertiary cyclones, both of the geometry shown in Figure 2.5, were operated individually or as a pair in series or parallel. These cyclones were fabricated from 18 gauge 304 stainless steel with the inside welds of the cyclones ground smooth to minimize solids re-entrainment. A PVC "Y" shaped flow splitter divided the flow exiting the secondary cyclone into two streams which flowed to the tertiary cyclones. At low gas flowrates, a single cyclone was used for tertiary solids separation, with the flow to the other cyclone blocked off by a blind flange. Improved solids separation was accomplished by operating the tertiary cyclones in series. For high gas throughputs, the two cyclones were used in parallel, with equal flow to each cyclone. Separated solids were collected in a conical bottom 304 stainless steel hopper and periodically returned to the solids inventory column.

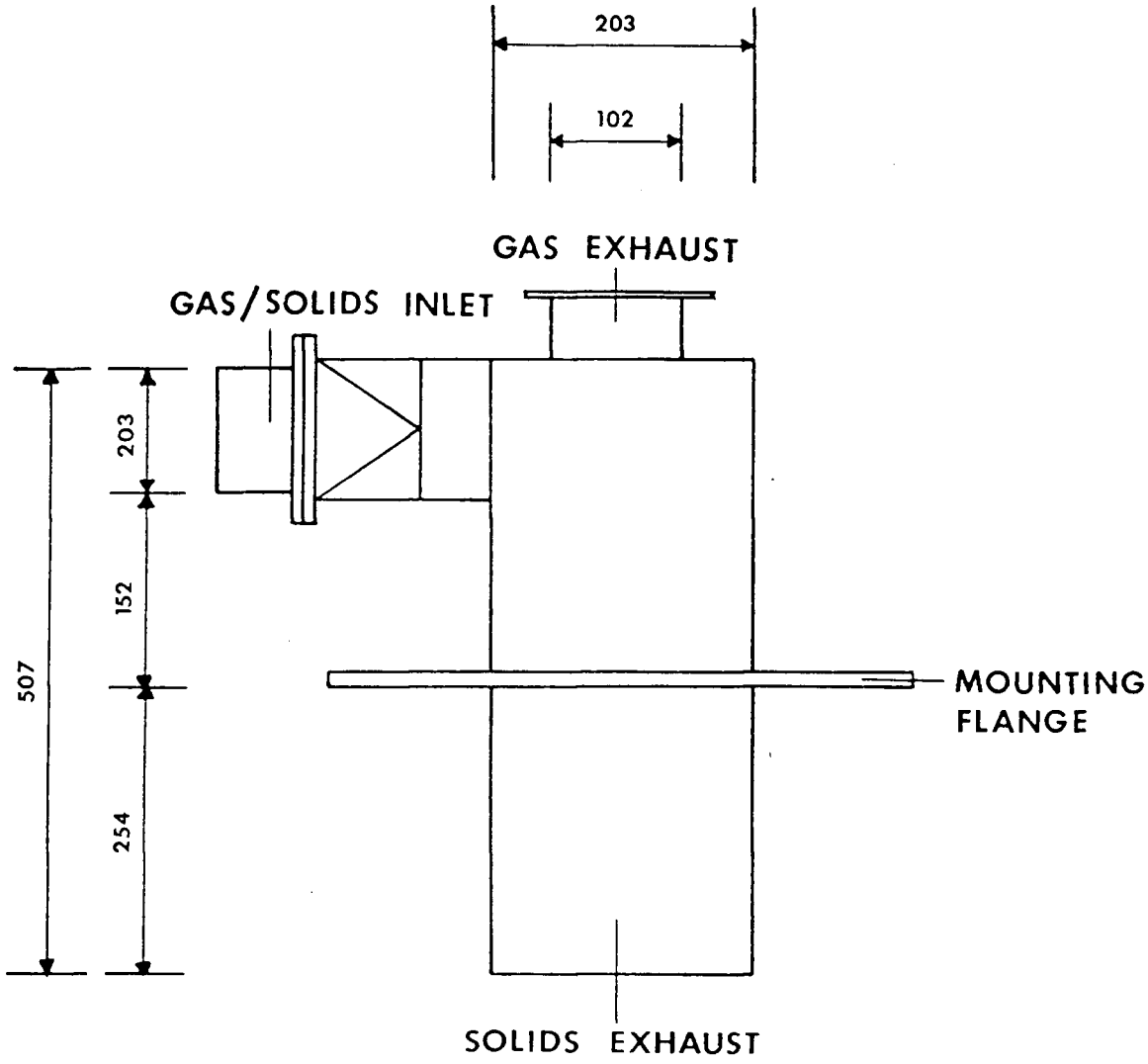

Figure 2.3 Primary cyclone. All dimensions shown are in mm.

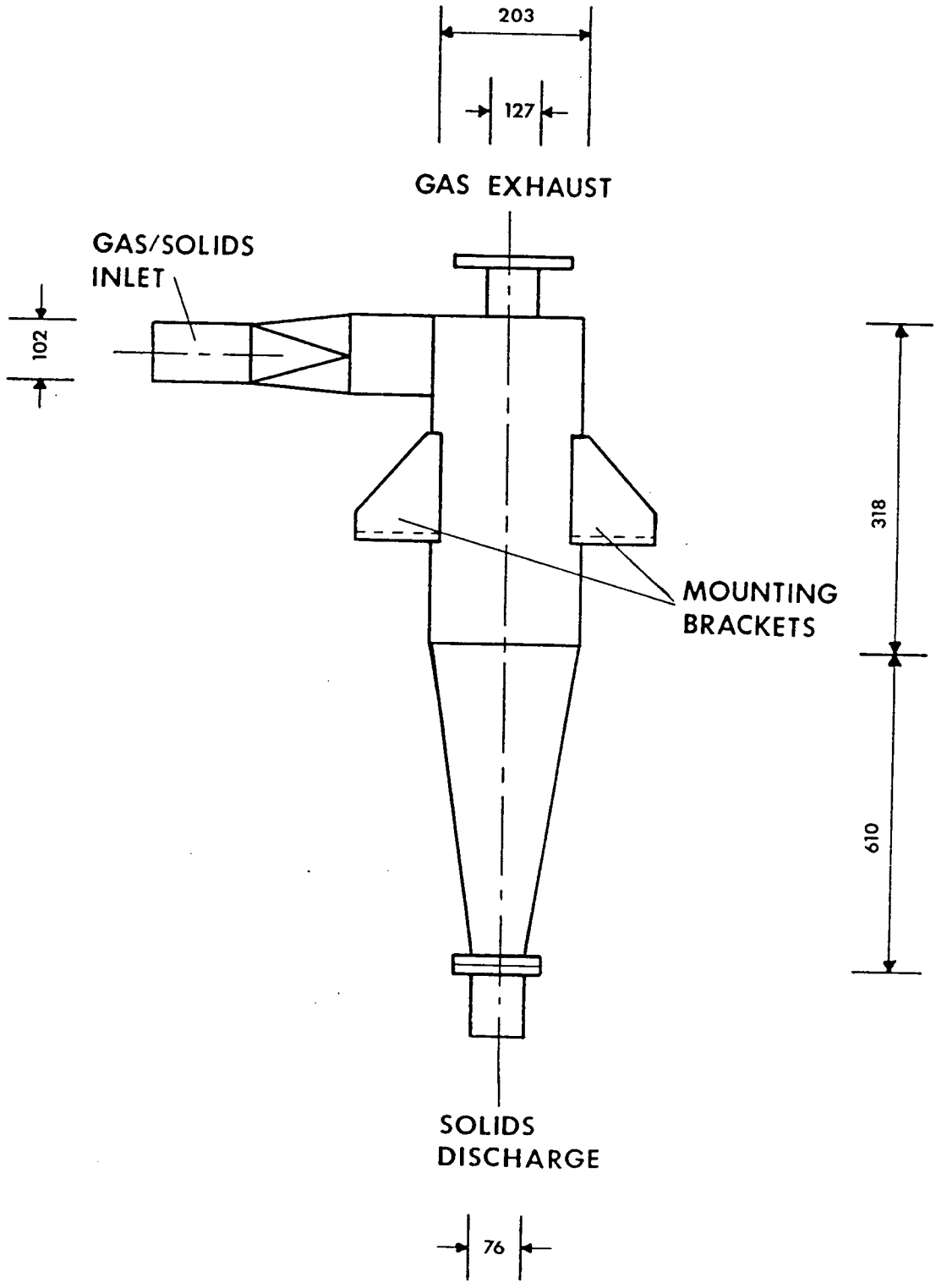

Figure 2.4 Secondary cyclone. All dimensions shown are in mm.

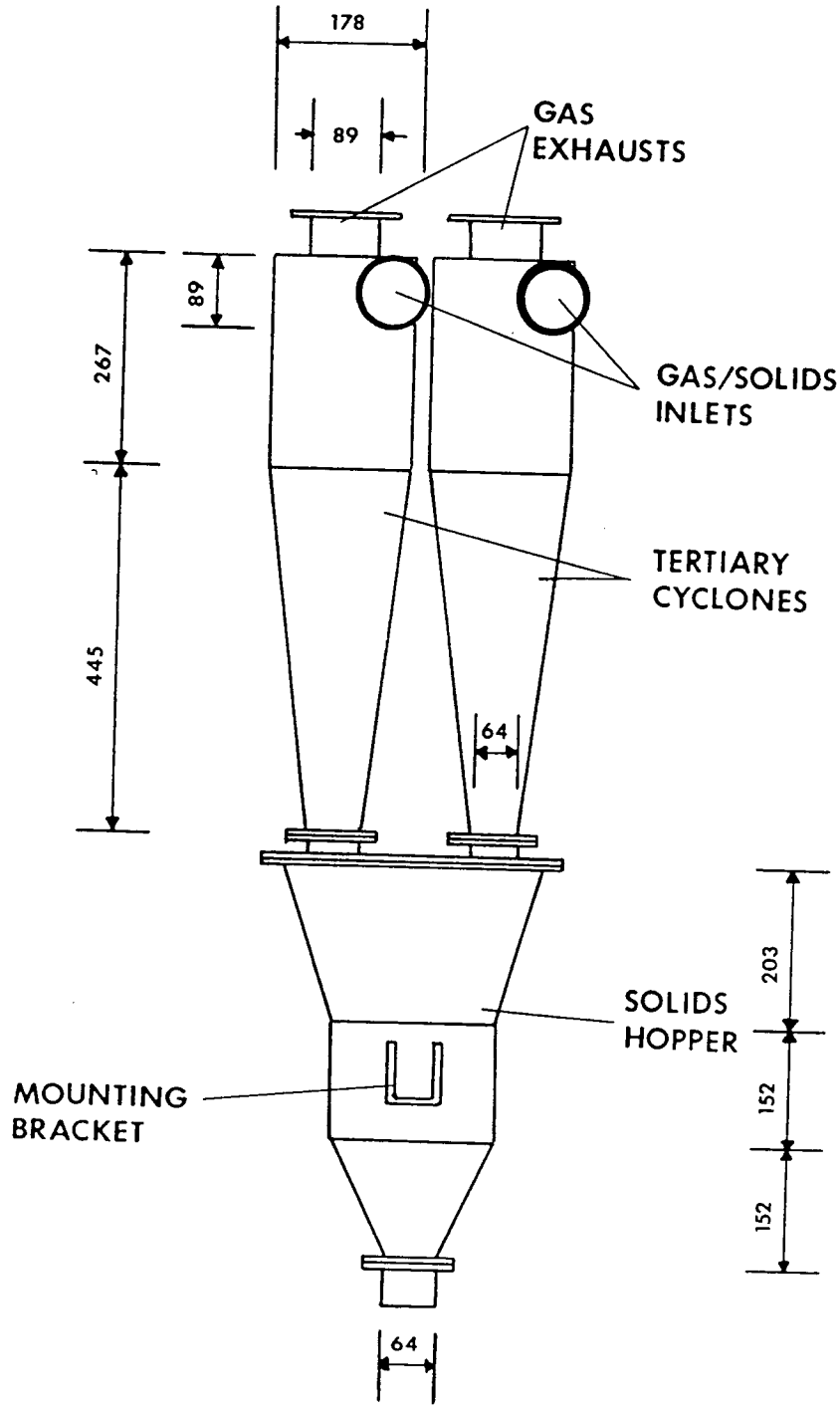

Figure 2.5 Tertiary cyclones and hopper. All dimensions are in mm.

2.1.4 Return Column

The 6.43 m tall return column, constructed of 0.343 m ID rolled acrylic tubing, 6.4 mm wall thickness, was assembled from a number of shorter flanged sections, varying from 0.48 to 1.40 m in length. Butadiene O-rings, 0.40 m ID, 3.18 mm diameter, provided seals between sections. The column served two functions: It provided a return route for solids to the upflow column; it served as a solids inventory vessel. The static solids bed height in the column was maintained at approximately 1.3 m. When the equipment was operating, the solids bed covered the return port of the secondary cyclone solids return line, thereby preventing gas and solids from bypassing through the secondary cyclone solids return line. During operation, the solids in the return column were fluidized to provide free movement to the L-valve.

Fluidizing air was supplied to the return vessel bed by a 0.03 m^3/s, 207 kPag compressor, metered by a rotameter and regulated by a 25.4 mm globe valve. Air entered the return vessel through a multi-orifice distributor at the bottom of the vessel and exited the standpipe by flowing up the column and primary cyclone and out with the gas exhausted from the primary cyclone. The distributor, with a free area of 1.2%, was composed of a piece of 200 mesh stainless steel screen sandwiched between two Dural aluminum distributor plates. The upper and lower plates were drilled with aligned 1.6 mm and 3.2 mm diameter holes respectively, on a 12.7 mm square pitch.

2.1.5 Modified Butterfly Valve

A modified butterfly valve, located in the return column 2.53 m above the distributor, was used to provide one measure of solids circulation rates as shown in Figure 2.6. The valve was made from two diametrically opposed semicircular aluminum plates attached along their diameters to rods with geared ends. The gears meshed together so that the movements of the butterfly valve leaves were synchronized. The plates were drilled with 1.6 mm diameter holes on a 12.7 mm square pitch, giving a free area of 1.2%. To prevent solids backflow through the orifices on the plates, each leaf was covered with 200 mesh stainless steel screen. The valve was operated by two levers, located outside the column, attached to the rods of the valve. The levers moved the plates over the range of vertically downward, fully open to horizontally opposed, fully closed. When closed, the valve prevented solids from flowing downward through the column but permitted gas to flow upward through the valve and accumulated solids. The upflowing gas maintained the accumulated solids in a fluidized state.

Solids accumulation rates were determined by monitoring the rate of change of pressure drop across the valve and accumulated solids. Pressure drops, measured by a Disa model 51D20 capacitance pressure tranducer used in conjunction with a Disa model 51E02-2 tuning plug and model 51E01 reactance converter and expressed as equivalent voltages, were displayed on a digital voltmeter, while permanent records were obtained using an Esterline, model S6015, chart recorder. The set-up is shown in Figure 2.7.

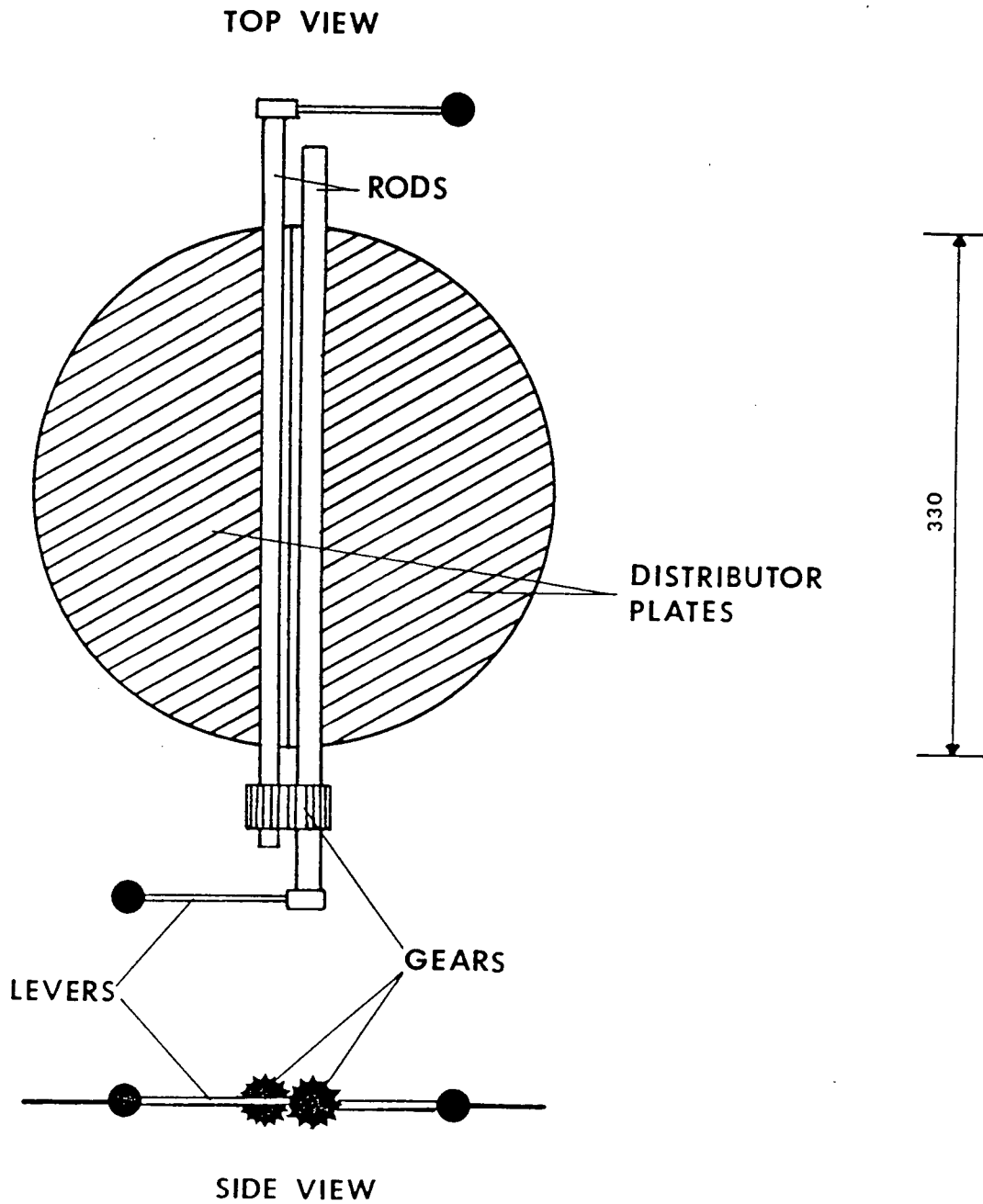

Figure 2.6 Modified butterfly valve. All dimensions shown are in mm.

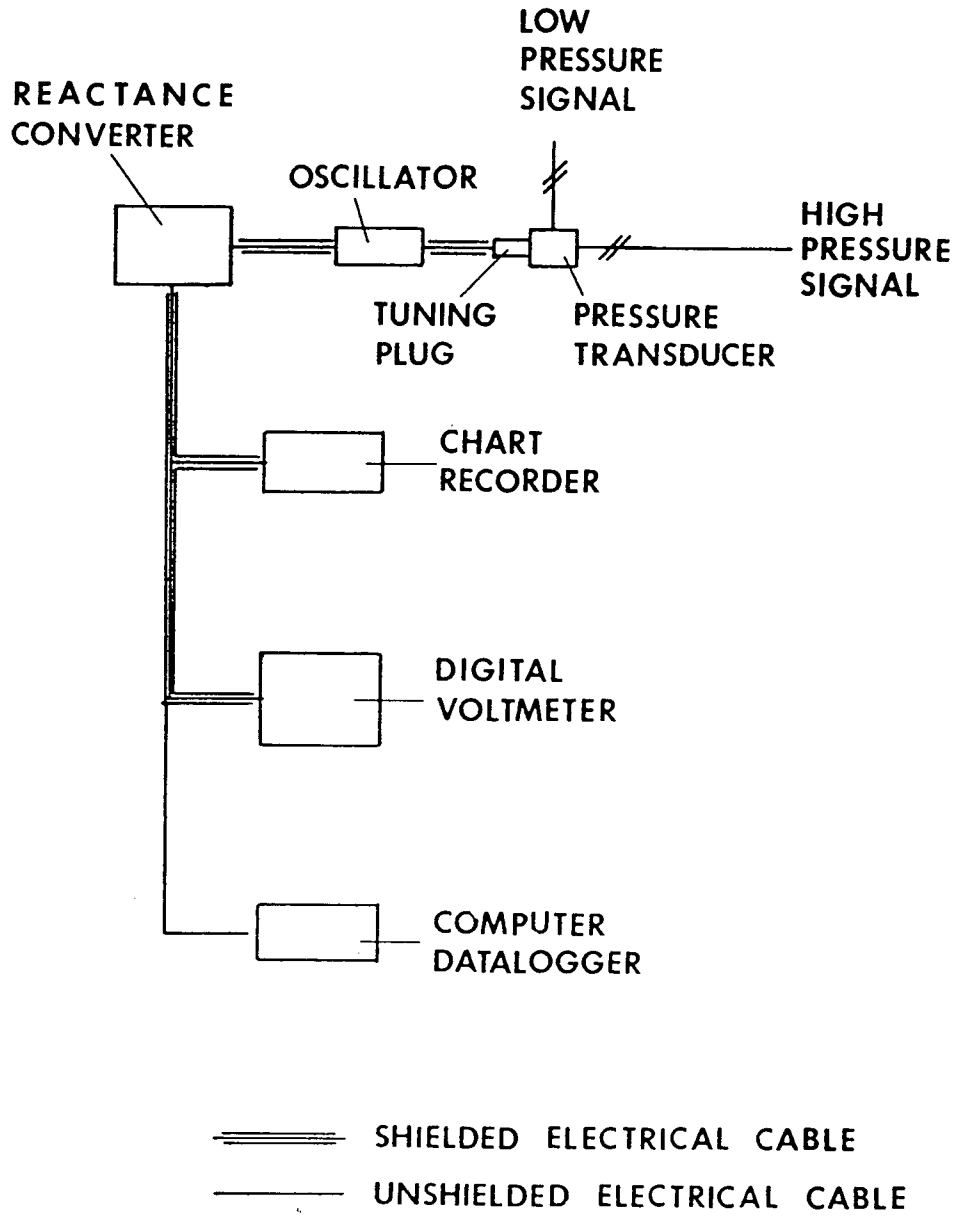

Figure 2.7 Schematic of the pressure measurement and recording apparatus.

2.2 Impact Flowmeter

The solids flow measurement technique of primary interest in this study was the impact flowmeter, Figures 2.8 and 2.9. This meter used a load beam to measure the force of the recirculating solids falling onto a pan extending across the solids return column.

The principle of using a load cell for force measurement was successfully demonstrated by Hosny (1983) in his study of forces on heat transfer tubes in bubbling fluidized beds. Although the magnitudes of the forces were considerably greater in that work, the use of load beams for dynamic force measurement in fluidized systems was shown to be feasible and reliable.

A commercially available series of solids flowmeters, operating on the same principal as the impact flowmeter, are marketted by Milltronics Inc., Canada. These meters measure the horizontal component of the force resulting from particles striking an inclined pan. Since only the horizontal component of the force is measured, the meters are not affected by solids accumulation on the pan. Flowrates as low as 0.5 Tonne/hr for particle sizes ranging from fine powders to 13 mm can be measured. However, it is necessary to concentrate the solids upstream of the flowmeter so that they flow through a 51 mm ID pipe.

2.2.1 Experimental Set-Up

The impact flowmeter was designed to measure solid fluxes ranging from 10 to 100 kg/m^2s, based on the fast bed column cross-sectional area. Solids impacted on a pan with a projected area of 0.033 m^2, (0.10 m wide and 0.33 m long), nearly spanning the diameter of the return column. The pan

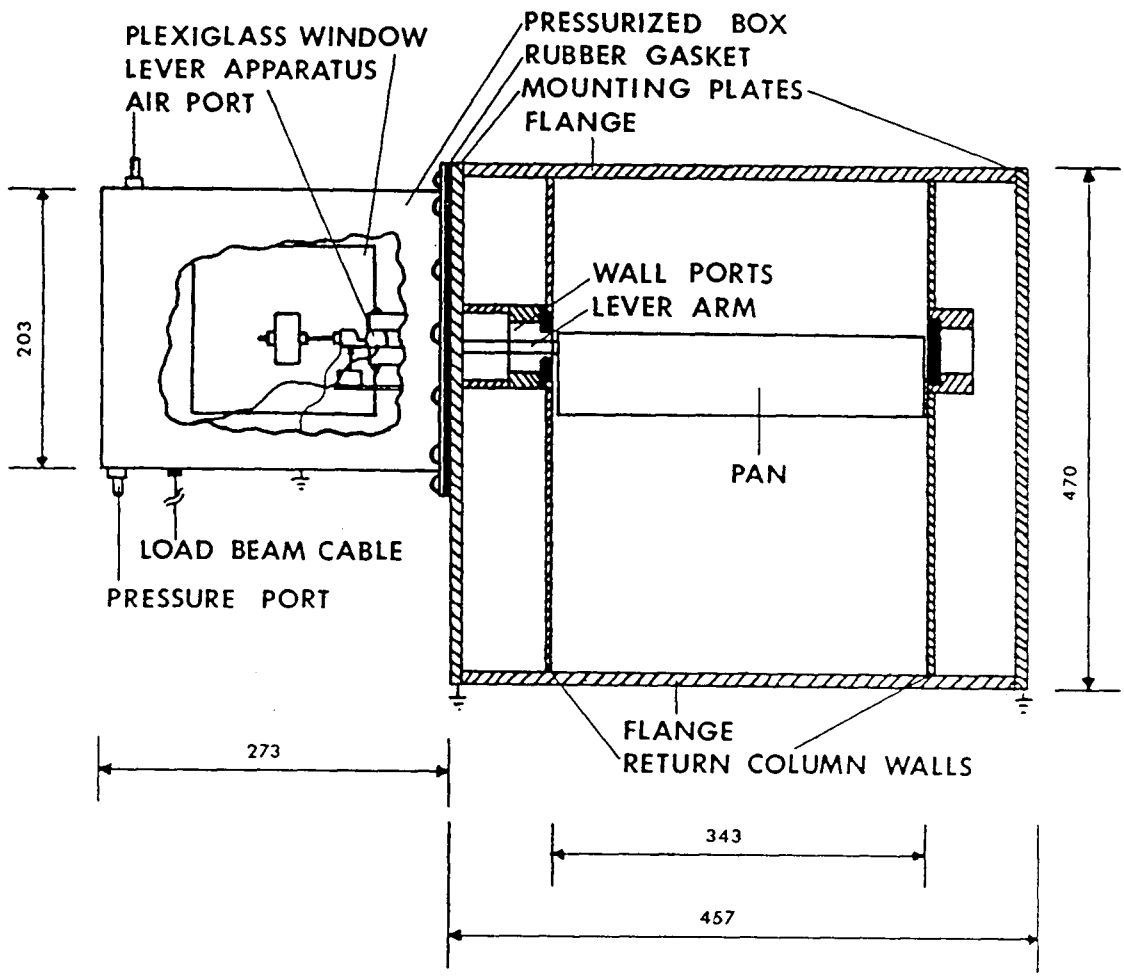

Figure 2.8 Impact flowmeter column section. All dimensions shown are in mm.

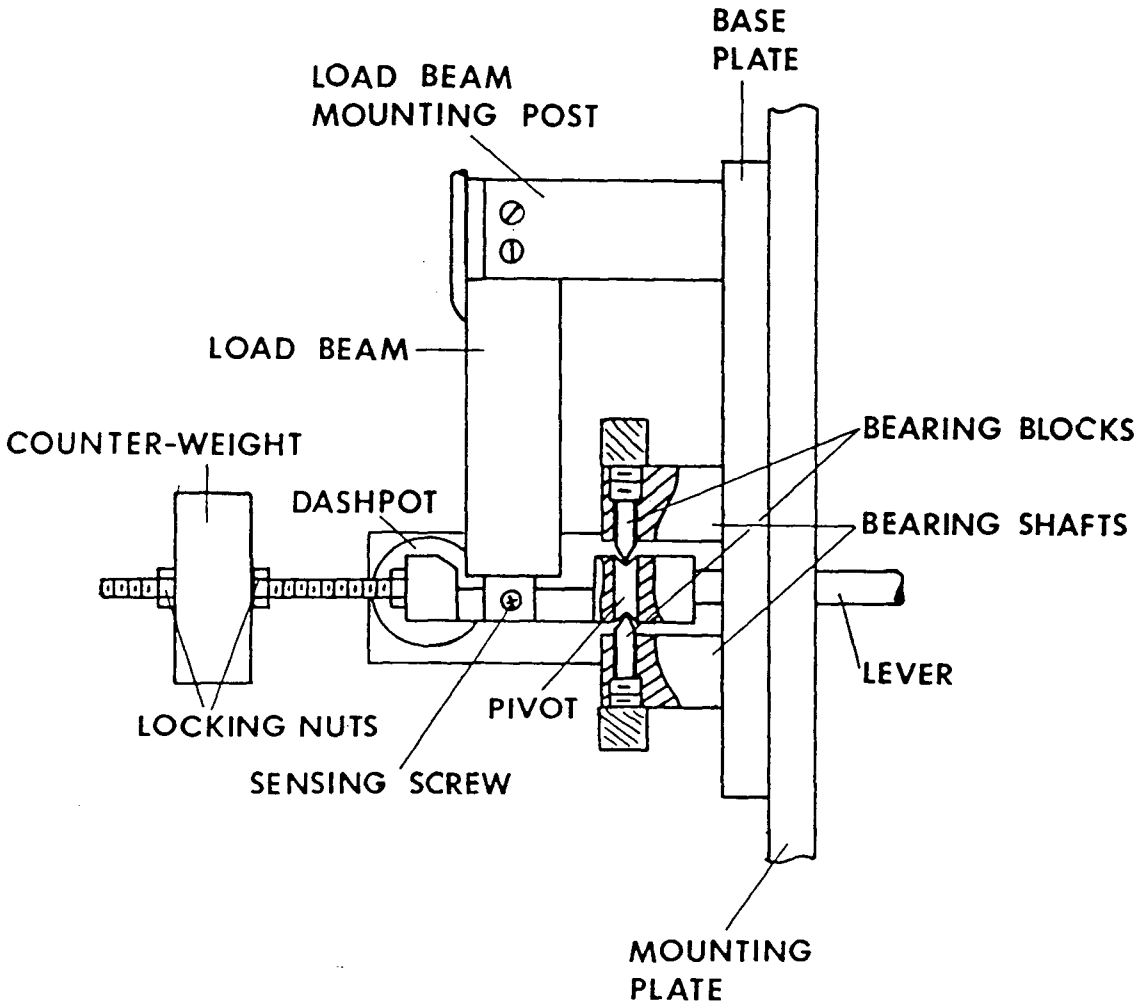

Figure 2.9 Impact flowmeter

was in the form of an inverted "V", with the angle of the sides exceeding the angle of repose of the solids, in order to prevent solids accumulation on the pan. Three pan angles, 30°, 45°, and 60° from the horizontal, were investigated in this study. The pan was attached at one end to a pivoted lever arm which passed through the wall of the return column, as shown in Figure 2.8. The pivot was located outside the column. An adjustable weight, to counter balance the pan and lever assembly, was attached to the end of the lever opposite the pan, Figure 2.9. An oil-damped dashpot, attached 75 mm from the pivot of the lever on the side opposite the pan, was used to dampen rapid oscillations of the lever system. The dashpot, Figure 2.8 and 2.9, had a 2.54 mm piston contained within a 3.15 mm cylinder which was filled with Mobil 600 w gear oil. The oil specifications are given in Appendix D.

A point contact bearing was used as the lever pivot in this study, Figure 2.9. This design of bearing was chosen because it fixed the location of the lever, minimized friction and allowed the equipment to be orientated in any plane. The pivot shaft of the lever, machined with a conical cavity in each end, was held between two hardened steel fixed pins with conical ends, pressing into the two cavities.

On the side of the lever opposite the pan, a 0.454 kg BLH load beam was located, Figure 2.10. A screw, machined with a conical end, was threaded into the sensing end of the load beam. The conical end of the screw contacted the lever assembly and provided a mechanical connection between the lever and the load beam. The centre of the pan assembly was 230 mm from the pivot point, while the load beam contact point was 51 mm from the pivot point. Thus, the force felt by the load beam was approximately four and one half times the force exerted on the pan.

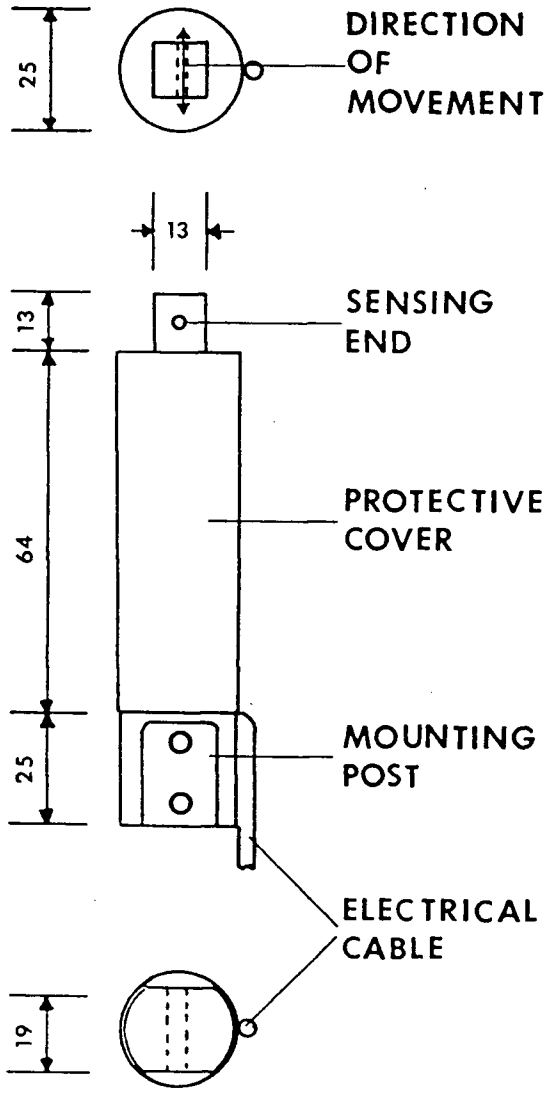

Figure 2.10 BLH load beam. All dimensions shown are in mm.

Exciting voltage and signal conditioning for the load beam were provided by a Bofors, model B-2-F, transducer amplifier module. The amplifier voltage was displayed on a digital voltmeter. Permanent records were made using an EMI UV Oscillograph, model SE 6150 Mk II. The instrumentation is shown in Figure 2.11.

To prevent solids from escaping from the return column through the lever port, the load beam apparatus outside the column was enclosed in a sheet metal box, 0.20 m deep by 0.25 m wide by 0.27 m long, equipped with an acrylic window to permit observation of the equipment. Air fed to the box flowed horizontally through the port in the column wall to the return column. The flow of air prevented solids from interfering with the load beam bearing assembly. The air flow was metered using a rotameter and regulated by a needle valve. The pressure differential between the box and column, measured using a water manometer, was maintained at 5 to 10 mm H_2O to ensure that the air flow was from the box to the column. Box pressure was adjusted by varying the airflow rate to the box.

2.2.2 Meter Location

The flowmeter was located in the solids return column between the bubbling bed surface and the primary cyclone solids exit, Figure 2.1. In this section, solids separated by the primary cyclone cascaded downward to the bubbling bed surface at near terminal velocities through the upward flowing fluidization gas.

The vertical elevation of the impact meter apparatus was chosen to minimize the effects of non-uniform solids distribution from above and particle projection from the bubbling bed surface below. Solids leaving

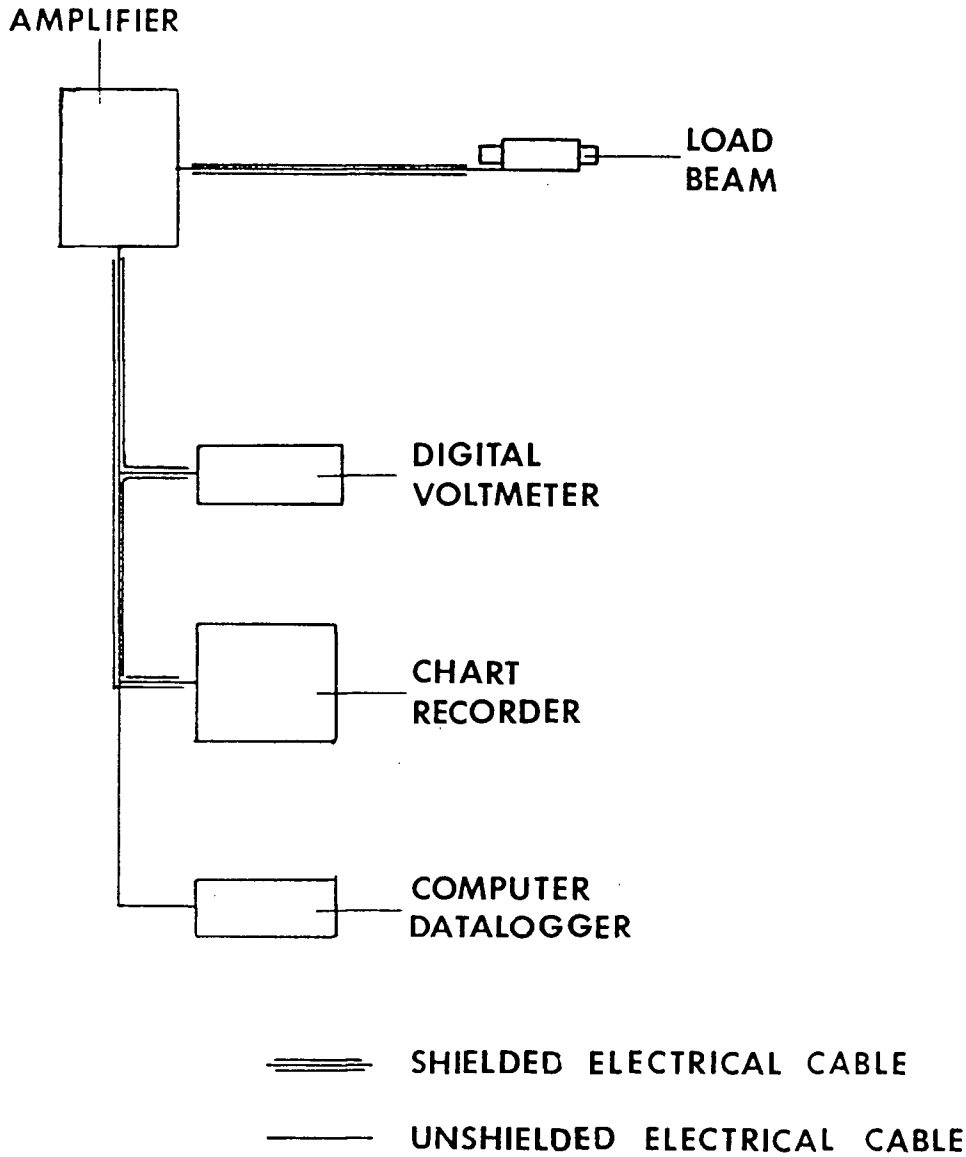

Figure 2.11 Schematic of the load beam signal conditioning and recording apparatus.

the primary cyclone followed a helical downward trajectory. As a result of the primary cyclone's centrifugal forces, the particles concentrated near the column wall, allowing some to escape contact with the pan by falling through the 6.4 mm gas between the ends of the pan and the wall. Particles projected upwards from the bubbling bed surface by erupting bubbles could reduce the net force acting on the pan. This was a minor problem since the bubbling bed was always operated at a flow low enough such that flow of particles projected upwards by bursting bubbles was negligible and the impact apparatus was 2.8 m above the bubbling bed surface.

A baffle, located at the column wall, deflected the particles inward, thus increasing the flow of solids in the core of column. The baffle, shown in Figure 2.12, was an annular sheet metal insert with 45° sides which projected 12.7 mm into the column from the wall.

A coarse screen assembly, extending across the entire column cross-section upstream of the impact meter and directly above the baffle, was used to dampen solids flowrate fluctuations and further promote uniform solids distribution as shown in Figure 2.12. The assembly consisted of a screen with 1 mm square openings supported on two rigid wire screens with 5 mm square openings aligned at 45° with respect to each other, Figure 2.13.

2.3 Modified Orifice

The flowmeter of secondary interest in this study was the modified orifice or venturi shown in Figure 2.13. This meter, suggested by Reh

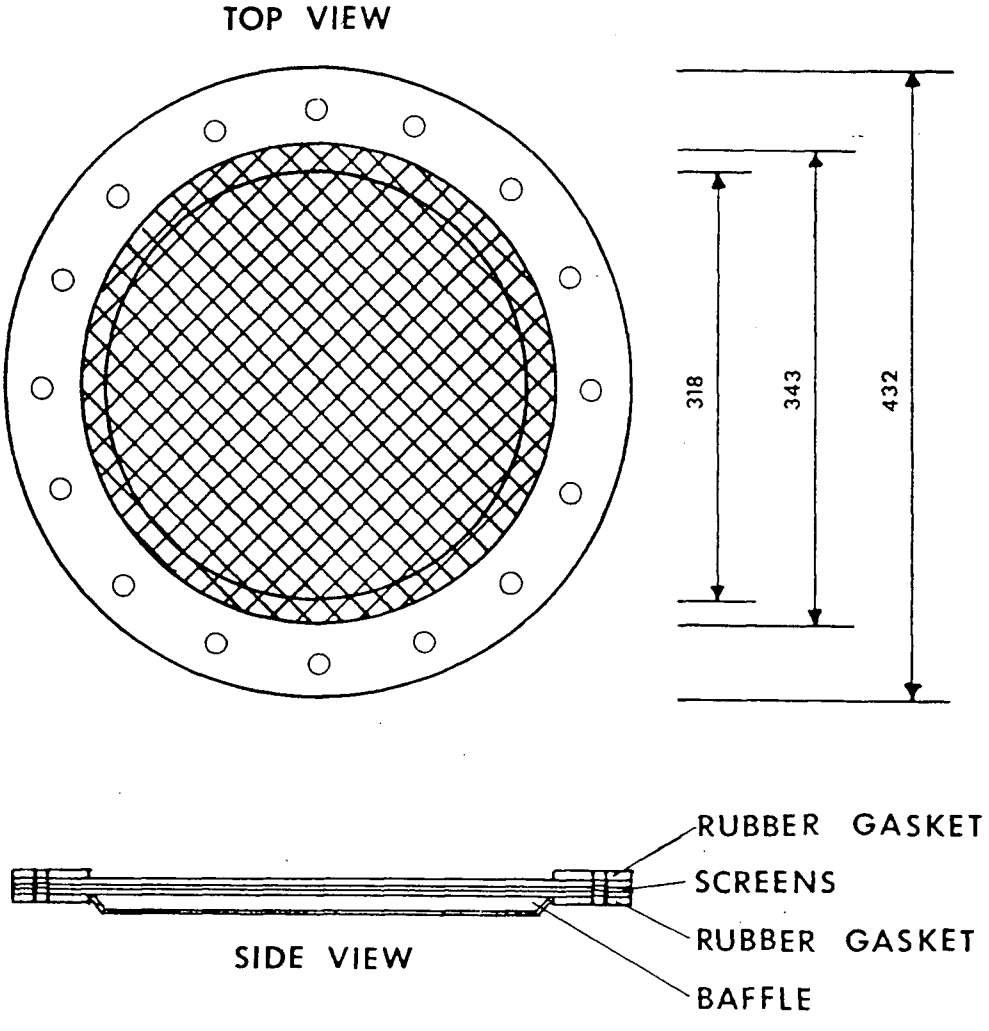

Figure 2.12 Baffle/screen assembly used to redistribute solids separated by primary cyclone. All dimensions shown are in mm.

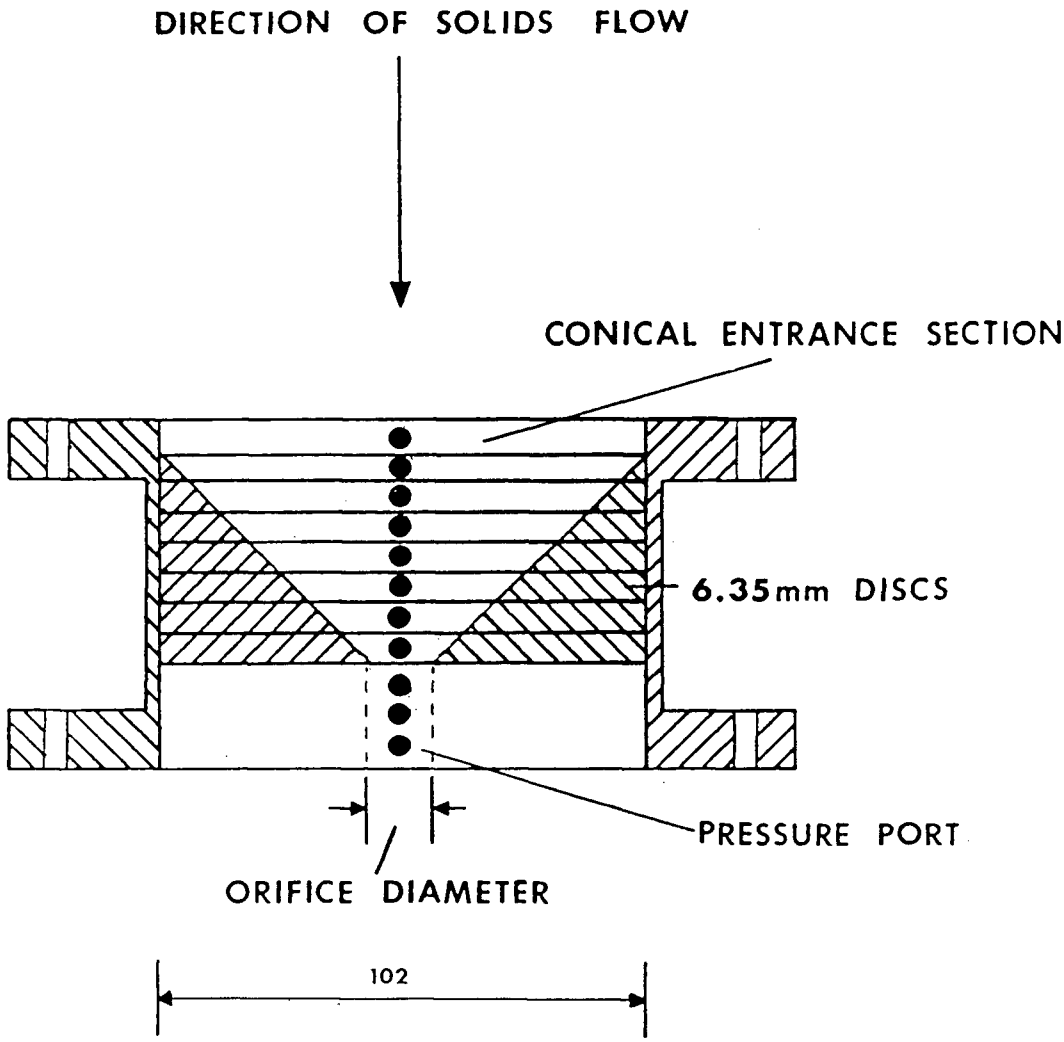

Figure 2.13 Modified orifice meter. All dimensions shown are in mm.

(1984), utilized an orifice with a conical entrance section to develop a pressure differential related to solids circulation rates. The orifice assembly was designed to study the feasibility of using an orifice with a conical entrance section to measure the solids flowrate in a counter-current flowing gas/solids suspension. The equipment permitted the effect of orifice geometry, i.e. cone angle and orifice-to-tube diameter ratio, to be studied.

The principle of using a constriction type flowmeter for measuring gas/solids flowrates was successfully demonstrated by Carlson (1948). In Carlson's study, it was found that the pressure differential for an orifice plate was insensitive to the presence of fine solids flowing with the gas. However, the pressure differential for a flow nozzle was sensitive to both gas and solids flowrates. Therefore, by using a flow nozzle in conjunction with an orifice plate it was possible to determine the gas and solids flowrates of a co-current gas/solid flow. It was postulated that the ability of a flow nozzle to measure solids flowrates resulted from its gradual throat constriction which permitted the solids to accelerate to the higher throat velocity. The rapid constriction of an orifice plate did not permit the solids to reach the higher throat velocity. Thus the solids did not affect the pressure drop across the orifice plate. The ability to use a constriction type flowmeter with a gradual throat constriction for the metering of co-current gas/solid flows was further demonstrated by Farbar (1953), who found that a venturi was capable of measuring the flowrate of solids carried with gas flowing through the meter.

In the present work, three modified orifices were studied under simulated CFB return vessel operating conditions to determine their performance and behaviour in measuring solids fluxes. The orifices were designed to measure solids fluxes ranging from 10 to 100 kg/m^2s flowing counter-currently to a low velocity upwards moving airflow, up to 0.03 m/s, which simulated the fluidization gas in the solids return column.

2.3.1 Modified Orifice Equipment

Each modified orifice was flanged between two vertical 1.52 m straight runs of 0.102 m ID acrylic tubing, Figure 2.14. To discourage solids accumulation in the throat, the inlet throat angles of 30°, 45° and 60°, as measured from the horizontal, exceeded the angles of repose of the solids used in this study. As shown in Figure 2.13, each orifice was constructed from a stack of 6.35 mm thick acrylic discs housed in a length of 0.102 m ID acrylic tubing. The conical entrance section was machined into the stack of discs with each disc equipped with a 3.2 mm diameter pressure tap port which aligned with a hole in the housing tube wall. The inlet and exit pipes were equipped with 3.2 mm ID pressure taps spaced 12.7 mm apart over the 0.31 m lengths immediately upstream and downstream of the orifice, on 25.4 mm spacing over the next 0.31 m in each direction, and 50.8 mm apart over the remaining lengths of each pipe. Air, to simulate the counter-current gas flow in the CFB solids return standpipe, was introduced at the bottom of the exit pipe of the apparatus. The flow of air was regulated and measured using a rotameter equipped with a needle valve.

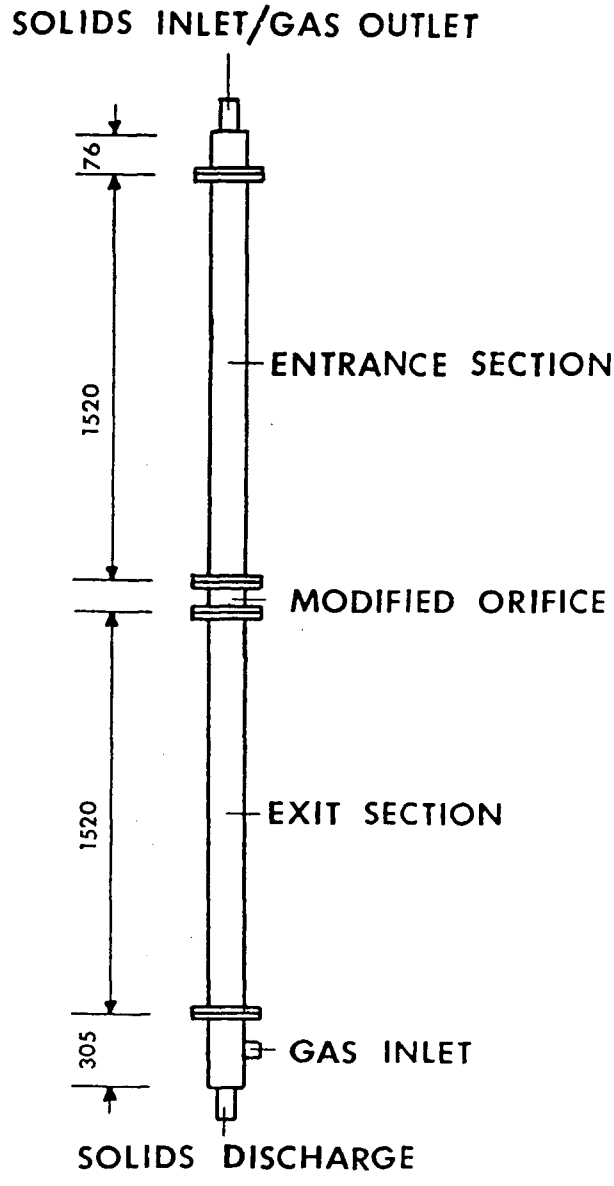

Figure 2.14 Modified orifice meter apparatus.
All dimensions shown are in mm.

2.3.2 Pressure Measurement

Pressure differentials were measured using a Disa model 51D20 capacitance pressure transducer in conjunction with a Disa model 51E02-2 tuning plug and model 51E01 reactance converter. Pressure differentials, in terms of corresponding voltages, were displayed on a digital voltmeter, while permanent records were made using an EMI UV Oscilliograph, model SE 6150 Mk II, chart recorder (see Figure 2.7).

2.3.3 Solids Feeding

Solids were supplied to the orifice apparatus using either: A solids feed funnel located at the solids inlet of the orifice apparatus or the secondary cyclone of the CFB apparatus. Solids feeding via the funnel permitted the flowrate of solids to be easily controlled. On the other hand, feeding of solids from the secondary cyclone provided a better simulation of the conditions which an orifice in the solids return loop of a CFB would experience.

In the first method, poured solids flowed through an orifice in the bottom of a large funnel to the solids inlet of the modified orifice. To ensure the flow of solids from the funnel did not vary, the inventory of solids in the funnel was maintained at a constant level by adding solids to funnel at the same rate as they were being discharged. Solids flowrate was varied by changing the diameter of the orifice used in the funnel. During these experiments, the solids were collected in a bin at the base of the modified orifice meter so that the solids flowrate through the meter could be determined.

Gas and entrained solids exiting the fast bed were sent directly to the secondary cyclone. Solids separated by the secondary cyclone were fed to the orifice assembly through a 0.102 m flexible hose. The gas/solids flow exiting from the secondary cyclone was sent to the primary and tertiary cyclones of the CFB unit for further solids removal and then exhausted to atmosphere. Solids feedrate by the secondary cyclone was adjusted by varying the solids loading of the gas entering the cyclone. This was accomplished by controlling the solids circulation rate using the L-valve. While setting up the experimental conditions, solids passing through the orifice were recirculated to the CFB unit. When steady state conditions were achieved, solids passing through the apparatus were collected in a bin attached to the end of the exit pipe of the equipment over a measured period of time.

2.4 L-valve Calibration

An additional area of interest was the relationship between the velocities of particles moving downward through the vertical section of the L-valve and the corresponding solids circulation rate. The effect of the circumferential point of measurement on the relationship between particle velocity and solids flux was also determined.

In this study, particle velocities were measured at five different circumferential positions, at 45° intervals starting in line with the horizontal leg of the L-valve, Figure 2.15. Particle velocities were determined by recording the time required for a particle to move through a 0.30 m length of the L-valve, starting 1.3 m above the base of the valve. Coloured alumina or sand particles, which were darker than the bulk of the

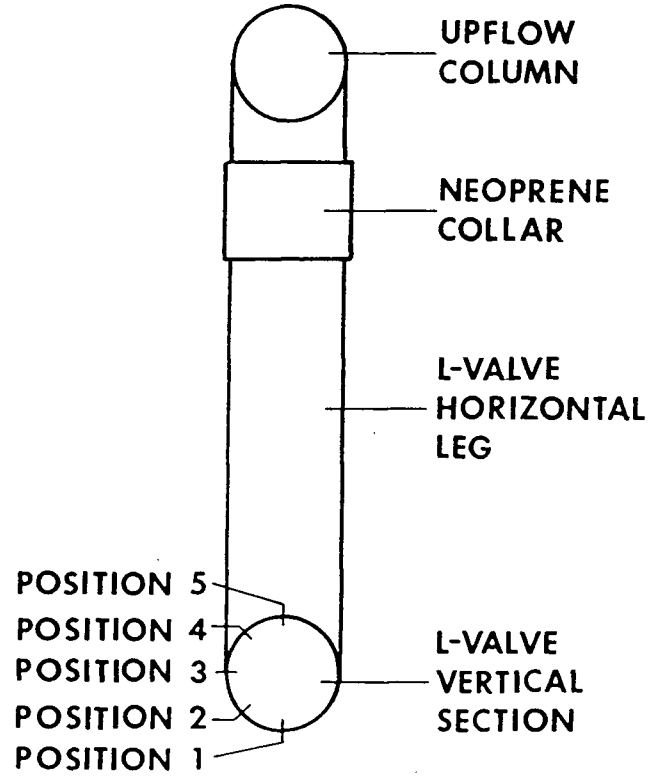

Figure 2.15 Particle velocity measurement positions

particulate material, were used to follow the movement of the solids through the valve. Solid circulation rates were measured with the butterfly valve.

2.5 Data Acquisition and Processing

The pressure transducer and load beam signals were datalogged using a Tecmar A/D, D/A programmable datalogging board in conjunction with an IBM XT computer. The programs used to set and start the clock and to determine the sampling rate of the Tecmar board are given in Appendices A.1 and A.2 respectively. This program was capable of sampling up to 30000 data points per second, but was limited to taking 27000 data points per run. The logged data points were stored in an array during sampling and transferred to the hard disk of the IBM XT computer at the end of each run.

The load beam was datalogged at a rate of 100 points per second for a 1 to 2 minute run duration. After each run, the data were integrated using Simpson's method to determine the average signal value. The integration program is shown in Appendix A.3. Trapezoidal integration was also carried out for comparison purposes. The standard deviation of the load beam signal about the time averaged valve was calculated using the program shown in Appendix A.4.

Pressure transducer measurements of the pressure differential across the orifice meter were datalogged at 100 points per second for a 1 to 2 minute run duration. These signals were then integrated and averaged as outlined above.

Pressure transducer measurements giving the pressure differential across the butterfly valve and accumulating solids were datalogged for a period of 10 to 30 seconds at 100 points per second. The relatively short sampling period was chosen to avoid excessive depletion of the solids inventory of the bubbling bed, since gas and solids would escape through the secondary cyclone return line if it became uncovered. The data were fitted by a straight line using the linear regression program presented in Appendix A.5.

2.6 Particle Properties

Two types of particles were used in this study: an alumina produced by Alcan and an Ottawa sand from the Ottawa Sand Company, Ottawa, Illinois. The respective properties of the particles are summarized in Table 2.1. Sauter mean particle diameters were calculated from the sieve analysis of the solids given in Appendix B. The loose packed bulk densities of the solids were found by pouring a weighed amount of solids into a graduated cylinder and recording the volume. The particle density of the alumina was found by mercury porosimetry. On the other hand, the sand particle density was found by pouring a weighed amount of solids into a measured volume of liquid and recording the displaced volume. The minimum fluidization velocities were estimated using an empirical correlation (Grace, 1982) and measured experimentally in a 0.15 m ID bed using pressure drop data, Appendix C. The angles of repose were found by measuring the slopes of the sides of poured piles of solids. The shapes and surface textures of the alumina and sand particles are shown in Figures 2.16 and 2.17 and Figures 2.18 and 2.19 respectively.

Table 2.1 Particle Properties

Property	Alumina	Ottawa Sand
Mean Particle Diameter, $\bar{d}p$ μm	64	148
Particle Density, ρ_p kg/m^3	3500	2650
Bulk Density, ρ_b kg/m^3	1140	1550
Loose Packed Voidage, ε	*0.67	0.42
Particle Terminal Velocity, U_t, based on gas properties at 25°C, m/s	0.36	0.99
Archimedes Number	31	290
U_{mf} Calculated m/s	0.006	0.023
U_{mf} Experimental m/s	0.010	0.021
Bulk Density at Minimum Fluidization, ρ_{mf}, kg/m^3	1100	1500
Bed Voidage at Minimum Fluidization, ε_{mf}	0.69	0.43
Angle of Repose	30°	29°

* includes internal voids of particles

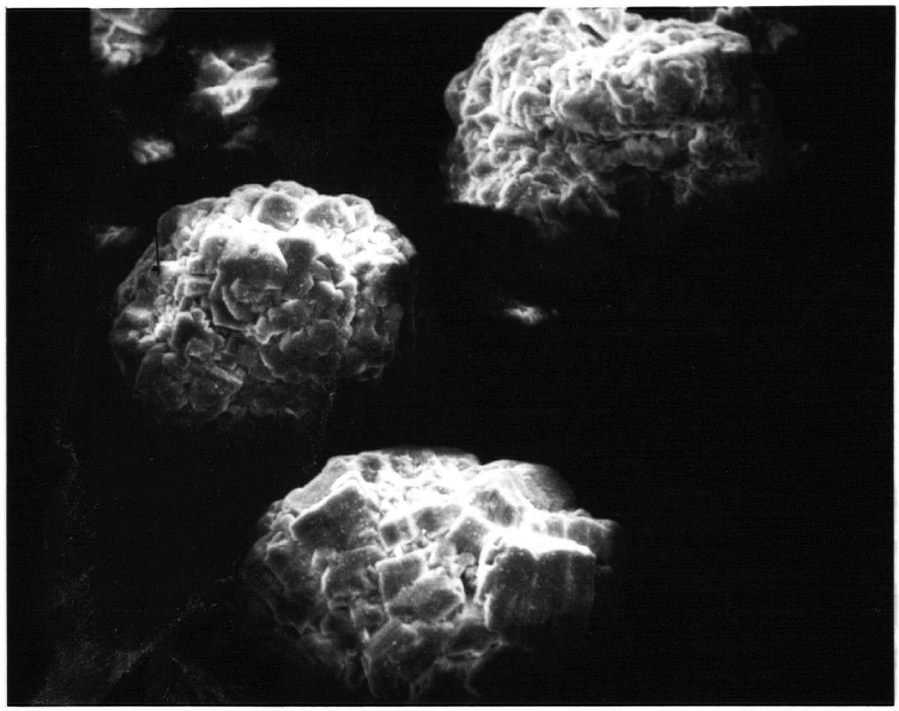

Figure 2.16 Photograph of the alumina particles at 400X magnification

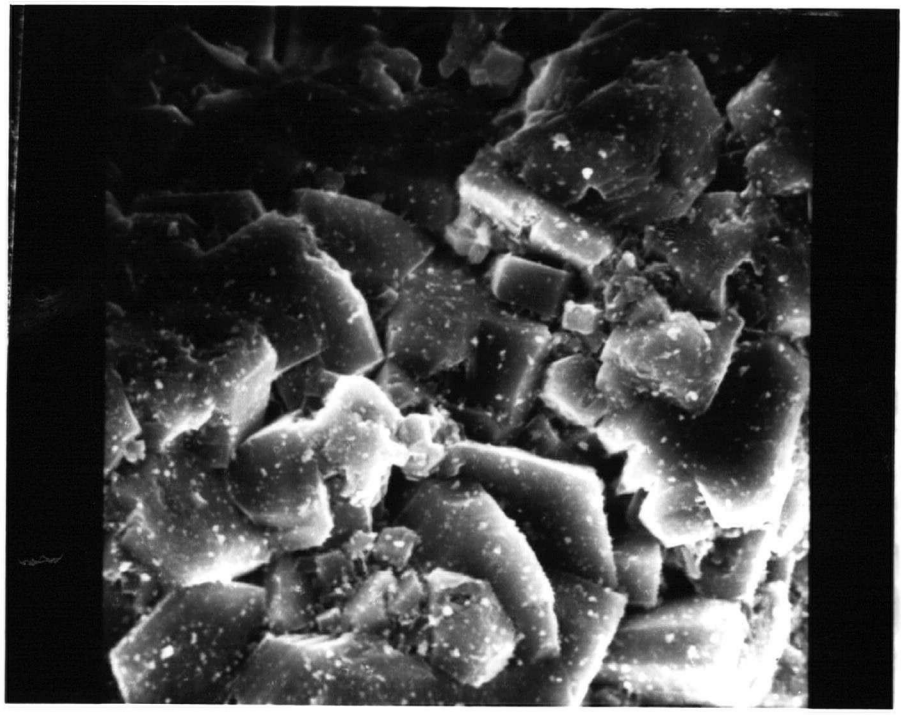

Figure 2.17 Photograph of the alumina particles at 2000X magnification

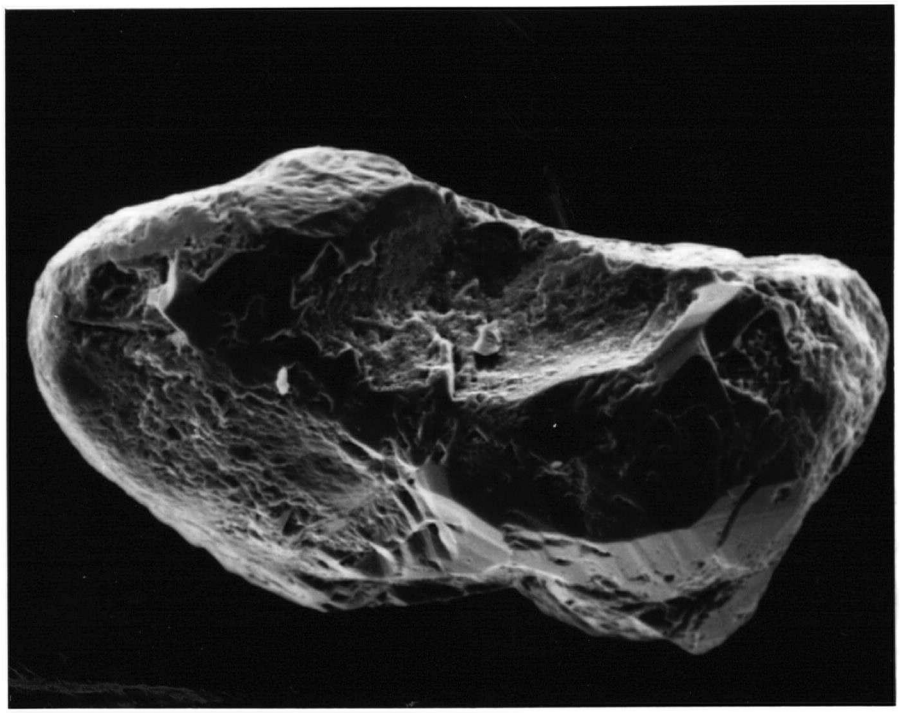

Figure 2.18 Photograph of the sand particles at 200X magnification

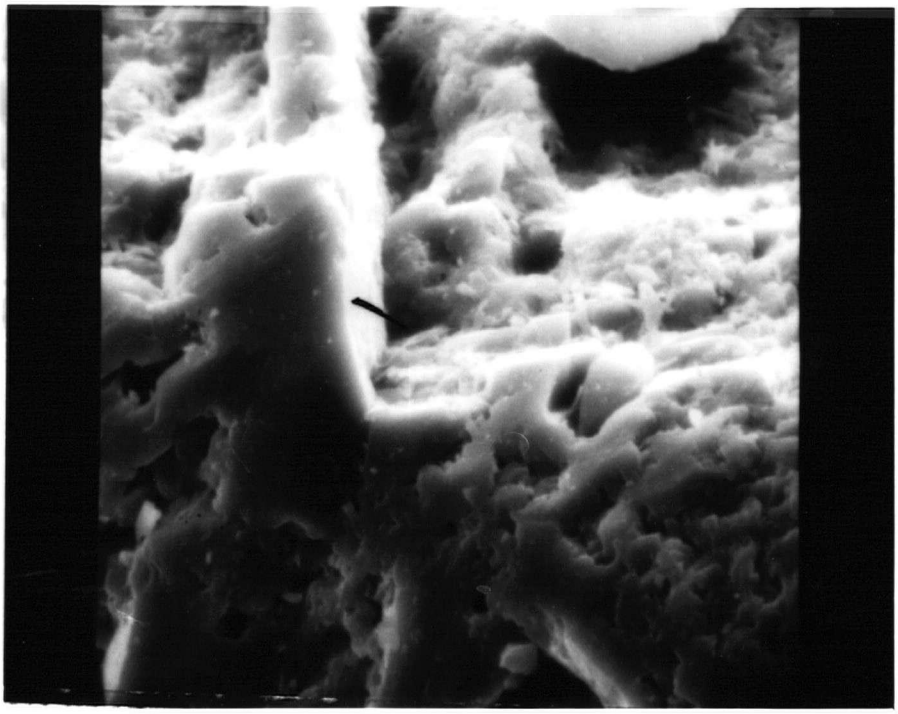

Figure 2.19 Photograph of the sand particles at 2000X magnification

3.0 Results and Discussion

3.1 Introduction

In this chapter the experimental results of this project are presented and discussed. The first section deals with general observations of the CFB unit during the course of this work. The remaining sections present and discuss the results and observations for the impact flowmeter, modified orifice meter and L-valve calibration.

3.2 General Observations

Throughout this study observations of phenomena which directly and indirectly affected the results of this research were recorded. These observations and their effects are summarized in this section.

3.2.1 Static Electricity

As a result of the particulate material rubbing against the plexiglass walls of the CFB unit, static charges were generated. The magnitude of these charges and rate of charging were dependent on the particulate material, the humidity of the air used in the fast and bubbling beds, the amount of solids circulating through the fast bed and the velocities at which they were travelling. Charge generation was found to be most severe when the outside air temperature and humidity was low, when the solids circulation rate was high and when the fast bed gas velocity was high.

The static charges tended to concentrate on the parts of the column assembly which were in intimate contact with the particles, such as the screen/baffle assembly, primary cyclone, impact flow meter, butterfly valve

and plexiglass walls containing the bubbling bed. Periodically, electrical discharges would occur from these areas of charge concentration to the grounded support structure. These discharges adversely affected the computer datalogging and operation of the impact flowmeter and the operation butterfly valve. Discharges from the column resulted in voltage spikes in the output signal of the load beam amplifier which prevented the Tecmar board from completing the analog-to-digital conversions. As a result, datalogging ceased when a voltage spike was encountered. Additionally, charge accumulation on the butterfly valve resulted in the valve operator receiving high voltage shocks whenever she/he went to close the valve. At times, the shocks were so intense that it was too uncomfortable to operate the valve.

To alleviate the problems of static discharge, the butterfly valve, primary cyclone, screen/baffle assembly and impact flow meter were electrically grounded to the support column using a heavy gauge copper wire. This prevented static build up and discharge from these pieces of equipment. The return column at the bubbling bed surface and immediately upstream and downstream of the impact flowmeter and the section of the upflow column adjacent to the impact flowmeter were covered with aluminum foil which was grounded to the support structure. This drew the charge away from the covered areas of the plexiglass columns. All of the electrical signal cables were replaced with shielded electrical cables, with the shields of the cables connected to an electrical ground.

The extensive grounding of the CFB unit allowed the equipment to operate without problems except on days when the outside temperature was below 0° celcius and the relative humidity was less than 70%. On these days, static discharges from the plexiglass column to grounded areas were observed. These discharges adversely affected the datalogging procedure.

To reduce this problem, the humidity of the fluidizing air was increased by adding water to the blower air line. The water was evaporated into the flowing air. This appeared to decrease the static charge generation. Since the water was added batchwise to the blower line, the effectiveness of this method decreased with time between additions. It also proved inconvenient to add water periodically to the blower line. An antistatic agent, ethylhexadecyldimethylammonium bromide dissolved in water, was also evaporated into the flow air but did not result in a noticeable static charge reduction. Therefore, the equipment was not operated when the outside temperature and relative humidity were low.

Under conditions of high static charge generation, it was observed that the behaviour of the solids would change. As static charges increased, an increasing amount of solids collected on the walls of the return columns. For the case of the Ottawa sand, operating under the worst static conditions, i.e. external temperature of -3°C and 60% relative humidity, irregular shaped voids were seen to form and travel downwards in the bubbling bed for short distances before disappearing. The build-up of static charge appeared to make the solids more cohesive and permitted the formation of agglomerates which were able to withstand higher shear.

3.2.2 Solids Circulation

The most effective method of setting and adjusting the solids circulation rate was found to differ for the two types of solids used in this study.

To circulate the alumina particles, it was necessary to aerate the solids in the vertical and horizontal legs of the L-valve before continuous solids feeding could be obtained. During start-up, the first step was to begin aerating the solids in the vertical leg using aeration point #16, Figure 2.2. When the airflow to point #16 was started, the solids were observed to bridge the 0.15 m column directly above the aeration tap. With time, solids fell from the lower surface of the bridge and the bridge was observed to travel up the vertical length of the L-valve to the bubbling bed. The gas was able to flow freely through the solids below the bridge, with bubbles travelling upward through the first 0.30 m of solids immediately above the aeration point and then dispersing so that detectable voids were not observed to flow through the solids above this point. Once the bridge had disappeared, the solids began to flow through the L-valve. However, the flow of solids occurred in pulses, with the solids sticking and slipping as they moved through the L-valve. At this point, the solids in the horizontal leg of the L-valve were aerated using aeration points #1 through #4, Figure 2.2. This resulted in the solids moving more smoothly through the L-valve. However, as the solids circulation rate was increased, the solids were found to stick and slip as they flowed through the valve. Adjustment of solids circulation was primarily by regulating the air flow to point #5. Minor flow adjustments were also made by varying the airflows to points #6 and #7.

Reinjection of the Ottawa sand using the L-valve tended to be much simpler than circulation of the alumina. Solids circulation was controlled using aeration points #6 and #7 in Figure 2.2. It was not necessary to aerate the solids in the vertical or horizontal legs of the L-valve. The solid circulation rate was increased by increasing the flowrate of air to the two aeration points. During all the experiments with the sand and the alumina, the flowrates to the two aeration points were kept equal. For the case of the sand, as the aeration rate was increased, a parabolic, concave void formed between the two aeration points. The void was in the form of a narrow lens between the two aeration points. The length which the void occupied increased with increasing air flow to the two aeration points. Periodically, the void collapsed and then reformed. This was not observed to have a significant effect on the solids circulation rate. As the solids flux was increased, the shape of the void became similar to that of a gas bubble in a bubbling fluidized bed. At circulation rates less than 20 kg/m^2s, solids movement through the valve was continuous, with only small fluctuations in feedrate being observable. As the circulation rate was increased past these rates, the flow of solids was found to fluctuate. This may have been due to the onset of choking in the fast bed column at the higher solids circulation rates which would have resulted in pressure fluctuations which could have caused variations in solids feeding.

3.3 Impact Flowmeter Results and Discussion

In this section the observations and results of the impact flowmeter are presented and discussed. The first subsection deals with observations of the behaviour of the impact flowmeter during operation. The remaining subsections are dedicated to presentation and analysis of the quantitative results obtained using the impact flowmeter.

3.3.1 General Observations

Figure 3.1 shows typical responses of the impact flowmeter to different circulation rates.

Initially, at low solids fluxes, the pan was observed to fluctuate at a very low frequency, with the displacements from the zero position occurring as single peaks with periods up to the order of seconds between them, Figures 3.1a. This type of response was observed for both alumina and sand for every pan. As the solids circulation rate was increased, the pan was found to oscillate with a higher frequency and with greater magnitude. Signal traces and pan observations showed the pan to be spending more time away from the zero position, but, it was still returning to its original position between peaks. The oscillations of the pan did not appear to be of a regular frequency. Deflections were found to occur as single pulses, with varying time intervals between pulses, and/or as a series of pulses in rapid succession, with overlap of successive deflections. Qualitatively, it appeared that the pan's response became less sensitive with increasing pan angle. However, comparison of the

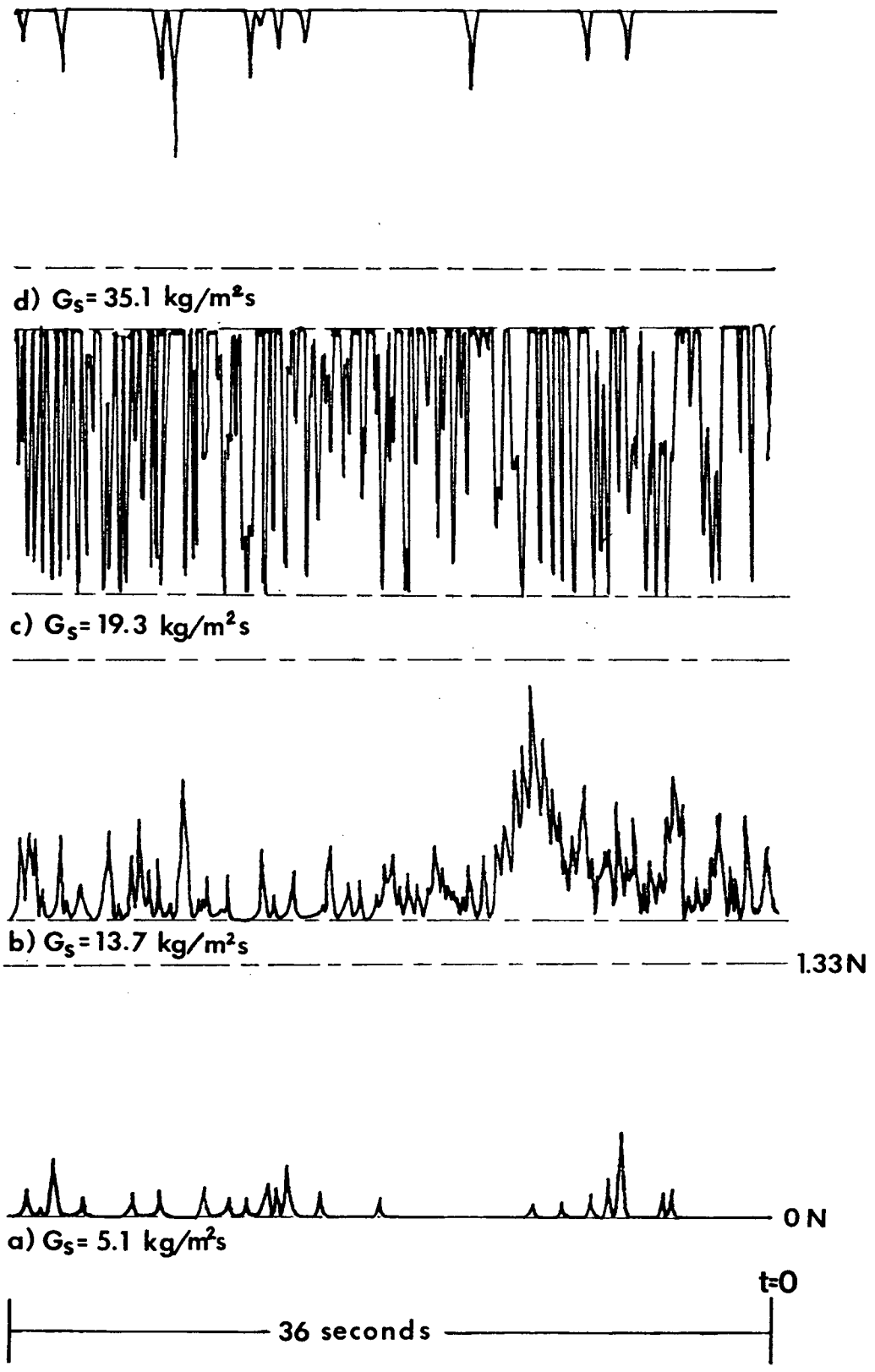

Figure 3.1 Effect of solids flux, based on the fast bed cross-sectional area, on oscillation of the 30° pan with sand, U_s = 0.024 m/s, U_f = 5.0 m/s.

traces for different pan angles did not allow this observation to be supported because the signals fluctuated rapidly with large amplitudes. With increasing solids circulation rate, Figures 3.1c and 3.1d, the load beam signal was seen to peak (i.e. reach a limiting value). This peaking was the result of the lever deflecting the load beam to such an extent that it contacted a mechanical stop which prevented overloading of the beam. The fraction of time during which the signal was peaked increased as the solids circulation rate increased. The circulation rate at which peaking occurred was found to increase with increasing pan angle and it was higher for alumina than for sand. At the higher circulation rates, the traces of the load beam amplifier signal showed the pan to be spending more time displaced from its original position. At the highest circulation rates studied, the pan was found to be peaked for the majority of the time.

The typical response of the impact flowmeter to circulating solids is shown in Figure 3.2. This figure shows the response of the pan over a 1 second period with the photographs being taken at 1 second intervals. The results show that the pan oscillates in the vertical plane when solids are flowing over it in the downward direction. This type of response was observed for all of the pan angles with both the alumina and sand being circulated. However, the frequency and amplitude of the fluctuations were found to change with the solid being circulated, the pan angle and solids circulation rate.

Originally, it was hoped that circulation solids would cause each pan to be deflected from its resting position and the trace of the load beam signal would show a fluctuating signal with an average value offset from the no-load signal value. As the solids circulation rate was increased the

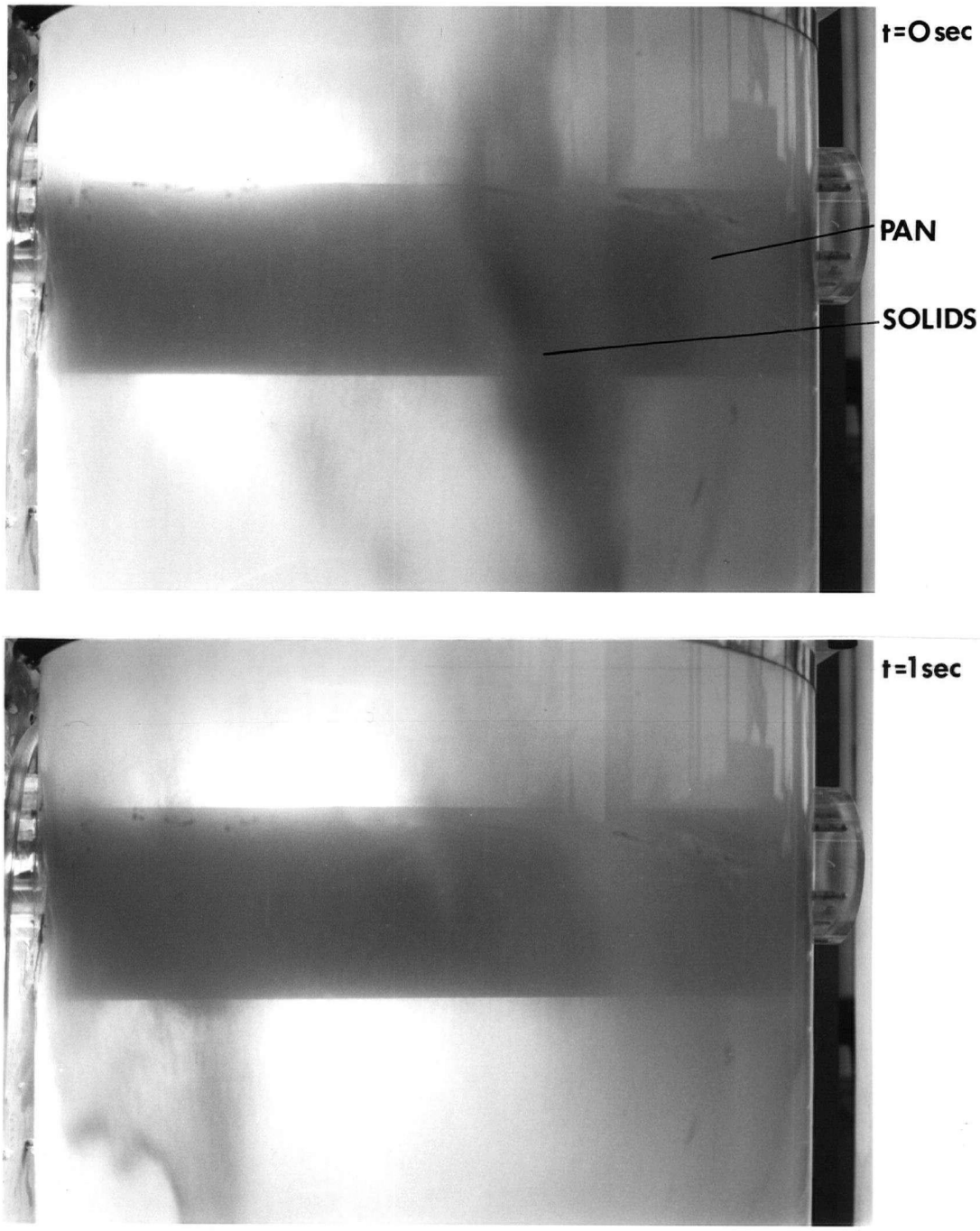

Figure 3.2 Photographs of the oscillating impact flowmeter 60° pan with sand, U_s = 0.024 m/s, U_f = 6.0 m/s, G_s = 25 kg/m^{2}s, based on the fast bed cross-sectional area.

difference between the average signal value and the no-load signal value was expected to increase monitonically. However, as shown by Figures 3.1a through 3.1d, the pan's responses with time were found to be composed of a series of peaks which increased in amplitude and frequency as the solids circulation rate increased. The traces are in agreement with the observations of the impact flowmeter which also showed the equipment to undergo oscillations.

Three possible explanations may explain the behaviour of the impact meter: During operation, the solids flowrate through the flexible hose connecting the fast bed exhaust port to the primary cyclone inlet was found to pulsate. The pulsations became increasingly evident as the solids circulation rate was increased. Observations of the flow through the acrylic sampling tube in the flexible hose, Figure 2.1, showed solids accumulating in the section tube for a period ranging from 1 to 2 seconds and then being blown out of the pipe very rapidly. The cycle then repeated itself. The period of the cycle did not appear to be affected appreciably by the bubbling bed or fast bed gas velocities or the solids circulation rates over the range of conditions studied. As a result of the pulsating flow through the flexible hose, the solids entered the primary cyclone with periodic pulsations. Thus, the flow of separated solids from the cyclone also showed pulsations. This may have been one of the causes of the impact flowmeter signal fluctuations. However, since the frequency of the meter oscillations increased with solids circulation rate, but the pulsing of the solids was not significantly affected by changing conditions, this is unlikely to be the entire cause of the fluctuating signal of the impact meter.

Solids from the primary cyclone were observed to move as a concentrated stream along a helical path, near the return vessel's wall, as they returned to the bubbling bed of the solids inventory vessel, Figure 3.3. The particles slowly dispersed as they fell counter-currently through the upward flowing gas. The pulsations in the solids flow exiting the primary cyclone did not seem to be affected by the screen. The solids were directed away from the column's wall by the baffle which concentrated the solids in the centre of the column, Figure 2.13 (see section 2.2.2). As a result of the baffle's action, the majority of the solids were found to strike the pan near its centre on one side. The trajectory of the solids was found to change slightly with time, solids circulation rate and fast bed gas velocity. However, the solids were always observed to preferentially strike the side of the pan closest to the front of the column, but in differing amounts as the trajectory of the solids flow changed, Figure 3.4. This could have contributed to the fluctuations which were observed for the impact flowmeter.

A third factor, likely to be significant, is that particles were observed to accumulate on and discharge from the pan at low solids circulation rates. At higher circulation rates it was not possible to observe the pan because of the dense flow of solids. However, at the end of a run with a high solids circulation rate, some solids were found to be resting on the pan. The rate and amount of solids accumulation and the frequency of solids discharged appeared to be affected by the pan angle and the solids circulation rate. For increasing pan angles the amount of solids accumulating on the pan was found to decrease. This was to be

Figure 3.3 Photograph of solids flow pattern exiting the primary cyclone, U_s = 0.024 m/s, U_f = 60 m/s, G_s = 25 kg/m^{2}s, based on the fast bed cross-sectional area.

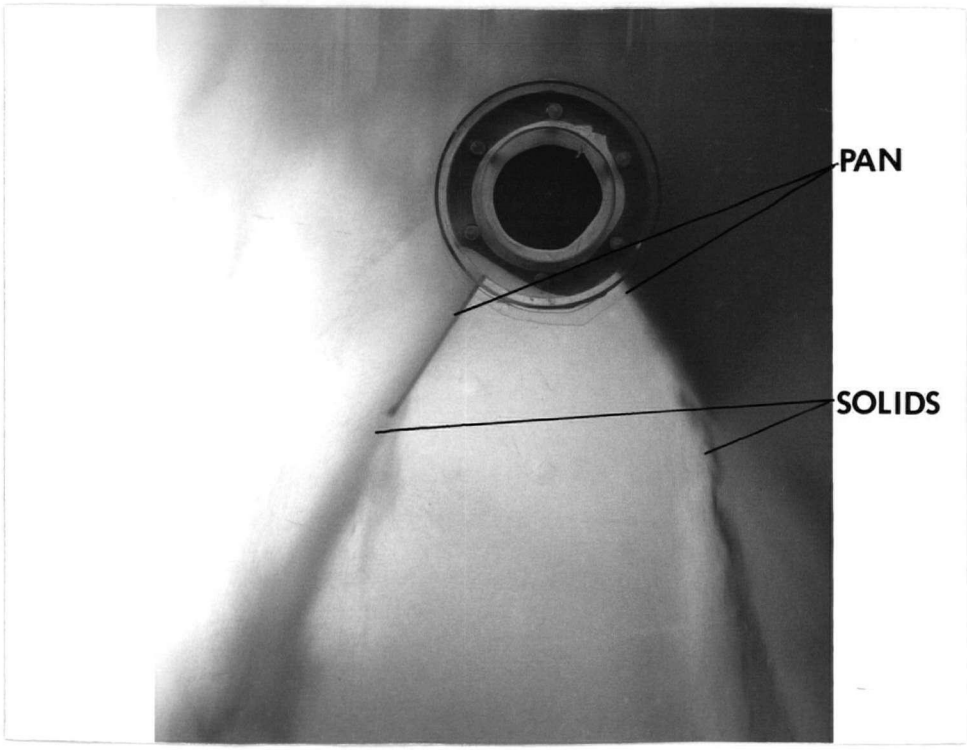

Figure 3.4 End view photograph showing sand striking the 60° pan U_s = 0.024 m/s, U_f = 6.0 m/s, G_s = 25 kg/m^{2}s, based on the fast bed cross-sectional area.

expected, since the slopes of the pan surfaces were becoming large with respect to the angle of repose of the two particulate materials studied. With increasing solids circulation rate, the solids accumulation on the pan and discharge frequency were also found to increase. The method of discharge of solids from the pan did not appear to follow a fixed pattern. Solids were observed to slide off from all areas of the pan at different frequencies and in varying amounts. Although the effect of discharging and loading of solids on the pan could not be observed separately from the other variables affecting the impact meter, it is evident that this type of response would result in a fluctuating signal. It is also important to note the possible influence of static charge. As discussed in section 3.2.1, the presence of a static charge seems to make the solids more cohesive and resistant to being dislodged by shear. If this is the case, it is plausible that variations in the static charge of the particles, as a result of changing humidity and/or static discharge, could affect accumulation of solids on the pan, and may result in significant changes in the amount of solids accumulating on the pan at different points in an experimental run.

Although the exact cause of the impact meter signal fluctuations remains uncertain, the suggested explanations may well be the entire cause or part of the cause of the observed fluctuations. In all likelihood, the fluctuations were caused by a combination of the above three suggested explanations. Variations in solids flux caused by the L-valve (see Section 3.2.2) and by turbulent fluctuations in the fast bed gas velocity may also have played a significant role.

3.3.2 Impact Flowmeter Results

The results of the impact flowmeter to changing solids circulation rates for the three pan angles and two solids are shown in Figure 3.5 through 3.10. The time-averaged effective impact flowmeter forces and solids circulation rates were converted from their equivalent voltage signals according to the procedures shown in Appendix E. The effective force represents the average force imparted to the pan by impacting particles at any instant. To determine the effective force, it is necessary to assume a value of X_{eff}, which is the distance from the point at which the effective force acts on the pan to the lever pivot. In this study, X_{eff} was assumed to be 230 mm, the distance from the centre of the pan to the lever pivot. The relationships between the force measured by the load beam, the force caused by impacting particles and the effective particle force are as follows:

$$F(t)_{eff} = \frac{F(t)_L \cdot X_L}{X_{eff}} = \sum_{i=1}^{n} \frac{F(t)_{P_i} X_{P_i}}{X_{eff}} \qquad (3.3.1)$$

The time-averaged effective force is given by:

$$\bar{F}_{eff} = \int_t^{t+\Delta t} \frac{F_{eff}(t)dt}{\Delta t} \qquad (3.3.2)$$

Solids circulation rates are expressed as solids fluxes based on the fast bed cross-sectional area and were measured by accumulation on the butterfly valve. For the reasons explained in section 3.6, only the first butterfly valve circulation rate measurements were used to calculate the solids fluxes.

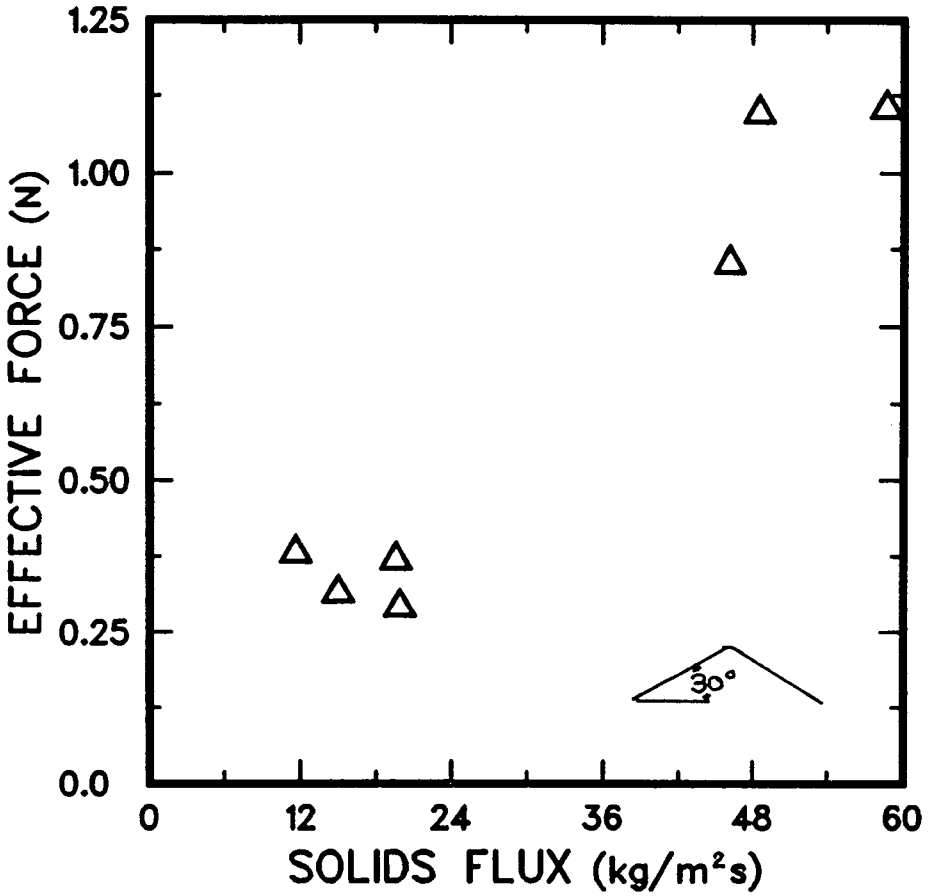

Figure 3.5 Influence of solids flux, measured by accumulation on the butterfly valve and based on the fast bed cross-sectional area, on effective force for the 30° pan with alumina, U_s = 0.014 m/s, U_f = 3.0 to 5.3 m/s.

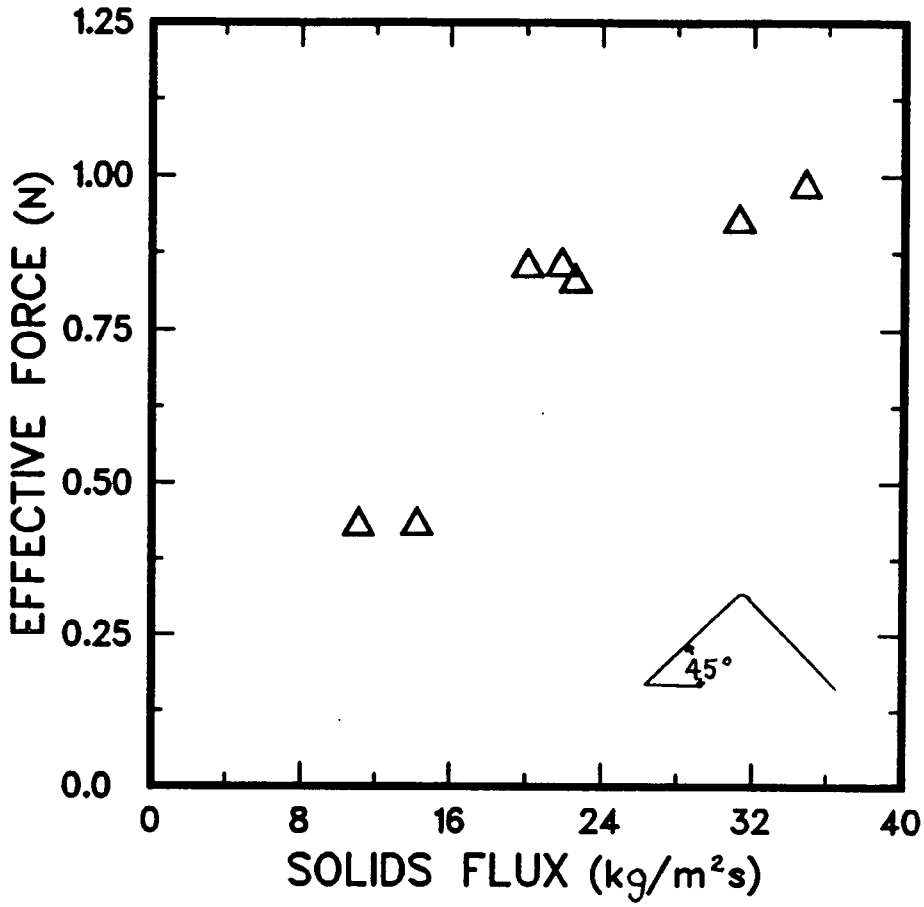

Figure 3.6 Influence of solids flux, based on the fast bed cross-sectional area, on effective force for the 45° pan with alumina,
U_s = 0.014 m/s, U_f = 3.2 to 3.8 m/s.

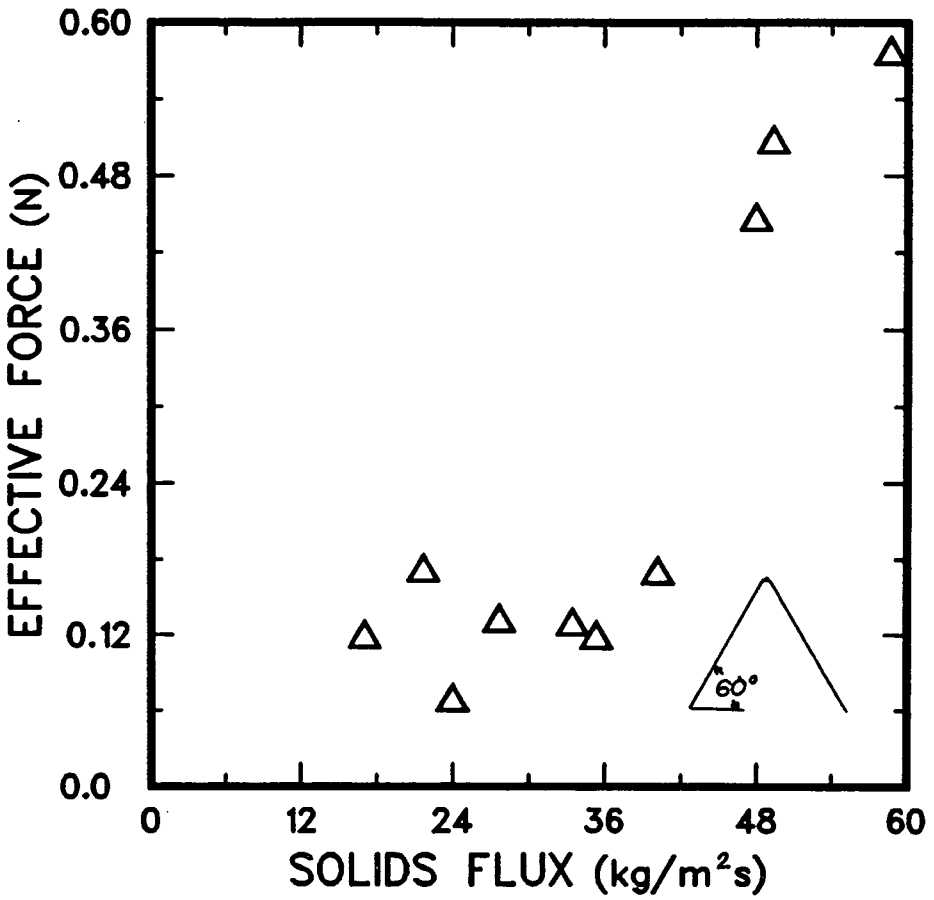

Figure 3.7 Influence of solids flux, based on the fast bed cross-sectional area, on effective force for the 60° pan with alumina,
U_s = 0.014 m/s, U_f = 3.0 to 4.4 m/s.

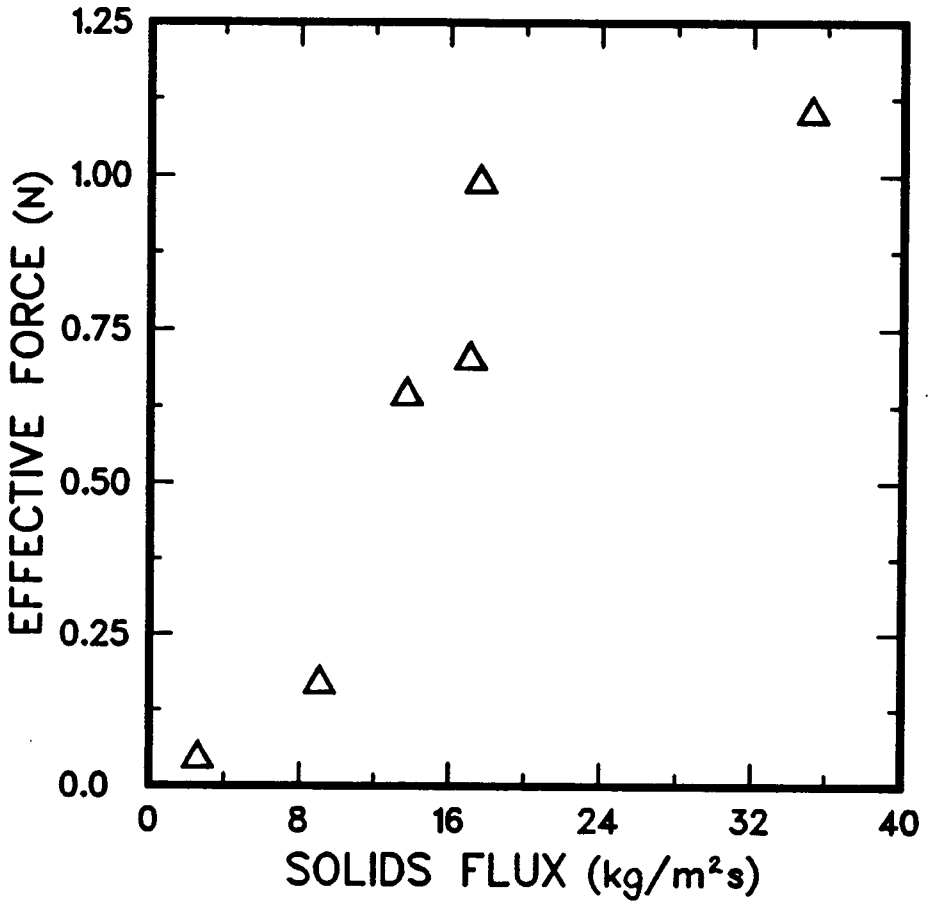

Figure 3.8 Influence of solids flux, based on the fast bed cross-sectional area, on effective force for the 30° pan with sand, U_s = 0.024 m/s, U_f = 3.5 to 5.0 m/s.

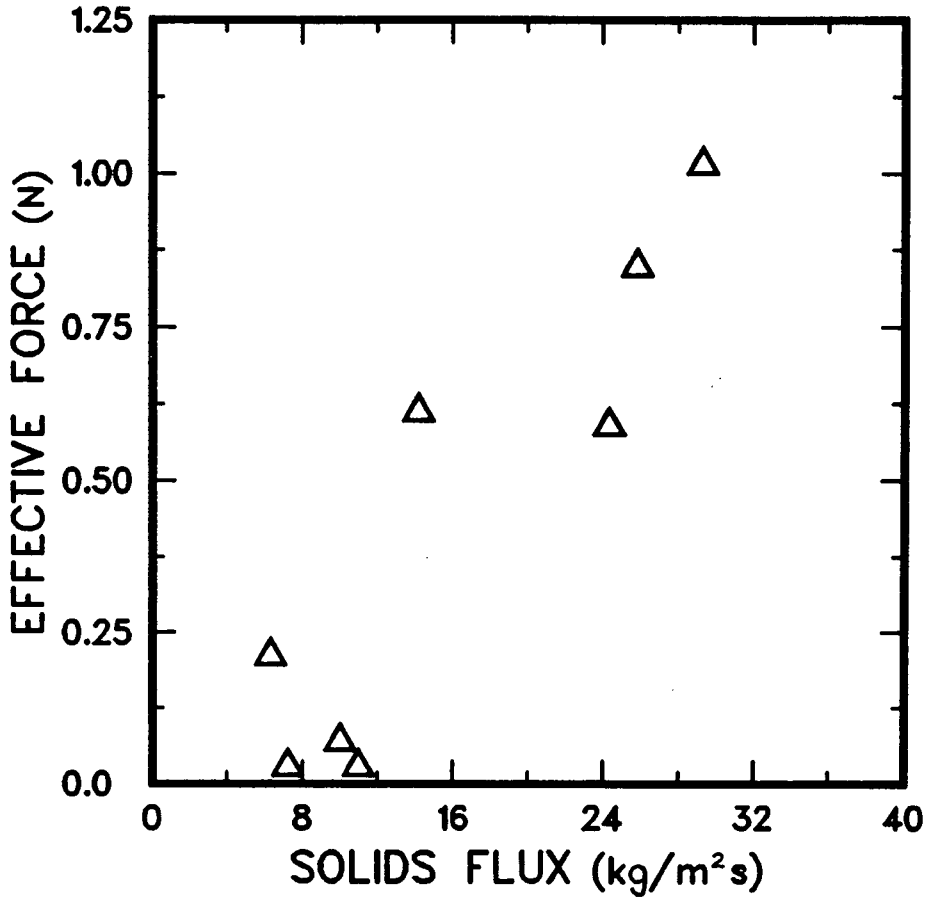

Figure 3.9 Influence of solids flux, based on the fast bed cross-sectional area, on effective force for the 45° pan with sand U_s = 0.024 m/s, U_f = 3.0 to 6.6 m/s.

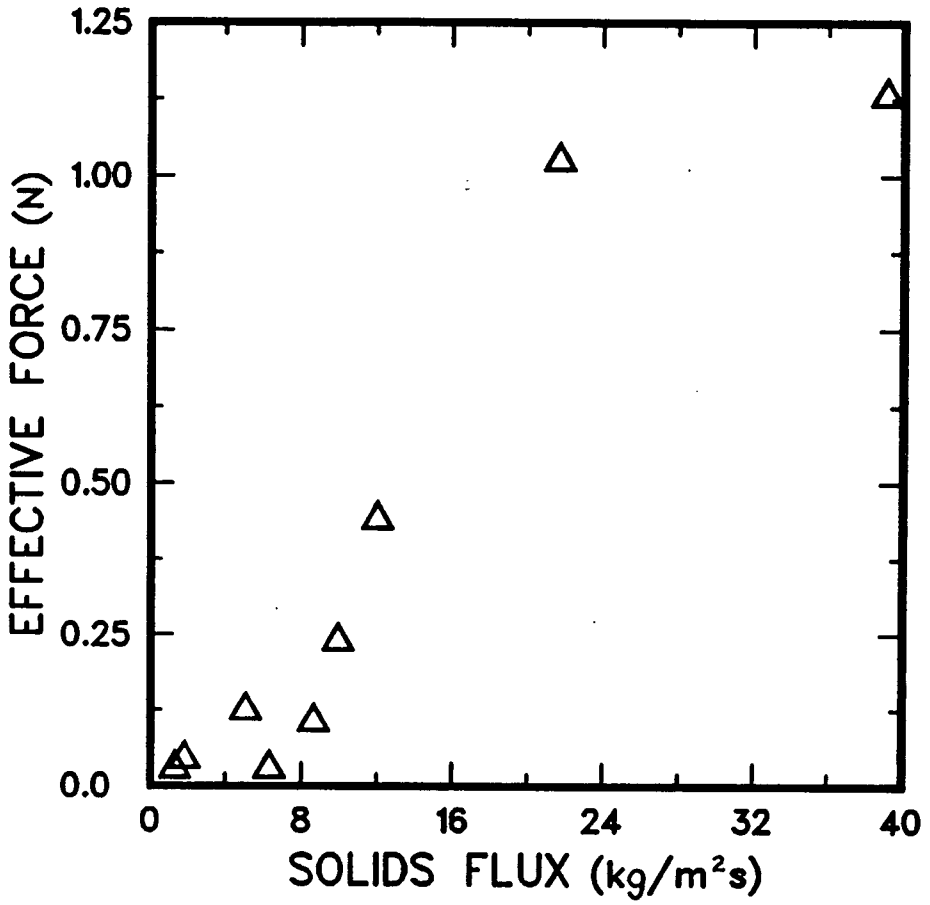

Figure 3.10 Influence of solids flux, based on the fast bed cross-sectional area, on effective force for the 60° pan with sand U_s = 0.024 m/s, U_f = 4.7 to 5.5 m/s.

The time-averaged load beam signals were found, in some cases, to vary significantly (see the raw data in Appendix F). The greatest fluctuations were found to occur at intermediate circulation rates, 10 to 50 kg/m^2s for the alumina and 10 to 30 kg/m^2s for the Ottawa sand. At these rates, the load beam signal was found to be very oscillatory, with the amplitude of the fluctuations being as great as 1.33N (converted from the signal traces by the procedure in Appendix E). The probable causes of the observed differences were that the datalogging period was too short and/or the solids circulation varied during the experimental run. It was not possible to use a longer sampling period due to computer limitations. The possible variation in solids flux, discussed in section 3.2.2, was not a controllable problem.

The results for the 30° and 60° pans for both the alumina and the sand, Figures 3.5, 3.7, 3.8 and 3.10, can be divided into three zones: At low circulation rates there is an initial zone where the effective force does not change significantly with changing solids flux. At intermediate fluxes, there is a sensitive region where the effective force increases rapidly with increasing solids flux. At higher circulation rates, the effective force is seen to be levelling off and reaching a maximum value. This type of response was not apparent in the results of the 45° pan for both the alumina and the Ottawa sand.

In the first zone, the effective force does not seem to respond to increases in the solids circulation rate. The extent of this zone is affected by the type of solids being circulated and the pan angle. For alumina, this zone persisted for circulation rates up to 35 kg/m^2s for the 30° and 60° pans. With sand, the response was observed for circulation

rates up to 8 kg/m^2s for both the 30° and 60° pans. This zone was most likely the result of frictional forces, which opposed the pan movement, being large with respect to the force of the particles impacting on the pan at low solids circulation rates. Both the lever bearing and load beam were observed to exhibit resistance to movement. However, it was not possible to measure the magnitude and extent of these resistances. The bearing, even when adjusted properly, was observed to stick. The resistance of the load beam was caused by the sensing end of the beam rubbing against the allen screws used to align it.

In the second region, the effective force was found to be sensitive to changes in the circulation rate. As expected, the results for the 30° and 60° pans, with both alumina and sand as the circulating solids, increased with increased solids flux. According to the simple model presented in Appendix H the slope of the response curve should increase as the pan angle decreases as a result of the greater change in the downward velocity of the particles caused by decreased pan angles. However, comparison of Figures 3.5 and 3.7 and Figures 3.8 and 3.10 shows that the slopes of the force versus solids circulation rate curves are essentially the same for the 30° and 60° pans. This applies for both alumina and sand. The reasons for this are not obvious, but it is possible that the effect of pan angle could not be distinguished because of inaccuracies in the measurements of the effective forces and the solids circulation rates.

The final zone corresponds to the equipment becoming overloaded. Two types of overloading occurred at higher circulation rates: Mechanical overloading of the load beam. Signal clipping of the load beam signal by the Tecmar board. It is the Tecmar board overloading wich has lead to the

third zone, apparent in the results. The Tecmar board was restricted to sampling voltages of 10 volts or less. When the equipment was mechanically overloaded the load beam voltage was approximately 12 volts. When the voltage exceeded the maximum voltage of the Tecmar board it was recorded as 10 volts. This maximum voltage corresponds to an effective force of 1.11 N when converted according to the procedure in Appendix E. Since, at the higher solids circulation rates the output voltage of the load beam amplifier exceeded the 10 volt maximum of the Tecmar Board for a greater fraction of the time, the time-averaged voltage levelled off and the effective force approached 1.11 N which was equivalent to a 10 volt load beam amplifier signal.

3.3.3 Standard Deviations

The standard deviations of the effective forces for the three pan angles and two solids versus the solids circulation rates, based on the fast bed cross-sectional area and measured by the butterfly valve, are shown in Figures 3.11 through 3.16. The standard deviations are plotted versus the effective force, as measured by the impact flowmeter, in Figures 3.17 through 3.22. The solid lines drawn on each figure represent the third order polynomials which best fit the data using least squares.

Figures 3.11 through 3.16 all show similar characteristics. At low circulation rates, the standard deviations of the effective forces are small. At these circulation rates, the meter's signal response, Figure 3.1, shows the pan fluctuations to be small and infrequent. Since the fluctuations of the pan are minor, variations in effective forces are also small. Therefore, standard deviations of the effective forces are small. As circulation rates were increased the pan of the impact meter was observed to fluctuate at a higher frequency with a greater amplitude for all three pans and both types of solids. The increase in fluctuations depended on the pan angle and solids type. The response was more sensitive for decreasing pan angles and with sand as the circulating material. The greater sensitivity and, thus, greater increase in fluctuations with increasing solids circulation rate are apparent when the Figures 3.11 through 3.13 or Figures 3.14 through 3.16 are compared. Comparison of these figures shows that the standard deviation of the effctive forces increases more rapidly as the angle of the pan decreases for both alumina and sand. This agrees with the observations of the pan which showed that decreasing the pan angle resulted in increased frequency and amplitude of

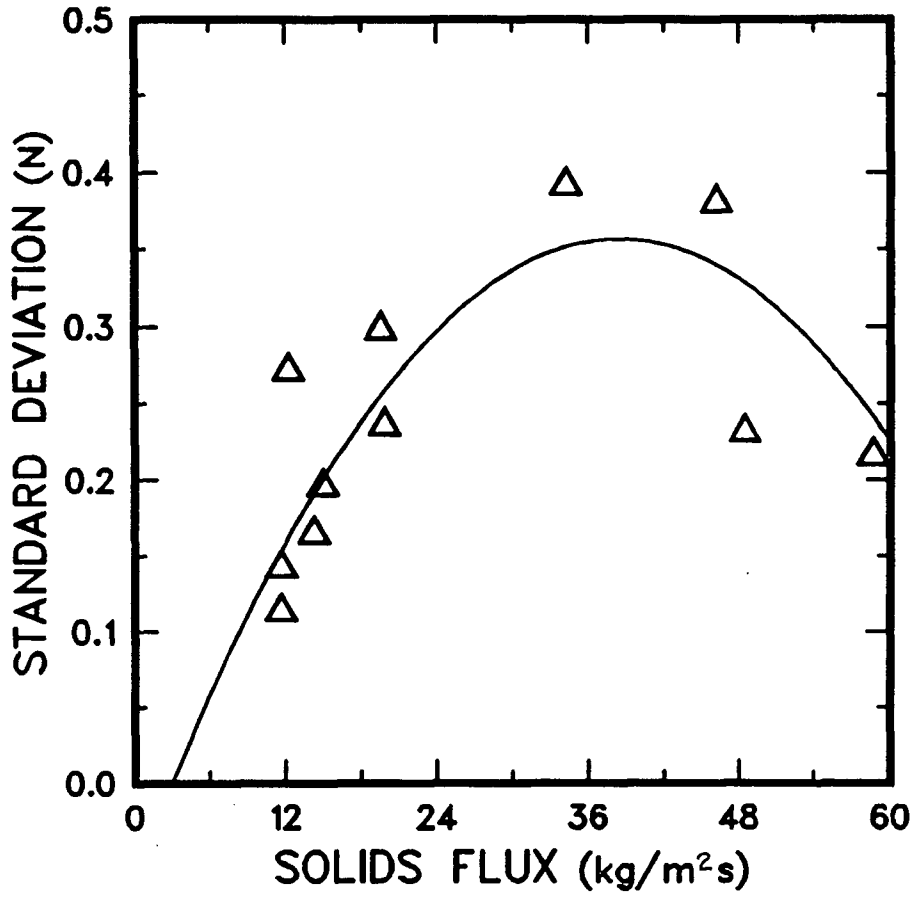

Figure 3.11 Effect of solids flux, based on the fast bed cross-sectional area, on standard deviation of the effective force signal for the 30° pan with alumina, U_s = 0.014 m/s, U_f = 3.0 to 5.3 m/s.

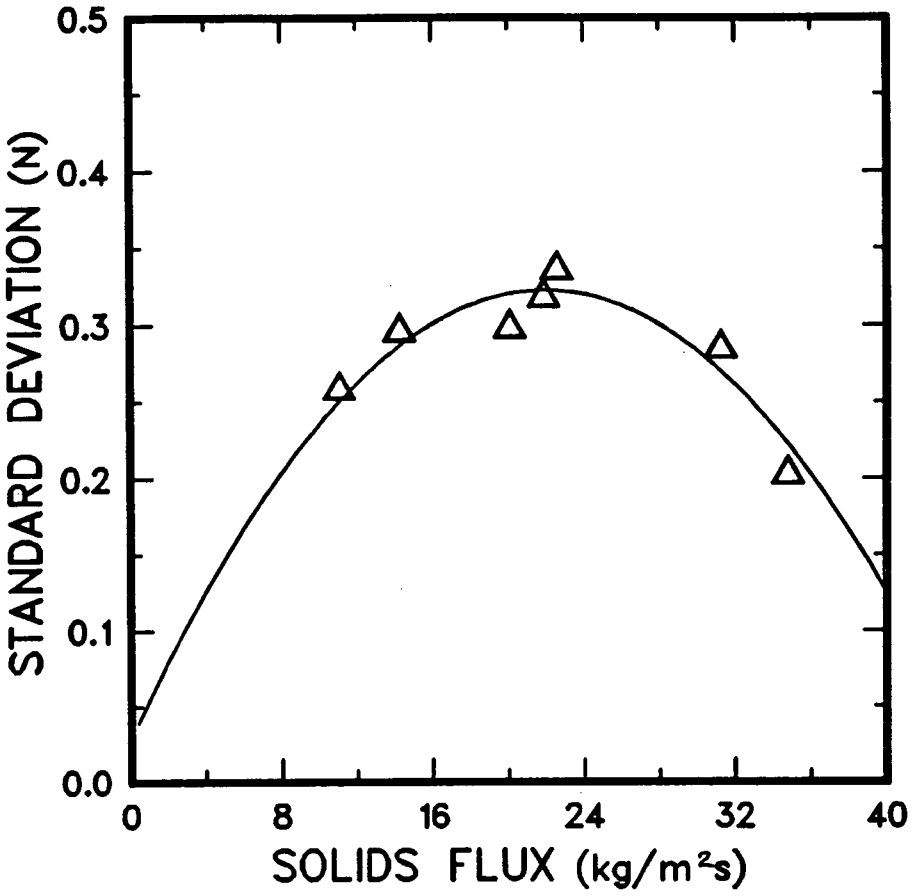

Figure 3.12 Effect of solids flux, based on the fast bed cross-sectional area, on standard deviation of the effective force signal for the 45° pan with alumina, U_s = 0.014 m/s, U_f = 3.2 to 3.8 m/s.

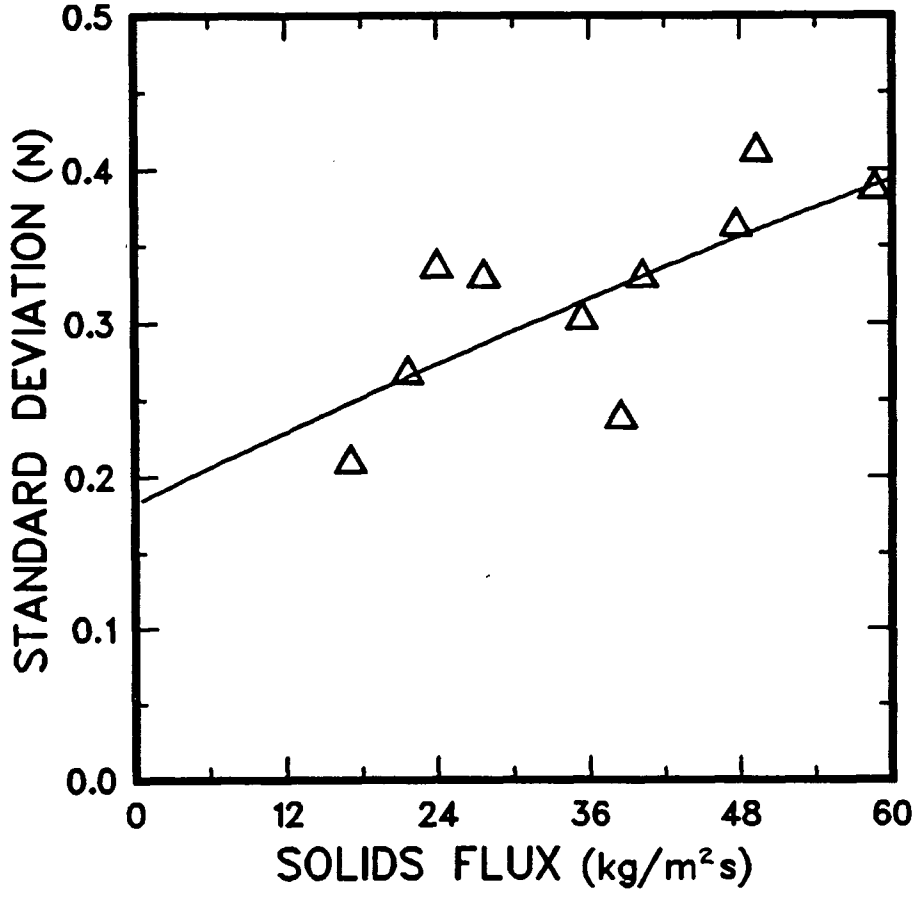

Figure 3.13 Effect of solids flux, based on the fast bed cross-sectional area, on standard deviation of the effective force signal for the 60° pan with alumina, U_s = 0.014 m/s, U_f = 3.0 to 4.4 m/s.

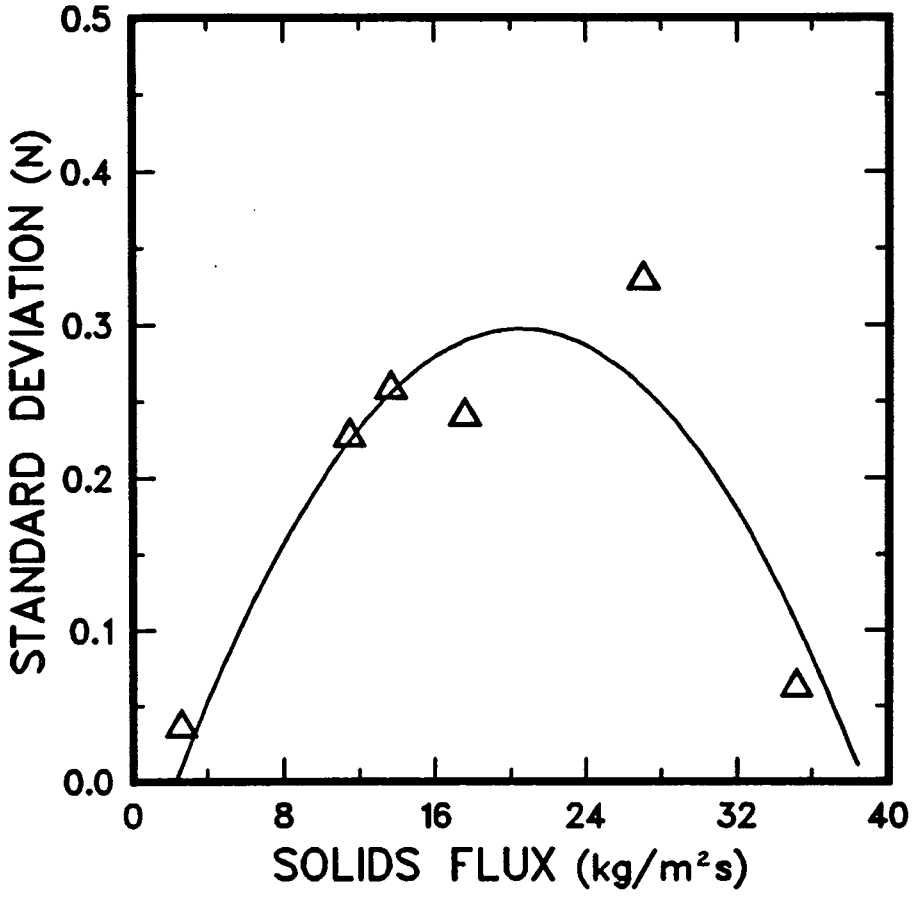

Figure 3.14 Effect of solids flux, based on the fast bed cross-sectional area, on standard deviation of the effective force signal for the 30° pan with sand, U_s = 0.024 m/s, U_f = 3.5 to 5.0 m/s.

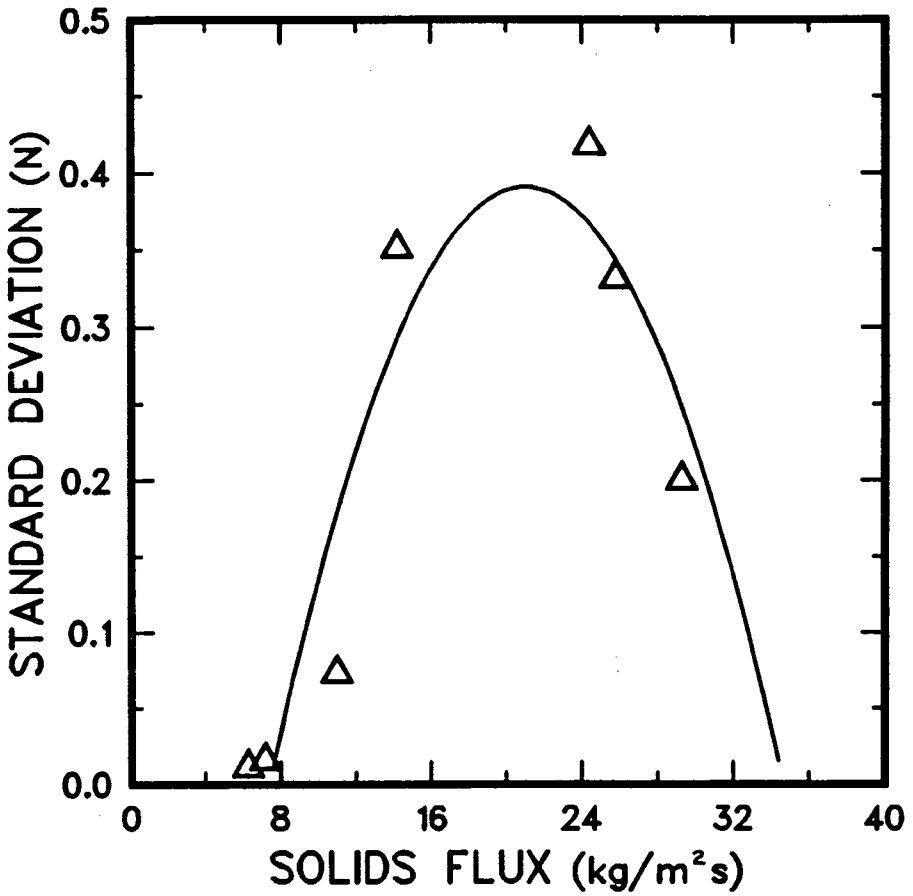

Figure 3.15 Effect of solids flux, based on the fast bed cross-sectional area, on standard deviation of the effective force signal for the 45° pan with sand, U_s = 0.024 m/s, U_f = 3.0 to 6.6 m/s.

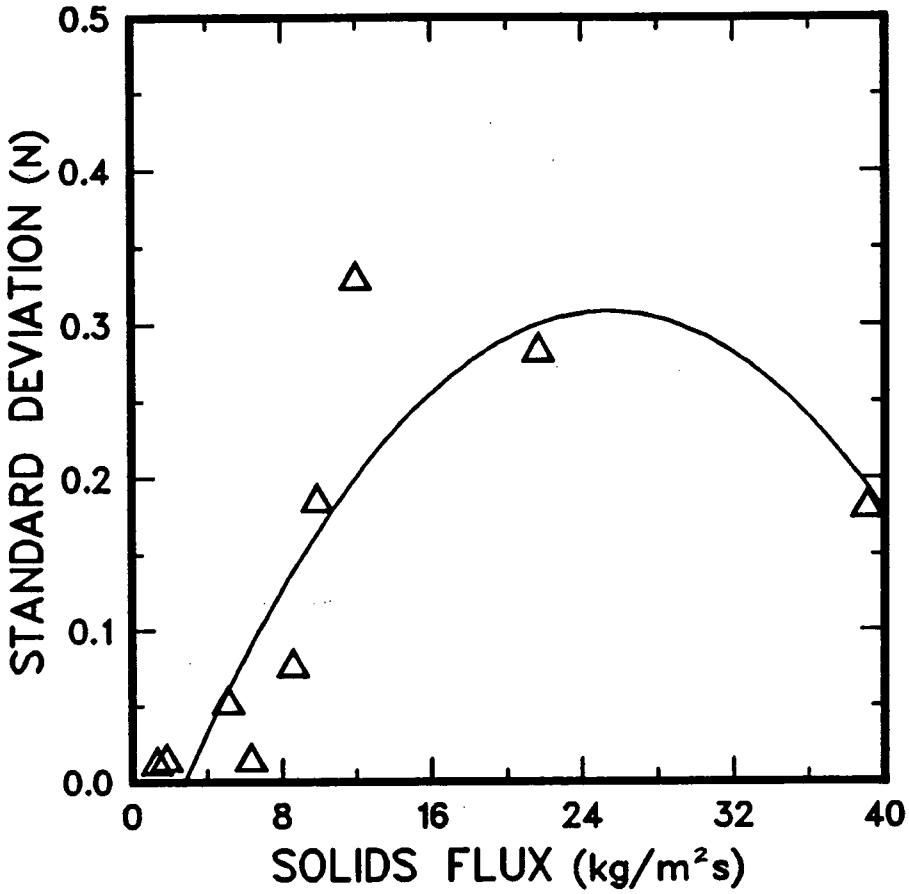

Figure 3.16 Effect of solids, based on the fast bed cross-sectional area, on standard deviation of the effective force signal for the 60° pan with sand, U_s = 0.024 m/s, U_f = 4.7 to 5.5 m/s.

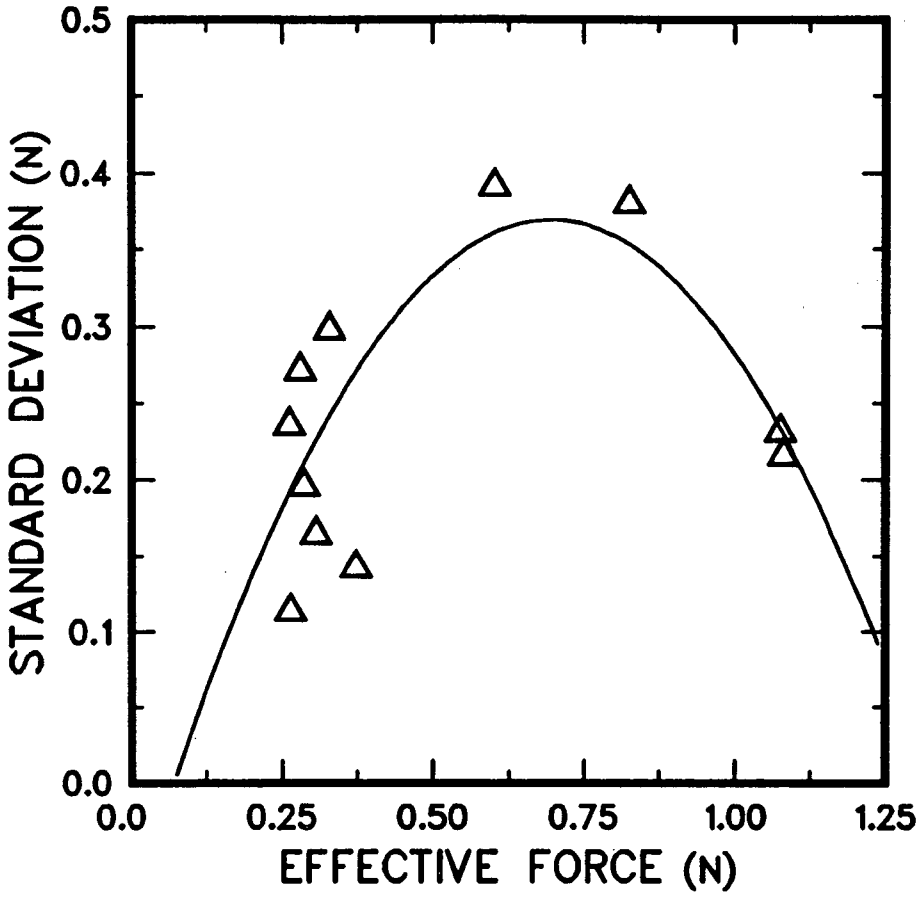

Figure 3.17 Influence of the effective force on standard deviation of the effective force signal for the 30° pan with alumina, U_s = 0.014 m/s, U_f = 3.0 to 5.3 m/s.

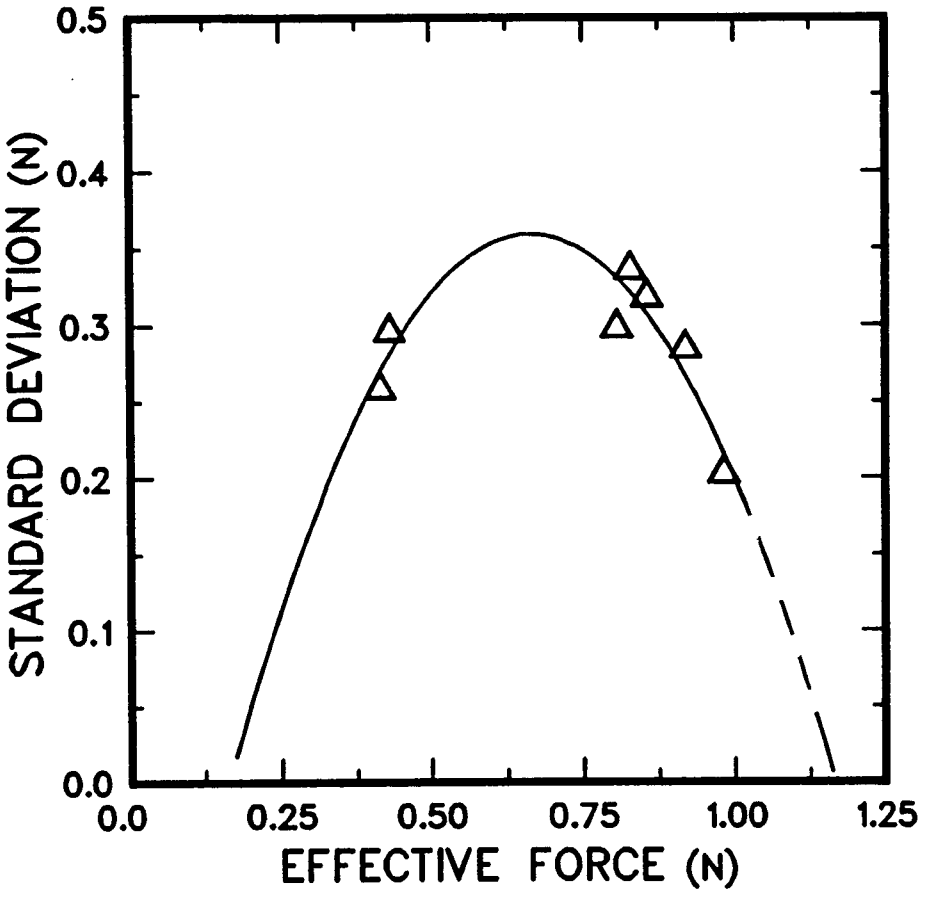

Figure 3.18 Influence of the effective force on standard deviation of the effective force signal for the 45° pan with alumina, U_s = 0.014 m/s, U_f = 3.2 to 3.8 m/s.

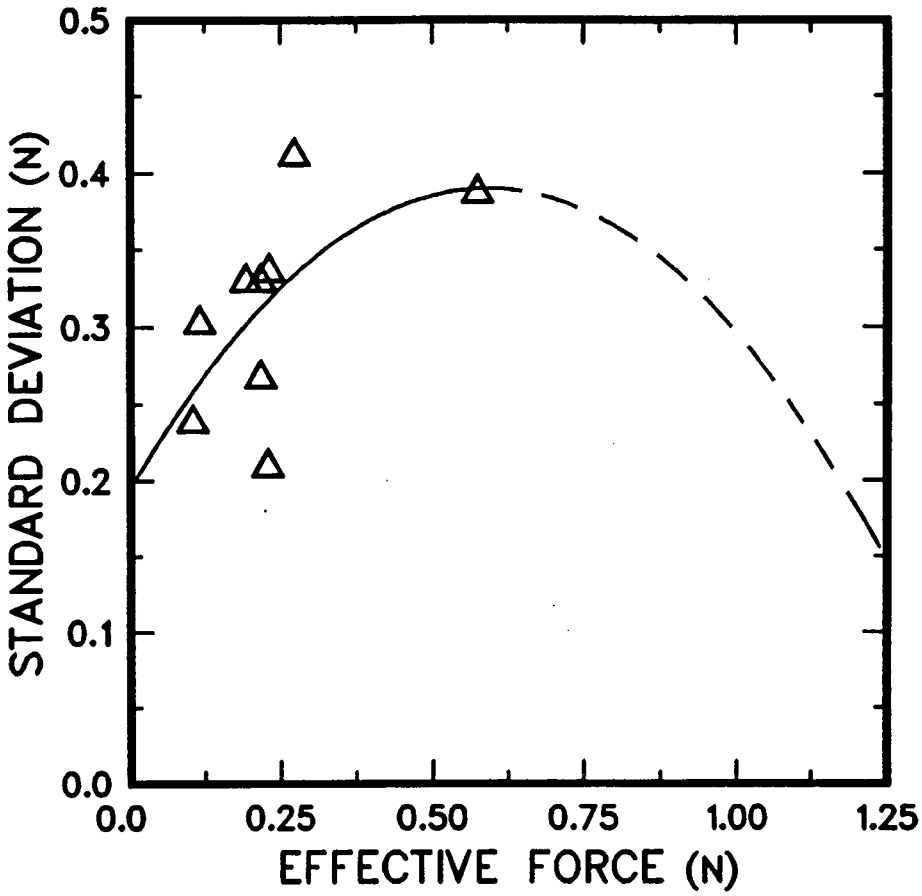

Figure 3.19 Influence of the effective force on standard deviation of the effective force signal for the 60° pan with alumina, U_s = 0.014 m/s, U_f = 3.0 to 4.4 m/s.

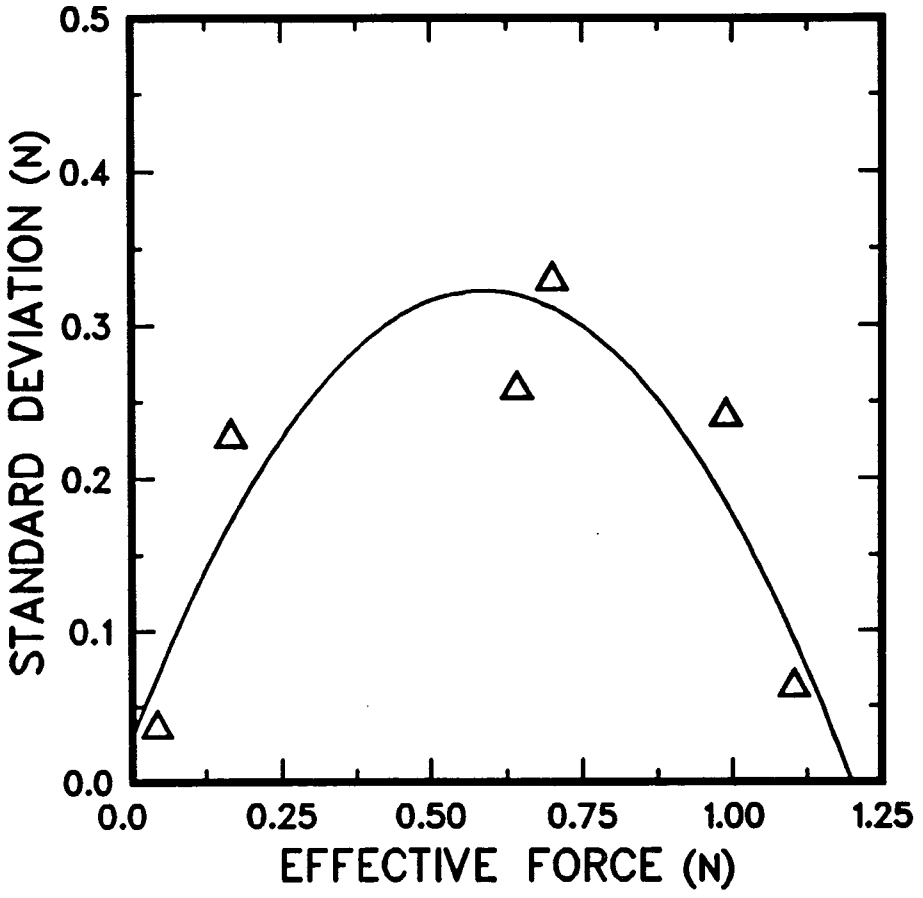

Figure 3.20 Influence of the effective force on standard deviation of the effective force signal for the 30° pan with sand U_s = 0.024 m/s, U_f = 3.5 to 5.0 m/s.

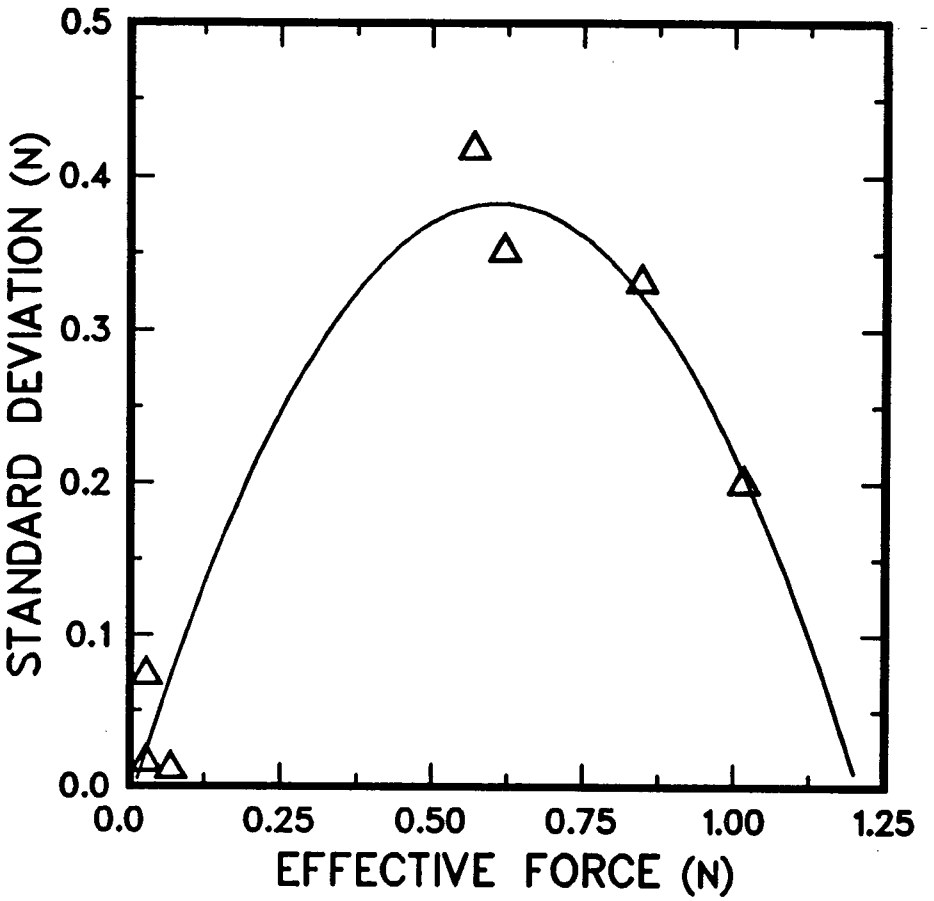

Figure 3.21 Influence of the effective force on standard deviation of the effective force signal for the 45° pan with sand, U_s = 0.024 m/s, U_f = 3.0 to 6.6 m/s.

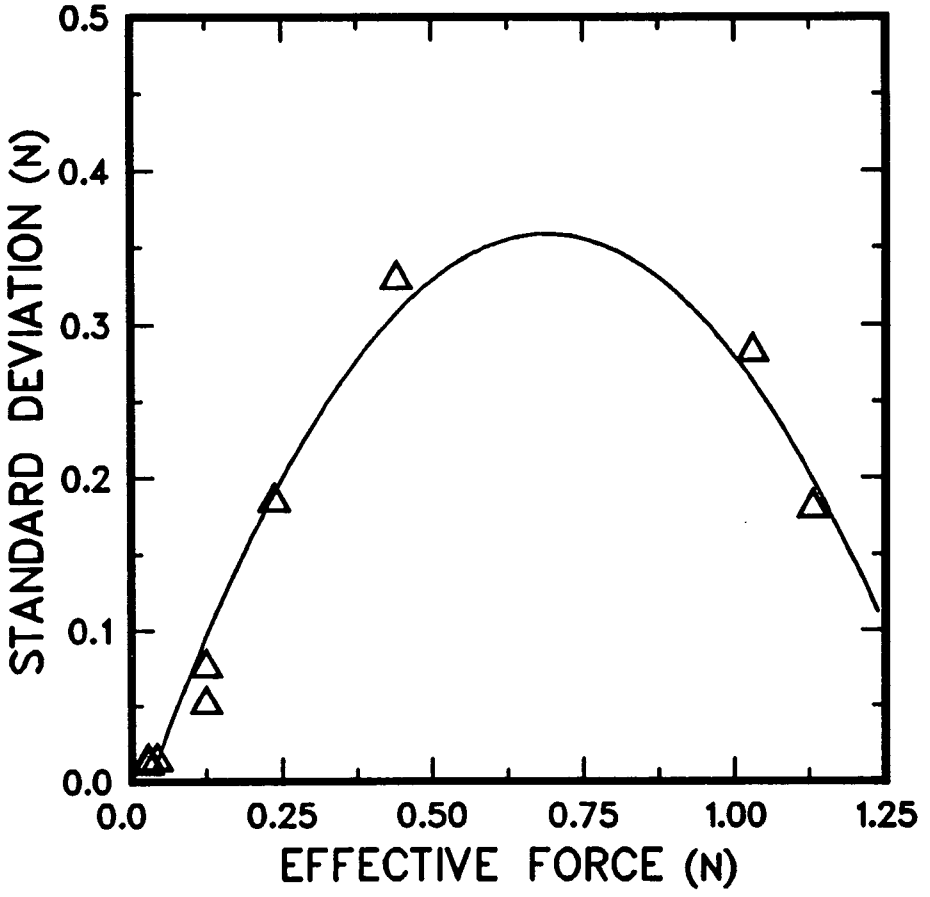

Figure 3.22 Influence of the effective particle force on standard deviation of the effective force signal for the 60° pan with sand, U_s = 0.024 m/s, U_f = 4.7 to 5.5 m/s.

fluctuations for a given solids flux. Comparison of Figures 3.11 and 3.14, and 3.12 and 3.15 and 3.13 and 3.16 show that the standard deviation of the effective force increases much more quickly for all the pan angles when sand rather than alumina is the circulating particulate material. This was expected, since all of the pans showed more vigorous fluctuations (higher frequency and greater amplitude) for the sand than for the alumina at the same solids fluxes. As the solids circulation rates were increased the standard deviations of the effective forces are seen to decrease. This reflects the pans being displaced from their zero positions for longer periods of time and the fact that the equipment was becoming overloaded. Since the signal could not exceed a maximum of 1.11 N, which corresponds to the maximum signal value which the Tecmar Board could measure, and the pan was permanently being displaced from the zero position, the range over which the pan oscillated decreased and correspondingly, the fluctuations in the effective force signals decreased. In reality then, the decrease in the standard deviation reflects the equipment becoming overloaded and not an improvement in the signal quality at higher circulation rates. The reduction in standard deviations occurred at lower circulation rates for decreasing pan angles. This is because the equipment became overloaded at lower circulation rates as the pan angle was decreased.

Figures 3.17 through 3.22 illustrate the relationship between the standard deviations of the effective forces and the values of the effective forces. From the similarity in the results it is evident that the standard deviations depend on the capacity at which the equipment is operating. When the effective forces are small, the standard deviations are small. As

the effective forces increase to approximately 50% of the capacity of the equipment, the standard deviations increase to a maximum value. For circulation rates greater than 50% of the capacity of the equipment, the apparatus begins to overload and the fluctuations of the pan reduce in amplitude. As a result, the standard deviations of the signals are seen to fall off and approach zero. When the equipment is completely overloaded, with the amplifier voltage always exceeding the 10V maximum sampling voltage of the Tecmar datalogging board, the standard deviation would be zero. The solids circulation rates at which the maximum standard deviations occur decrease with decreasing pan angle and occur at lower circulation rates when sand is the bed material.

3.3.4 Response of the Impact Flowmeter to Butteryfly Valve Closure and Stoppage of Solids Circulation

Changes in the operation of the CFB unit as a result of the closure of the butterfly valve could not be detected by the impact flowmeter. This insensitivity was noted for all three pan angles and both solids. The lack of sensitivity of the impact flowmeter arises from the nature of the load beam signal, the long sampling times required to obtain a representative signal when using this method and the inaccuracies associated with this measurement technique. The fluctuating load beam signal did not enable the effect of the butterfly valve closure to be easily observed. To obtain a representaive average voltage, sampling periods of 1 minutes were used to calculate the averages. As a result, the equipment could not measure rapidly changing average signal strengths. Additionally, the inaccuracies of this measurement technique made it impossible to determine whether a

change in the effective force represented a response to the butterfly valve closure or was the result of noise in the experimental measurement.

The impact flowmeter was not able to measure the transient response of the flowrate of solids out of the fast bed resulting from a change in solids feedrate to the upflow column. The meters insensitivity resulted from the problems outlined in the previous paragraph. Observation of the load beam signal trace showed the oscillations to decrease in magnitude and frequency over a period of time when the solids circulation rate was stopped. The period of decay was found to increase with increased solids hold-up in the fast bed and with decreased fast bed gas velocity. The usefulness of these observations is limited since the decay rates could not be quantified and the decay time could not be accurately determined.

3.4 Modified Orifice Results and Discussion

The modified orifice, as studied (see section 2.3), was not able to provide a signal from which the solids circulation rate could easily be determined. Initial studies with the 45° modified orifice, using an orifice to tube diameter ratio of 0.5, with the solids being fed by the funnel apparatus, showed the change in the pressure differential resulting from the flow of solids to be very small, and approximately equal in magnitude to the zero drift of the pressure transducer, Figure 3.23a. As a result, it was not possible to determine pressure differentials. In the case of solids being fed by the secondary cyclone to the modified orifice apparatus, for the same orifice and orifice diameter as before, the pressure differential was found to vary wildly, with pressure fluctuations up to 25 mm H_2O, Figure 3.23b. Due to the large magnitude of the

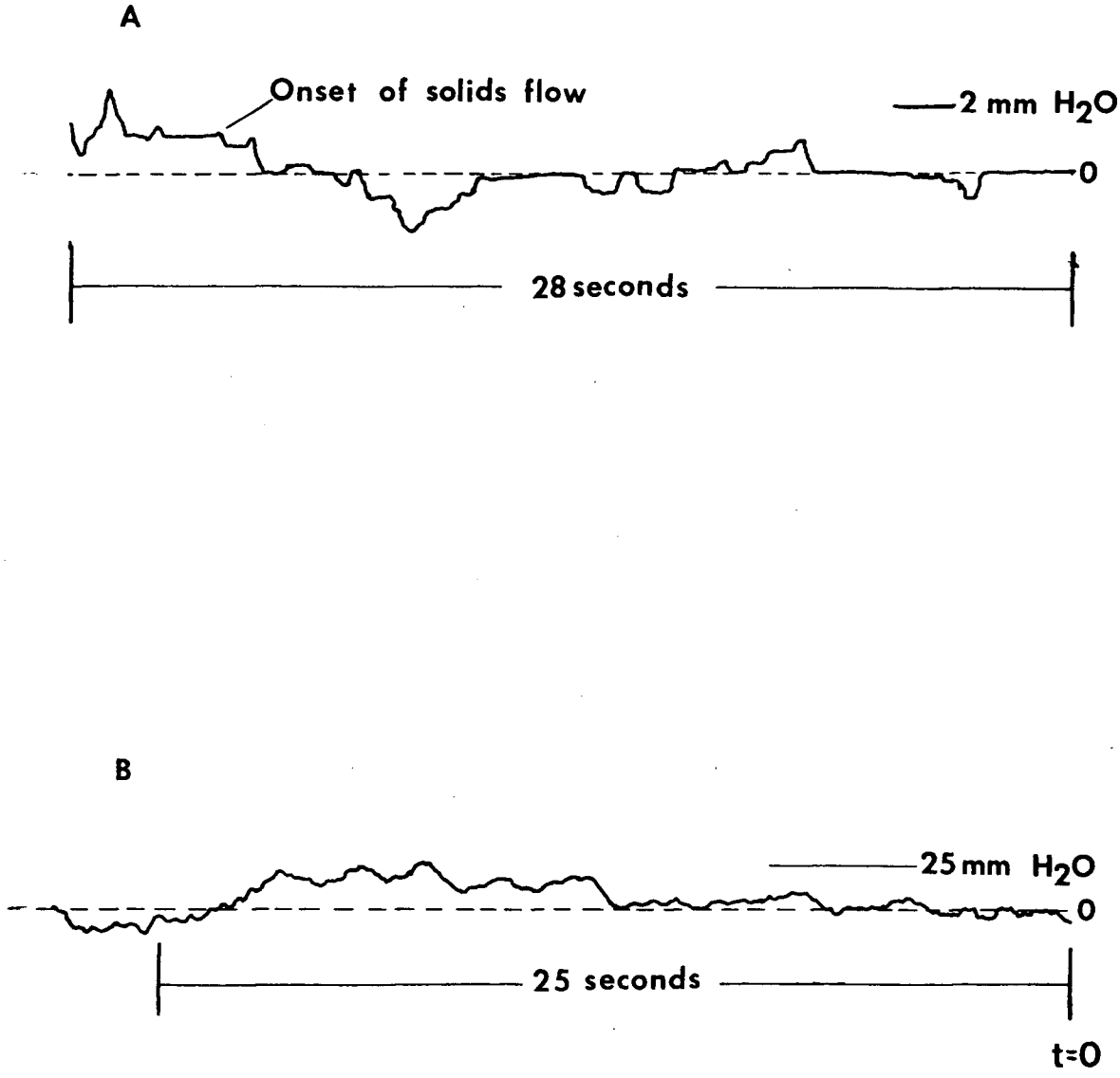

Figure 3.23 Effect of solids flux on modified orifice pressure differential. A) Alumina fed by funnel, G_s = 25 kg/m^{2}s based on the orifice tube cross-sectional area, U_o = 0.014 m/s.
B) Sand fed by secondary cyclone, G_s = 22 kg/m^{2}s based on the orifice tube cross-sectional area, U_o = 0.024 m/s.

fluctuations, it was not possible to detect an apparent change in the pressure differential as a result of a change in solids flux. The source of the oscillations was not studied in detail, but they may have been caused by variations in the solids and/or gas flowrates through the apparatus. The possible sources of solids flowrate variations are discussed in Section 3.2. The variations in gas flowrate may have resulted from bubbles from the bubbling bed and secondary solids return line aeration tap travelling up the solids return line to the orifice apparatus.

To understand why the modified orifice did not measure an appreciable change in the pressure differential between the orifice throat and upstream pressures with changing solids flowrates, it is necessary to review the principles which predict the behaviour of an orifice meter. Analysis of orifice meters and other constriction type flowmeters is generally based on Bernoulli's theorem which, for negligible frictional losses, requires that the total head of a flowing stream remain constant, i.e.:

$$H = \frac{P}{\rho g} + \frac{V^2}{2g} + y = \text{constant} \qquad (3.4.1)$$

This relationship provides a basis for determining the pressure response of a fluid undergoing a change in velocity. For the simplest case, where the fluid is incompressible, the flow is non-turbulent, frictional head losses are small and elevation changes are negligible, the relationship between velocity and pressure may be expressed as:

$$(P_1 - P_2) = \frac{\rho}{2} (V_2^2 - V_1^2) \qquad (3.4.2)$$

In reality, particularly when dealing with gases, the fluid is compressible and frictional head losses cannot be ignored. This situation is often modelled using a modified form of Bernoulli's theorem which incorporates a head loss term.

In the case of two phase counter-current flow of gas and solids through an orifice, the previously mentioned deviations from the non-ideal case apply. In addition, one must consider the problem of having two components undergoing different velocity changes. In the case of the gas, the gas is expected to accelerate rapidly to a higher throat velocity as it enters the orifice and to decelerate rapidly to the lower tube velocity having passed through the orifice. No doubt, the solids affect the behaviour of the gas as it passes through the orifice. The extent of this effect is not known. However, this should still result in the upstream pressure being greater than the orifice pressure. The particles, moving counter-currently downward through the upward flowing gas, at or near their terminal velocities, encounter an increasing upward gas velocity as they enter the conical section of the modified orifice. The particles must therefore slow down when viewed from a fixed point of reference. If Bernoulii's theorem applies to the particle flow, the decrease in velocity of the particles should cause a pressure differential between the orifice and upstream pressure taps, with the orifice pressure being larger than the upstream pressure. The net change in pressure would depend on the ratio of the gas to solid flowrates, the magnitude of the velocity change which each

component undergoes, as well as the effects of turbulence, frictional head losses and density changes. Clearly this net change in pressure is very difficult to calculate and would have to be determined experimentally.

In the case of counter-current gas/solids flow, the maximum gas velocity, which occurs at the point of maximum constriction, i.e. at the throat of the orifice, should probably not exceed the terminal velocity of the particles being studied. If an upward gas velocity in excess of the terminal velocity of the smallest particles is used, this could result in the entrainment of some of the particulate material. The severity of this problem would increase as the gas velocity is increased. The response to increasing gas velocity would depend on the solids flux. At high solids fluxes the solids may behave in a manner similar to solids in a CFB, where the solids are observed to flow both co- and counter-currently to the gas. This could lead to slugging of gas and solids through the orifice as the result of solids accumulating on the orifice.

The low gas velocities are probably responsible for the lack of sensitivity of the modified orifice meter in the present work. The maximum gas velocities at the throat of the orifice did not exceed 0.24 m/s. The relatively small change in gas velocities, (c.f. Carlson (1948) who worked with velocity changes up to 44 m/s and Farbar (1953) who used gas velocity changes up to 55 m/s), provides one possible explanation of why the orifice meter did not detect any noticeable changes in pressure differential as the solids circulation rate was changed.

3.5 L-Valve Calibration Results

The results of the L-valve calibrations for alumina and Ottawa sand are shown in Figures 3.24 and 3.25 and Figures 3.26 and 3.27 respectively. These figures show the average particle velocity vs. the solids circulation rate, based on the fast bed cross-sectional area. The solid lines drawn through Figures 3.26 and 3.27 represent the straight lines which best fitted the data using least squares. The dashed lines indicate the expected results assuming that the bulk density of the solids flowing through the L-valve is the same as the bulk density of the solids at minimum fluidization.

Velocity measurements were taken over a variety of operating conditions, with fast and slow bed velocities between 1 and 5 m/s and 0.02 and 0.15 m/s respectively and solids circulation rates up to 60 kg/m^2s with the alumina and 40 kg/m^2s with the Ottawa sand, based on the fast bed cross-sectional area. It was found that these variations with these ranges did not have a discernable effect on the particle velocity vs. solids flux relationship.

Figures 3.24 and 3.25 illustrate the effect of the circumferential position of measurement on particle velocity. Each data point represents the average of up to five measurements taken at each circumferential position and set of operating conditions. For both the sand and the alumina, it appears that the circumferential position used for measurement does not affect the relationship between particle velocity and solids flux. This result agrees with the findings of Goldblatt (1985) who observed that solids moved through the vertical section of an L-valve in plug flow until they neared the corner of the L-valve.

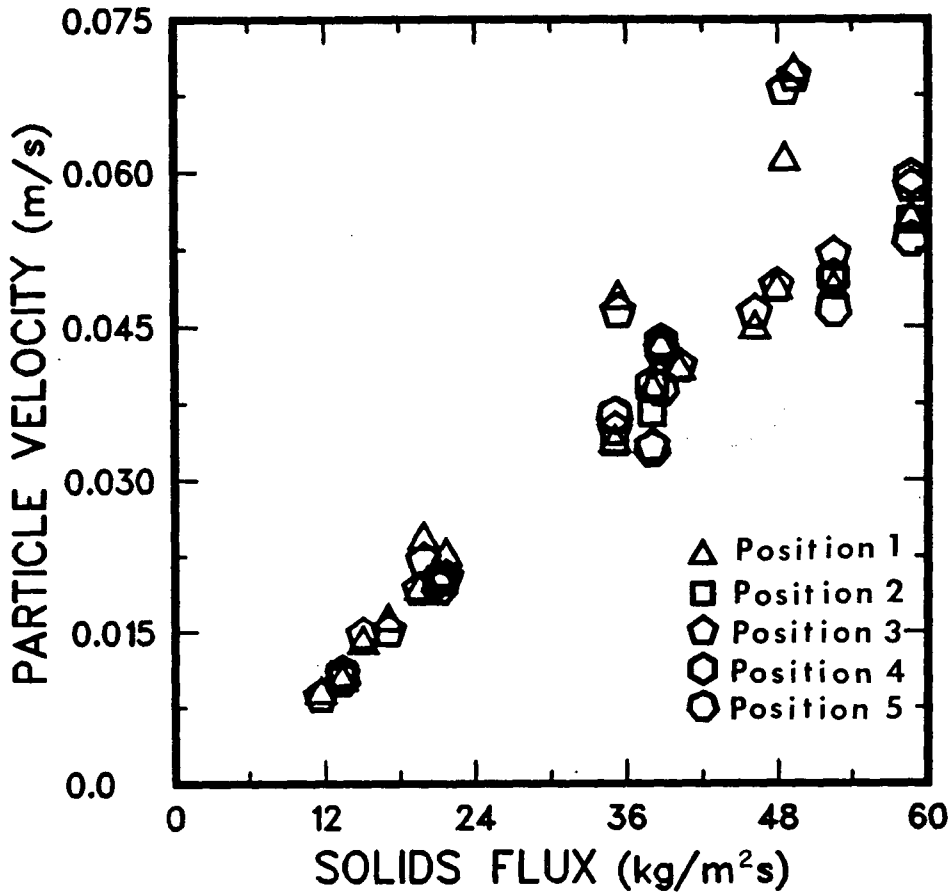

Figure 3.24 Effect of solids flux, based on the fast bed cross-sectional area, on average particle velocity measured at different circumferential positions for alumina, U_s = 0.014 m/s, U_f = 2.8 to 4.8 m/s.

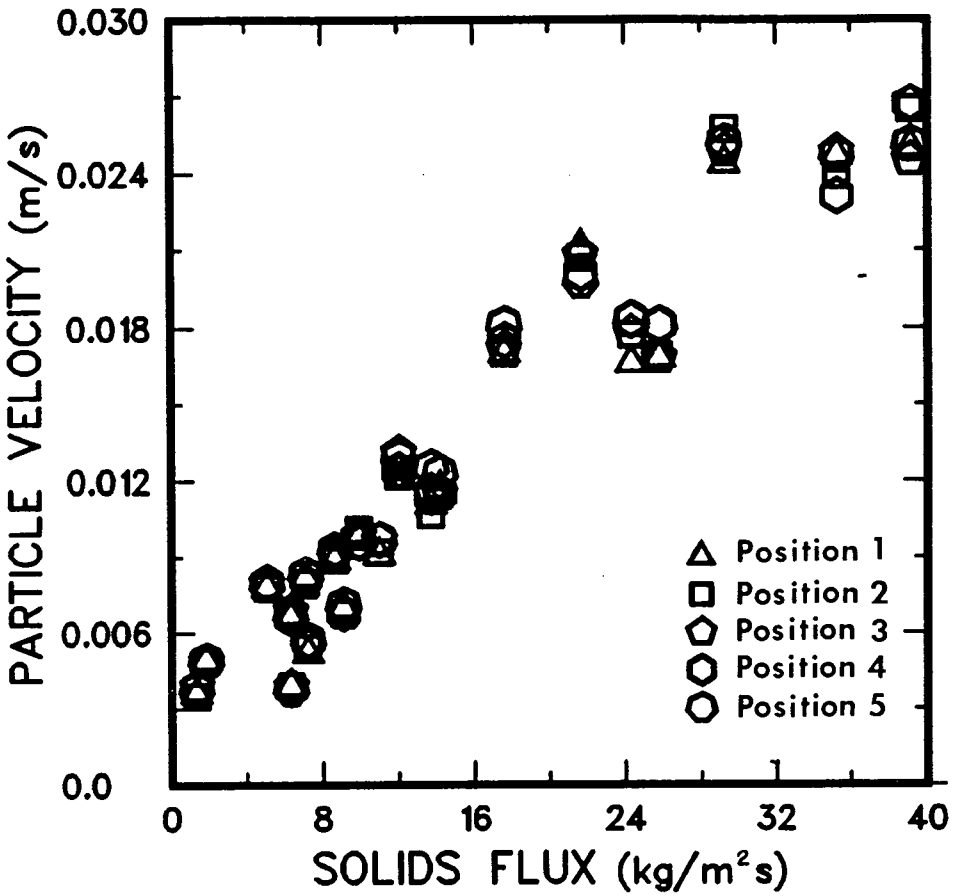

Figure 3.25 Effect of solids flux, based on the fast bed cross-sectional area, on average particle velocity measured at different circumferential positions for sand, U_s = 0.024 m/s, U_o = 3.0 to 6.0 m/s

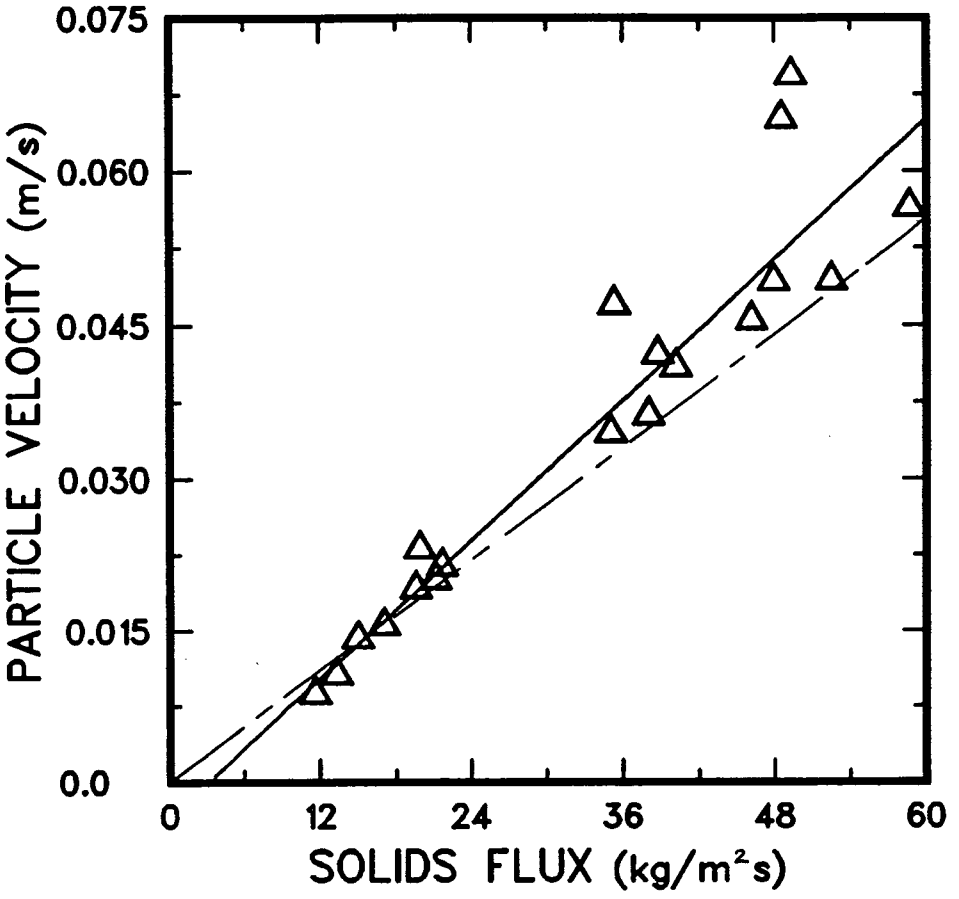

Figure 3.26 Effect of solids flux, based on the fast bed cross-sectional area, on average particle velocity for alumina, U_s = 0.014 m/s, U_f = 2.8 to 4.8 m/s.

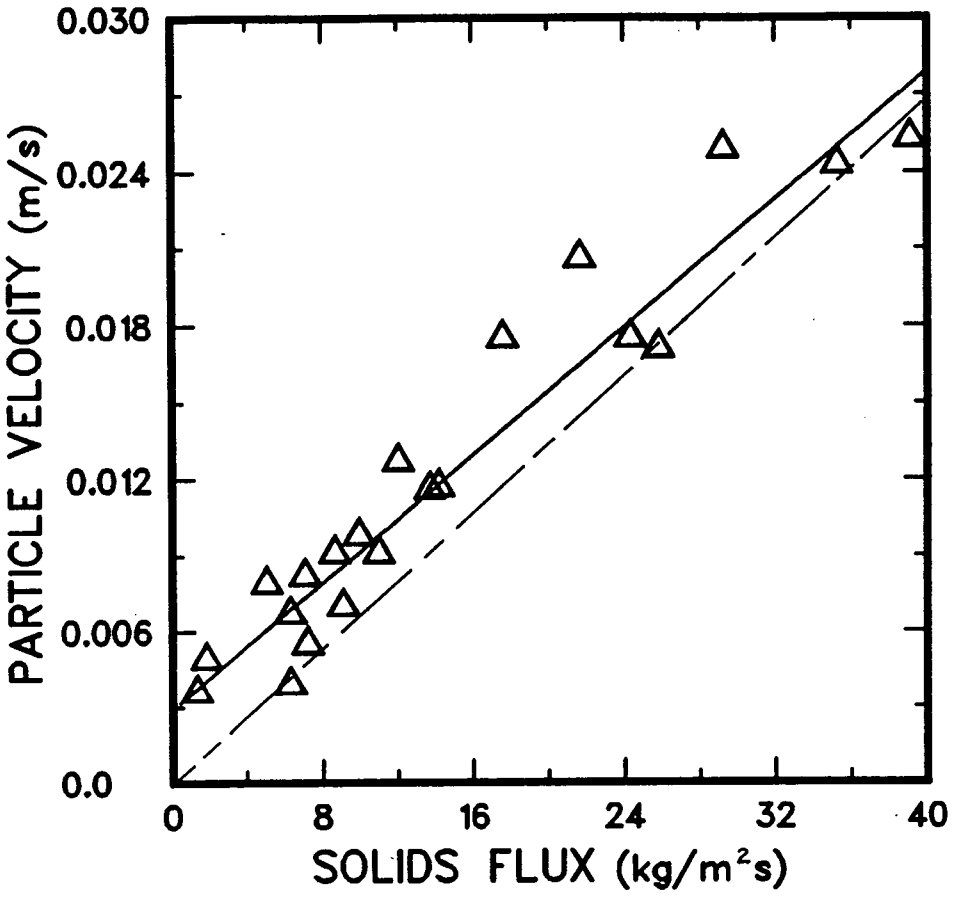

Figure 3.27 Effect of solids flux, based on the fast bed cross-sectional area, on average particle velocity for sand, U_s = 0.024 m/s, U_f = 3.0 to 6.0 m/s.

In Figures 3.26 and 3.27, particle velocities have been determined by averaging all of the measurements, taken at the five circumferential positions, for each set of operating conditions. The results, for both alumina and sand, show good agreement with the best fitted lines at low circulation rates, less than 24 kg/m^2s for alumina and 12 kg/m^2s for Ottawa sand. This is not surprising, since at these circulation rates, the fast bed did not exhibit choking or slugging and the solids moved smoothly through the L-valve. As circulation rates were increased, a stick/slip solids flow pattern developed in the L-valve, with the length of slip and the duration of the periods of sticking increasing with increasing circulation rate. The development of the stick/slip flow pattern resulted in larger deviations between particle velocity measurements for a given set of operating conditions. Since the slip length and duration of sticking periods were becoming large with respect to the overall length and the residence time in the L-valve, the velocity measurements were increasingly affected by the behaviour of the solids when they entered the measuring zone. If the solids were to stop immediately on entering the measurement area, the particle velocity was found to be lower than the mean particle velocity. On the other hand if the solids were found to slip through all or most of the measurement zone, the solids velocity was found to be greater than the average of the measured solid velocities. This probably partially accounts for the poorer agreement with the best fitted lines at higher circulation rates. Additionally, the inaccuracies of the butterfly valve circulation rate measurements may have also contributed measurements at higher fluxes to the poorer agreement with the best fitted lines.

If the solids circulation rate is zero it is apparent that the particle velocity in the L-valve should also be zero. Thus, the plots of particle velocity versus solids flux should pass through the origin. However, for both the alumina and sand it was found that the best fitted lines did not pass through the origin, but had a positive intercept for the alumina and a negative intercept for the sand. This likely arises from inaccuracies in both the particle velocity measurements as discussed above and solids flux measurements via the butterfly value (see Section 3.22) at the higher solids circulation rates. However, the deviations are not considered to be significant.

The alumina experimental results were found to agree well with the expected results at circulation rates less than 24 kg/m^2s, Figure 3.26. At rates greater than 24 kg/m^2s the deviations between experimental and expected results increased, with the expected results underestimating the particle velocity. The increased deviation can be partially attributed to the inaccuracies of the data at higher circulation rates. However, it is also possible that the poorer agreement at higher circulation rates arises from the solids bulk density in the L-valve decreasing at the higher rates.

Comparison of the experimental results for sand with the expected results (see figure 3.27) shows the expected results to always underestimate the particle velocity. However, the slopes of the best fitted and expected results lines are similar. The poorer agreement probably results from inaccuracies in the measurements of particle velocities and solids fluxes and in the assumed bulk density.

3.6 Butterfly Valve

3.6.1 Introduction

During the course of this work, the butterfly valve (see Figure 2.1 and 2.7) was found to provide a simple method of measuring solids circulation rates. However, the butterfly valve was prone to frequent problems so that the results of butterfly valve circulation rate measurements were not always consistent.

3.6.2 Butterfly Valve Operating Difficulties

Several problems were encountered with the operation of the butterfly valve: The valve became misaligned with use and, as a result, tended to stick in the closed position. Solids found their way into the bearings of the rods of the butterfly valve, causing sticking, erosion and fatigue of the valve.

To correct for misalignment, the bolts securing the valve were removed and the sections of the column resting on the valve were lifted off so that the valve position could be changed. The valve was then positioned so that it did not contact the column walls. The overlying sections of the return column were then lowered and the securing bolts were re-installed.

The second, more serious problem, required removal of the valve at periodic intervals for maintenance. This problem arose from solids getting between the two rods of the butterfly valve and the plexiglass flanges which held and acted as bearings for the rods. The solids tended to gall the aluminum rods and to erode the plexiglass bearing areas. As a result,

the movement of rods became difficult, and solids eventually escaped the column by flowing out through the bearings. The increased difficulty in moving the rods, coupled with the sticking of the butterfly valve in the closed position, led to splaying of the gears used to synchronize the movement of the two valve plates and fatigue of the levers and points of attachment. Eventually, the metal gave way.

3.6.3 Effect of Butterfly Valve Closure

The impact flowmeter was not able to detect any effect of closing of the butterfly valve, at least for periods of 1 minute after the closure. However, comparison of the trace of pressure drop across the butterfly valve and accumulated solids of the first circulation rate measurement at a constant set of operating conditions with the traces of the second and subsequent measurements, recorded within 4 minutes of the previous measurement showed some differences, Figures 3.28a and 3.28b. The trace for the first circulation rate measurement taken at a given set of operating conditions was a smooth, monitonically increasing curve. On the other hand, the traces of the second and following circulation rate measurements were not smoothly increasing curves. Instead, the pressure drop was observed to increase, but with superimposed fluctuations. The differences between the first and subsequent curves, taken at constant operating conditions, were observed only if the CFB unit had been operating smoothly, i.e. with only small variations in the fast bed gas velocity and the flowrate of solids through the valve, for at least 10 minutes prior to the first butterfly valve circulation rate measurement. If this was not the case, the first and following traces of the pressure drop across the

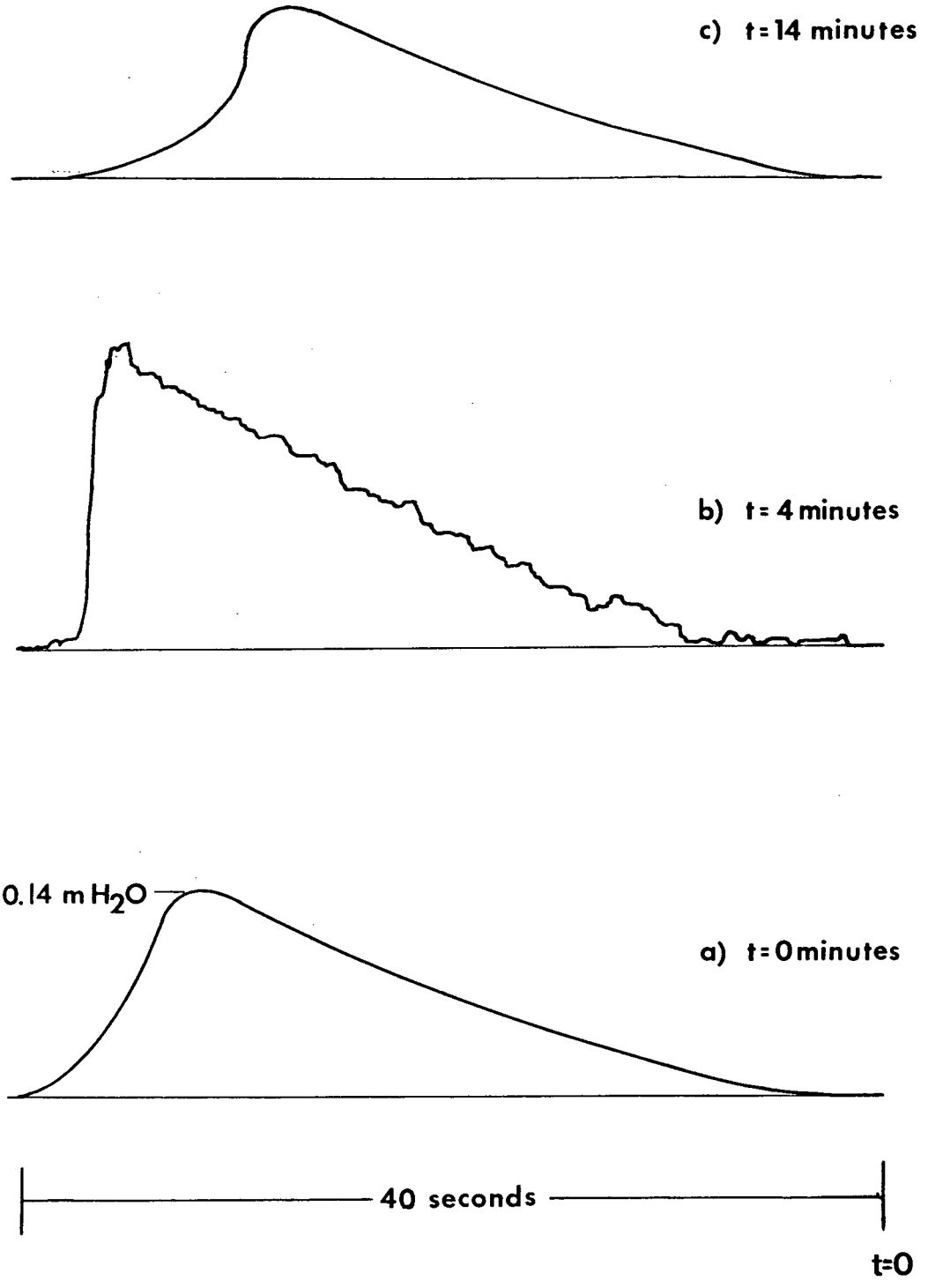

Figure 3.28 Pressure drop across the butterfly valve versus time for three successive circulation rate measurements.

butterfly valve during circulation rate measurements were found to be of the fluctuating increasing curve type. If the time between circulation rate measurements was approximately 10 minutes or more and the CFB unit was operating smoothly, the pressure drop curves for the first and following circulation rate measurements were all found to be smooth and monitonically increasing curves, Figures 3.28a and 3.28c.

The fluctuations observed with short intervals between closures may actually be an artifact of the circulation rate measurement technique. During the first circulation rate measurement of an experimental run, solids may have seeped through the holes on the distributor plates and collected between the plates and the screen. If this was the case, during the following measurement, the collected solids may have blocked holes on the distributor plates, thus causing the pressure fluctuations. This could not be substantiated by observations while the solids were circulating. However, after the solids circulation was stopped solids were found to be trapped between the screens and the plates. The solids slowly flowed from between the butterfly valve plates and screens after the valve was opened.

The pressure drop versus time data for successive butterfly valve circulation rate measurements starting 10 seconds after the butterfly closure and ending 10 seconds before the release of the accumulated solids, were fitted with straight lines using least squares. The slopes of the fitted lines for measurements taken within 4 or 10 minutes of each other were found to be similar for the successive circulation rate measurements. The slopes of the lines best fitting the data of the second and subsequent circulation rate measurements were sometimes greater and sometimes less than the slope of the line best fitting the data of the first butterfly

valve circulation rate measurement, with the differences typically being ±15%. It appears as if the butterfly valve closure does not significantly affect the time averaged solids circulation but does affect instantaneous circulation rates for successive measurements taken within 4 minutes of each other. It also appears that the solids circulation rate varies naturally with time, since the slopes of the lines best fitting the smoothly increasing pressure data of measurements taken 10 minutes apart were also found to vary typically by ± 15%. Since the circulation rate seemed to vary with time, it was decided to use the slope of the line fitting the pressure data of the first circulation rate measurement to calculate the solids flux. This measurement was taken immediately after the particle velocity and impact flowmeter determinations and thus should give a better representation of the actual solids flux during the data-taking period.

The appearance of the trace of the first butterfly valve circulation rate measurement (e.g. Figure 3.28a) gives no indication that the closure of the butterfly valve affects the CFB unit, at least during the 1 minute periods in which measurements were taken. Therefore, it seems that the butterfly valve closure does not perturb the CFB unit, at least over brief periods. However, perturbations appear to result from the subsequent dumping of the solids accumulated during a measurement. The exact sources of these perturbations following a previous measurement are unknown. One possible cause is that the opening of the valve and release of the accumulated solids upsets the flowrates of gas in the CFB. An alternative explanation is that the dumping of accumulated solids affects the reinjection of solids into the fast bed.

During operation, the pressure drop across the upflow column was measured by the pressure transducer and recorded on an Esterline, model S6015, chart recorder. The pressure drop was found to oscillate slowly at 1 to 2 cycles/min. with a superimposed 1.5 Hz fluctuation. The closure of the butterfly valve and dumping of the solids accumulated on the valve did not cause a detectable change in the pressure drop across the bed, or correspondingly, the solids loading of the fast bed for periods up to 1 minute after the butterfly valve closure. The oscillations in pressure drop across the fast bed did not seem to be affected by the butterfly valve closure.

4.0 Conclusion

The butterfly valve, impact flowmeter and particle velocity in the vertical section of the L-valve could all be used to determine the solid circulation rate in a CFB unit. On the other hand, the modified orifice meter, at least in the form studied, was not able to detect the movement of solids flowing counter-currently to a gas. The key conclusions for each circulation rate measurement method are summarized in the following paragraphs.

The butterfly valve was found to provide the simplest method of measuring solids circulation rates. Solids flux was easily determined from the pressure data once the pressure transducer had been calibrated. Successive measurements, at constant operating conditions, were found to vary by ± 15%. However, the butterfly valve itself was not dependable, as a result of sticking, erosion and breakage. Frequent maintenance of the butterfly valve was required to allow continued operation. Perturbations in the operation of the CFB unit were also detected when using the butterfly valve. It was found that traces depended on the duration of the preceding smooth operation. If the system had operated continuously for at least 10 minutes prior to the measurement, the change in pressure drop across the valve with time followed a smooth, monitonically increasing curve. Traces of the succeeding rate measurements, taken after shorter periods of operation, were increasing curves with similar slopes but showing distinct fluctuations. The source of these differences appeared to be the dumping of the solids accumulated on the butterfly valve affecting the gas flow pattern in the CFB unit and solids reinjection to the upflow column.

The impact flowmeter was found to respond to changes in the solids circulation rate. However, the equipment was found to have inherent limitations: The meter was not able to sense changes in solids flowrate at low circulation rates. The sensitive range of the equipment was restricted to a narrow range of circulation rates. The geometry of the equipment, coupled with the datalogging system employed, resulted in the magnitude of the effective force reaching an upper limit at circulation rates much less than the desired maximum of 100 kg/m^2s. The response of the meter was oscillatory, with the frequency and amplitude of the fluctuations being affected by the solids circulation rate, pan angle and particulate material. To calculate the average value of the pan's response, it was necessary to integrate the load beam signals for periods up to 1 minute before the time-averaged signal values were found to be consistent at identical operating conditions. The impact flowmeter must also be calibrated, introducing further inaccuracies into the impact flowmeter results. The effects of these problems restricted the usefulness of the impact flowmeter. It was limited to operating over a narrow range of circulation rates and in this range, the results showed considerable scatter.

Particle velocity in the vertical section of the L-valve was found to be the simplest and most reliable solids circulation rate measurement technique once the equipment was calibrated. Particle velocities were easily measured. Only the presence of identifiable particles flowing with the solids was required. The circumferential position of velocity

measurement did not affect the magnitude of the velocities. The relationship between particle velocity and solids flux was found to reasonably agree with a straight line fitted by least squares. The data for both alumina and sand were found to be scattered about the best fit line. This probably resulted from inaccuracies in measuring solids fluxes. At low circulation rates, the agreement between the experimental data and the line best fitting the data was good. However, with increasing circulation rate the agreement of the data with the best fitted line became poorer. The poorer agreement resulted from the increase of sticking and slipping of the solids flowing through the L-valve with increasing circulation rates. This method suffered the previously mentioned disadvantages of requiring calibration using the butterfly valve. Particle velocities were found to be underestimated when calculated, assuming the bulk densities of the solids in the L-valve were the same as at minimum fluidization.

The failure of the modified orifice in measuring solid circulation rates resulted from the small velocity changes which the gas and solids experienced while passing through the orifice. Typically, the velocity changes were less than 0.24 m/s. As a result, the corresponding pressure differentials across the orifice were too small to be detected by the pressure transducer and the effects of changing solids circulation rates could not be measured. Use of this technique would appear to demand considerable constriction of the return line, leading to risks of bridging. Hence this technique appears to be unsuitable for circulating bed systems.

It does not appear that any of these meters are ideally suited for use in a high temperature and/or pressure CFB. The butterfly valve is prone to breakage and is difficult to operate. The impact flowmeter, as studied, was not able to accurately measure solids flux. Particle velocity measurements, would be difficult in an industrial CFB.

5.0 Recommendations

A new butterfly valve should be designed and built for measuring solids circulation rates. The new valve should eliminate the problems of valve closure and sticking, solids erosion of the valve bearings and solids accumulation between the valves distributor plate(s) and the screen covering the plate(s). The new valve should be used to investigate the causes of the perturbations, if they still exist, seen in the pressure data obtained using the previous butterfly valve.

The geometry, bearing and dashpot of the impact flowmeter should be re-designed to eliminate the problems of overloading, sticking and signal fluctuations respectively. The effective multiplier of the impact flowmeter should be decreased so that the operating range of the equipment can be extended. To do this, the distance between the load beam/lever contact point and lever pivot should be increased. The bearing of the impact flowmeter should be replaced by a bearing which offers less resistance to movement. This would increase the sensitivity of the meter at low solids circulation rates. The dampening effect of the dashpot should be increased to reduce the load beam signal fluctuations. This can be accomplished in four ways: A more viscous fluid can be used as the dashpot liquid. A larger piston-to-cylinder ratio would increase the resistance of the fluid to displacement is greater. Increasing the diameter of the piston and cylinder would increase the volume of displaced fluid. The connection of the piston rod to the lever could be moved a greater distance from the lever pivot so that the piston travel is increased, thus increasing the fluid displacement and dampening force.

Regardless of whether any of these changes are made, the impact flowmeter should be studied using a variety of different circulating solids, with the average particle diameter and apparent particle density being varied independently. The results, if consistent, should then be modelled so that the force versus circulation rate relationship can be predicted empirically, based only on the particle properties. Work should also be carried out to optimize the baffle and screen designs and to distribute the flow of solids exiting the cyclone so that the movement of solids past the flowmeter is more dispersed and steady. Finally, the impact flowmeter pans should be rebuilt to eliminate accumulation of solids on the pan. This may involve both pan material and geometry changes.

The modified orifice does not appear to offer any potential for measuring the flowrate of solids moving counter-currently to a flow of gas and thus, continued investigation under these operating conditions should not be undertaken. However, the ability of the modified orifice to measure solids flowrates in a co-current gas/solids stream is worthy of investigation. Such a meter could be installed in the line connecting the fast bed to the primary cyclone. Under these conditions, it is possible that the modified orifice may provide an effective method of measuring CFB solids circulation rates.

Nomenclature

$F(t)_{eff}$	Effective force of particles impacting on the pan at any instant (MLT^{-2})
$\bar{F}_{eff}$	Time averaged effective force over a time period Δt (MLT^{-2})
$F(t)_L$	Force felt by the load beam at any instant (MLT^{-2})
$F(t)_{Pi}$	Force caused by the ith particle impacting on the pan at any instant (MLT^{-2})
g	Acceleration due to gravity (LT^{-2})
Gs	Solids flux based on the fast bed cross-sectional area ($ML^{-2}T^{-1}$)
H	Total head of flowing fluid (L)
P	Static pressure ($ML^{-1}T^{-2}$)
P_1	Static pressure of the fluid at position 1 ($ML^{-1}T^{-2}$)
P_2	Static pressure of the fluid at position 2 ($ML^{-1}T^{-2}$)
t	Time (T)
U_f	Upflow column superficial gas velocity (LT^{-1})
U_o	Orifice tube superficial gas velocity (LT^{-1})
U_s	Return column superficial gas velocity (LT^{-1})
V	Absolute velocity of the flowing fluid (L)
V_1	Velocity of the fluid at position 1 (LT^{-1})
V_2	Velocity of the fluid at position 2 (LT^{-1})

X_{eff}	Distance from the lever pivot point to the point at which the effective force acts (L)
X_L	Distance from the lever pivot point to the load beam contact point (L)
X_{Pi}	Distance from the impaction point of the ith particle on the pan to the lever pivot (L)
y	Vertical height coordinate (L)
Δt	Time period over which the load beam signal was averaged (T)
ρ	Density of the fluid (ML^{-3})

References

Anonymous, Battelle's Multisolid Fluidized-Bed Combustion Process, Report to Battelle Development Corporation, 1-18 (1981).

Anthony, E.J., Desai, D.L. and Friedrich, F.D., Fluidized Bed Combustion of Suncor Coke, CANMET Report #EAP/ERL 81-27(TR), 1-32 (1981).

Arundel, P.A., Boothroyd, R.G. and Eng, M.I., Measurement of Local Solids Velocity in Pneumatic Conveyor from Correlated Electrostatic Signals, Paper Presented at Pneumotransport 1, First International Conference on the Pneumatic Transport of Solids in Pipes, Paper D1 (1971).

Avidan, A.A., Turbulent Fluid Bed Reactors Using Fine Powder Catalysts, Proc. of Chem. Eng. Joint Meeting, Beijing, China (1982).

Base, B.E., Bergougnou, M.A., Baker, C.G.J. and Mills, P.E., Velocity Measurements and Isokinetic Sampling in a Two Phase Solids in Gas Flow, in "Fluidization Technology", Vol. II, Keairns, D.L. ed., Hemisphere Publishing Corporation, Washington, D.C., 231-237 (1976).

Beer, J.M. and Sarofim, A.F., Fluidized Combustion - Research Needs, NSF Workshop, Paper presented at Fluidization and Fluid-Particle System-Research Needs and Priorities, Rensselaer Polytechnic Inst. Troy, New York, 1-15 (1979).

Bierl, T.W., Gajdos, L.J., McIver, A.E. and McGovern, J.J., Studies in Support of Recirculating Bed Reactors for the Processing of Coal, Carnegie-Mellon University, 24-27, 52-58 (1980).

Cankurt, N.T., Turner, D.H., Avidan, A.A. and Yerushalmi, J., The Turbulent Fluidized Bed, Report for the Clean Fuels Institute, 1-25 (1977).

Carlson, H.M., Frazier, P.M. and Engdahl, R.B., Meter for Flowing Mixtures of Air and Pulverized Coal, Transactions of the ASME, 70, 65-79 (1948).

Clift, R., Grace, J.R. and Weber, M.E., Bubbles, Drops and Particles, Academic Press, New York (1978).

Cohen, L.S., Johnson, W.B. and Parlee, M.C., Fluidized Bed Combustion: The Advantages of the Solids Circulation Fluid-Bed Boiler, Chem. Eng. Prog., Vol. 80, No. 1, 55-60 (1984).

Do, H.T., Grace, J.R. and Clift, R., Particle Ejection from Fluidised Beds, Powder Technology, 6, 195-200 (1972).

Doss, E.D., Analysis and Application of Solid-Gas Flow Inside a Venturi with Particle Interaction, Int. J. Multiphase Flow, Vol. 2, No. 4, 445-458 (1985).

Engstrom, F., Development and Commercial Operation of a Circulating Fluidized Bed Combustion System, Paper presented at the 6th International Fluidized Bed Combustion Conference, Atlanta, Georgia, Vol. II, 616-621 (1980).

Farbar, L., The Venturi as a Meter for Gas-Solids Mixtures, Transactions of the ASME, 75, 943-951 (1953).

Fitzgerald, T., Bushnell, D., Crane, S. and Yeong-Cheng S., Powder Technolgoy, 38, 107-120 (1984).

Fusey, I., A Novel Circulating Fluidized Bed, M.A.Sc. Thesis, University of British Columbia, Vancouver, B.C. (1985).

Geldart, D. and Abrahamsen, A.R., Fluidization of Fine Porous Powders, Recent Advances in Fluidization, AIChE Symposium Series, Vol. 77, No. 205, 160-165 (1981).

Goldblatt, W., U.B.C., personal communication (1985).

Grace, J.R., Fluidized-bed Hydrodynamics, in "Handbook of Multiphase Systems", ed. G. Hetsroni, Hemisphere, Washington, 8.5-8.64, (1982).

Grace, J.R. and Matsen, J.M., Fluidization, Plenum Press, New York, New York (1980).

Hartke, W., Helmrich, H., Kroger, H. and Schugerl, K., Non-Catalytic Decomposition of Sodium Bicarbonate in a Circulating Fluidized Bed Reactor, Ger. Chem. Eng., 4, 203-208 (1981).

Heertjes, P.M., Verloop, J. and Willems, R., The Measurement of Local Mass Flow Rates and Particle Velocities in Fluid-Solids Flow, Powder Technology, 4, 38-40 (1970/71).

Hirama, T., Tomita, M., Adachi, T. and Horio, M., An Experimental Study of Low NO_x Fluidized-Bed Coal Combustor Development. 2. Performance of Two-Staged Fluidized Bed Combustion, Environmental Science and Technology, Vol. 14, No. 8, 960-965 (1980).

Horio, M., Taki, A., Hsieh, Y.S. and Much, I., Elutriation and Particle Transport Through the Freeboard of a Gas-Solid Fluidized Bed, in "Fluidization", Grace, J.R. and Matsen, J.M. eds., 509-518 (1980).

Hosny, N.M., Forces on Tubes Immersed in a Fluidized Bed, Ph.D. Thesis, University of British Columbia (1982).

Jones, O., Initial Operation of Conoco's South Texas Fluidized Bed Combustor, Paper presented at: 10th Energy Technology Conference & Exposition, Washington, D.C., 1-13, (1983).

Knowlton, T.M. and Hirsan, I., L-Valves Characterized for Solids Flow, Hydrocarbon Processing, 3, 149-156 (1978).

Knowlton, T.M. and Hirsan, I., Solids Flow Control Using a Non-Mechanical L-Valve, Paper Presented at the 9th Synthetic Gas Symposium, Chicago, Illinois, 1-36 (1977).

Knowlton, T.M. and Hirsan, I., Wet and Dry Limestone Feeding using an L-Valve, Paper presented at the 6th International Conference on Fluidized Bed Combustion, Vol. II, Atlanta, Georgia, 565-570 (1980).

Kunii, D. and Levenspiel, O., Entrainment and Elutriation from Fluidized Beds, Journ. of Chem. Eng. Japan, Vol. 2, No. 1, 84-88 (1969).

Lund, T., Lurgi Circulating Fluid Bed Boiler: Its Design and Operation, The 7th International Conference on Fluidized Bed Combustion, Vol. I, Philadelphia, 38-46, (1982).

Mann, U. and Tubinovitch, M., A Method for Measuring Local Particle Flow Rates in Fluidized Beds, Paper presented at the 75th Annual AIChE Meeting, Los Angeles, California (1982).

Oakes, E.J., Jave, J. and Engstrom, F., Startup and Operating Experience at the Kattua 22-MWe Cogeneration Circulating Fluidized-Bed Combustion Plant, Proc. of the Amer. Power Conf., Vol. 44, 64-68 (1982).

Oki, K., Walawender, W.P. and Fan, L.T., The Measurement of Local Velocity of Solids Particles, Powder Technology, 18, 177-178 (1977).

Reh, L., Fluidized Bed Processing, Chem. Eng. Prog., Vol. 67, No. 2, 58-63 (1971).

Reh, L., Lurgi Corporation, personal communication (1984).

Rickman, W.S., Holder, N.D. and Young, D.T., Circulating Bed Incineration of Hazardous Wastes, Chem. Eng. Prog., Vol. 81, No. 3, 34-38 (1985).

Sahagian, J., Commercial Development of Fluidized Beds for Direct Combustion of Tar Sands and Other Oil Bearing Materials, Energy Progress, Vol. 4, No. 1, 51-53 (1984).

Sneyd, R.J., Energy Recovery from Fluidized Bed Combustion, Chem. Eng. Prog., Vol. 80, No. 1, 48-54 (1984).

St. John, B., Analysis and Comparison of Five Generic FBC Systems.

Themelis, N.J. and Freeman, G.M., Fluid Bed Behavior in Zinc Roasters, Journal of Metals, 52-57 (1984).

Tomita, M., Hirama, T., Adachi, T. and Yamaguchi, H., Two-Stage Fluidized Bed Combustion of Coal, Paper Presented at the 6th International Fluidized Bed Combustion Conference, Atlanta, Georgia, Vol. II, 623-631 (1980).

van Breugel, J.W., Stein, J.J.M. and deVries, R.J., Isokinetic Sampling in a Dense Gas-Solids Stream, Proc. Instn. Mech. Engrs., Vol. 184, Pt. 3C, 18-23 (1969/70).

Yerushalmi, J. and Cankurt, N.T., Further Studies of the Regimes of Fluidization, Powder Technology, 24, 187-205 (1979).

Yerushalmi, J. and Cankurt, N.T., High Velocity Fluid Beds, Chemtech., Vol. 8, No. 9, 564-571 (1978).

Yerushalmi, J., Turner, D.H. and Squires, A.M., The Fast Fluidized Bed, Ind. Eng. Chem. Process Des. Dev., Vol. 15, No. 1, 47-53 (1976).

Appendix A

Computer Programs

Appendix A.1 - Datalogging Program

```
10  PRINT "This program datalogs either channel 0 or 1 of the Tecmar board"

20  PRINT "There are facilities to input a base voltage which will be
          subtracted"

30  PRINT "from the data being logged.  This program is designed to be used
          in the"

40  PRINT "case where the equipment has not been calibrated for each run,
          but a"

50  PRINT "base voltage has been determined by some other means

60  PRINT "PRESS ANY KEY TO RUN THE PROGRAM"

70  X$=INPUT$(1)

80  CLS

90  REM $LINESIZE: 132 $PAGESIZE: 55

100 WIDTH 80: CLS

110 DEFINT I,J,K,L,M

120 DIM A%(27000),L$(3)

130 DIG=0!: FSL=0!: PRES=0!: NOTE=0!: TOT=0: M=1

140 PRINT

150 PRINT "HARDWARE:  IBM personal computer,"

160 PRINT "Tecmar Lab Master A/D & D/A converter,"

170 PRINT "(2 channel, 0 & 1, single-ended, gain=1, -10.V to +10.V):"

180 PRINT "Channel 0 Hardware;"

190 PRINT "BLH 1 Kg Load Beam,"

200 PRINT "Bofors signal amplifier and conditioner."

210 PRINT "Channel 1 Hardware;"

220 PRINT "Disa pressure transducer."

230 PRINT

240 INPUT "Enter the name of the file to be used for data storage: ",FIL$
```

Datalogging Program - Continued

```
250 OPEN FIL$ AS #1 LEN=8

260 FIELD #1, 4 AS X$, 4 AS Y$

270 IF NOTE=1 THEN GOTO 310

280 INPUT "Enter the investigators name:   ",NAM$

290 INPUT "Enter the date:    ",S$

300 IF NOTE=0! THEN GOTO 340

310 PRINT "Are the sampling conditions the same?"

320 I$=INPUT$(1)

330 IF I$="Y" OR I$="y" THEN GOTO 420

340 INPUT "Enter the length of the sampling period in seconds:  ",T

350 INPUT "Enter the desired sampling rate in points/second
        (1-30000)",S%

360 NN%=T*S%

370 IF NN%<=27000 THEN GOTO 410

380 CLS:  PRINT: PRINT

390 PRINT "Choose a smaller sampling rate or period such that the product of
    the two is less than 27000!"

400 CLS:  GOTO 340

410 IF NOTE=0! THEN GOTO 450

420 PRINT "Are the operating conditions the same?"

430 I$=INPUT(1)

440 IF I$='Y" OR I$='y' THEN GOTO 590

450 INPUT "Base voltage?", VOL

460 CLS:  PRINT "Operating Conditions:":PRINT

470 PRINT "Fast bed conditions"

480 INPUT "Orifice diameter, inches?",OD$
```

Datalogging Program - Continued

```
490 INPUT "Pressure upstream of the orifice meter, cm of Hg?",UP$
500 INPUT "Pressure drop across the orifice meter, cm of H2O?",PD$
510 PRINT: PRINT
520 PRINT "Slow bed conditions;"
530 INPUT "Slow bed fluidization gas flowrate, rotameter reading?",SB$
540 INPUT "Rotameter #1 Setting?",R1$
550 INPUT "Rotameter #2 Setting?",R2$
560 INPUT "Rotameter #3 Setting?",R3$
570 INPUT "Rotameter #4 Setting?",R4$
580 INPUT "Rotameter #5 Setting?",R5$
590 LPRINT CHR$(27)"E":LPRINT
600 LPRINT CHR$(14) "INVESTIGATOR:"TAB(20) NAM$
610 LPRINT CHR$(14) "DATA FILE:" TAB(20) FIL$
620 LPRINT CHR$(14) "DATE:" TAB(20) S$
630 LPRINT "------------------------------------------------------------"
640 LPRINT
650 LPRINT "BASE VOLTAGE:";VOL
660 LPRINT "BED CONDITIONS:":LPRINT"FAST BED;"
670 LPRINT "ORIFICE DIAMETER:" TAB(40) OD$;"in."
680 LPRINT "UPSTREAM PRESSURE:" TAB(40) UP$;" cm of Hg"
690 LPRINT "PRESSURE DROP ACROSS ORIFICE:" TAB(40) PD$;" cm of H2O
700 LPRINT "SLOW BED:"
710 LPRINT "BUBBLING BED ROTAMETER READING:" TAB(40) SB$
720 LPRINT "#1 ROTAMETER READING:" TAB(40) R1$
730 LPRINT "#2 ROTAMETER READING:" TAB(40) R2$
```

Datalogging Program - Continued

```
740 LPRINT "#3 ROTAMETER READING:" TAB(40) R3$

750 LPRINT "#4 ROTAMETER READING:" TAB(40) R4$

760 LPRINT "#5 ROTAMETER READING:" TAB(40) R5$

770 LPRINT

780 LPRINT "SAMPLING RATE:";S%;" points/second"

790 LPRINT "SAMPLE LENGTH:",T;" seconds"

800 LPRINT "NUMBER OF DATA POINTS READ:";NN%: LPRINT: LPRINT

810 CLS: PRINT "Unit to be datalogged, pressure transducer or load beam?"

820 V$=INPUT$(1)

830 IF V$="P" OR V$="p" THEN C%=1 ELSE C%=0

840 P%=0:IF S%>2000 THEN P%=0 Plot if < 2000 pts/sec

850 CLS

860 CLS: PRINT "PRESS ANY KEY TO START DATA LOGGING."

870 I$=INKEY$:IF I$="" THEN 870

880 CLS

890 F%=0 'Initialize overrun flag

900 CALL TIMER(A%(1),F%,P%,NN%,C%,S%)

910 IF F%<>0 THEN PRINT "Warning--data taken too fast!":NN%=NN%-F%

920 IF F%<>0 THEN LPRINT:  LPRINT "ACTUAL NUMBER OF DATA POINTS READ:
    ";NN%: LPRI NT

930 PRINT "DATA LOGGING COMPLETE"

940 FOR I-1 TO NN%

950 TIME=I/S%

960 IF A%(I)>32767 THEN A%(I)=A%(I)-65535!

970 P=A%(I)/204.8-VOL
```

Datalogging Program - Continued

```
980  LSET X$=MKS$(TIME): LSET Y$=MKS$(P)
990  PUT #1, I
1000 NEXT
1010 CLOSE #1
1020 LPRINT CHR$(27)CHR$(12)
1030 CLS: PRINT "Do you want to take another set of data?"
1040 I$=INPUT$(1)
1050 IF I$="Y" OR I$="y" THEN NOTE=1!" C=C%: CLS: GOTO 240
1060 STOP
1070 END
```

Appendix A.2 - Clock Setting Program

```
        PAGE, 132
        TITLE TIMER
;       SUBROUTINE TO DO TIMED DATA COLLECTION FROM TECMAR A/D/A BOARD
;       CALL FROM BASIC WITH CALL OF FORM:
;       CALL TIMER (A%(1),F%,P%,N%,C%,S%)
;       WHERE  A% IS ARRAY WHERE DATA ARE TO BE STORED
;              F% IS OVERRUN FLAG--SET TO ZERO UPON NORMAL EXIT
;                 OTHERWISE SET TO VALUE OF CX REGISTER TO GIVE
;                 NUMBER OF POINTS NOT COLLECTED
;              P% IS 0 TO OMIT REAL-TIME PLOT, OTHER TO PLOT
;              N% IS NUMBER OF POINTS TO BE COLLECTED
;              C% IS CHANNEL NUMBER OF A/D
;              S% IS NUMBER OF DATA POINTS PER SECOND
;                 S% MUST BE < = SPEED OF A/D
;                 IF S% < 0 THAT MEANS WE WANT THAT MANY SEC/POINT
;
CSEG    SEGMENT
        ASSUME CS:CSEG, DS:NOTHING
TEMP    DW      ?                       ;TEMP. STORAGE
PLOT    DW      ?                       ;PLOT FLAG
TEMPSI  DW      ?                       ;TEMP. STORAGE FOR SI REGISTER
OVRUN   DW      ?                       ;OVERRUN OF A/D FLAG
;DEFINITIONS:
ADD0    =1808                           ;I/O ADDRESS OF TECMAR BOARD
ADD4    =ADD0+4                         ;A/D CONTROL BYTE
```

Clock Setting Program - Continued

```
ADD5    =ADD0+5                 ;A/D CHANNEL NUMBER
ADD6    =ADD0+6                 ;SOFTWARE START CONVERSION
ADD8    =ADD0+8                 ;TIMER 9513 DATA PORT
ADD9    =ADD0+9                 ;TIMER 9513 CONTROL PORT
        PAGE
        PUBLIC  TIMER
TIMER   PROC    FAR
        PUSH    BP              ;SAVE BP
        MOV     BP,SP           ;SET BASE PARAMETER LIST
        MOV     DI,[BP]+6       ;GET DATA POINTS/SEC.
        MOV     AX,[DI]         ;INTO BX REGISTER
        MOV     BX,AX
        MOV     DI,[BP]+8       ;GET CHANNEL NUMBER
        MOV     AX,[DI]         ;AND STORE AS AX
        MOV     DX,ADD5         ;AND OUTPUT TO A/D
        OUT     DX,AL           ;(USE ONLY LOWER BYTE)
        MOV     DI,[BP]+10      ;GET NUMBER OF DATA POINTS
        MOV     CX,[DI]         ;STORE IN CX REGISTER
        MOV     DI,[BP]+12      ;GET PLOT FLAG
        MOV     AX,[DI]         ;STORE IN MEMORY
        MOV     PLOT,AX
        MOV     AL,128
        MOV     DX,ADD4         ;EXTERN. START CONVERSION, ALL INTERRUPTS
        OUT     DX,AL           ;GAIN=1)
        MOV     AX,0            ;SI IS X-VALUE OF POINT TO BE
```

Clock Setting Program - Continued

```
MOV     AX,6            ;SET UP HIGH RESOLUTION GRAPHICS MODE
INT     10H
MOV     DX,ADD6         ;RESET DONE FLIP-FLOP OF A/D
IN      AL,DX
MOV     DX,ADD9         ;SET DATA POINTER TO MASTER MODE REGISTER
MOV     AL,23
OUT     DX,AL
MOV     DX,ADD8         ;SET MASTER MODE REGISTER FOR SCALER
                        CONTROL=
MOV     AL,23
OUT     DX,AL
MOV     DX,ADD8         ;SET MASTER MODE REGISTER FOR SCALER
                        CONTROL=
MOV     AL,0            ;BCD DIVISION, ENABLE INCREMENT 8-BIT BUS,
OUT     DX,AL           ;FOUT ON, DIVIDE BY 16, SOURCE=F1
MOV     AL,128          :COMPARATORS DISABLED, TOO DISABLED
OUT     DX,AL
MOV     DX,ADD9         ;SET DATA POINTER TO COUNTER MODE OF
MOV     AL,5            ;REGISTER 5
OUT     DX,AL
MOV     DX,ADD8         ;SET COUNTER 5 FOR COUNT REPETITIVELY,
MOV     AL,33           ;BINARY COUNT, COUNT DOWN, ACTIVE HIGH
OUT     DX,AL           ;TC, DISABLE SPECIAL GATE, RELOAD FROM
                        LOAD,
CMP     BX,31           ;CHECK IF <31 POINTS/SEC
JL      MED             ;IF SO JUMP
PAGE
```

Clock Setting Program - Continued

```
;BRANCH TO HERE FOR 31 TO 20000 POINTS/SEC--USE 1 MHz CLOCK

FAST:  MOV     AL,11          ;COUNT AT 1 MHz (NO GATE, RISING
       OUT     DX,AL          ;EDGE OF F1)
       MOV     AX,10000       ;DIVIDE 1000000 BY PTS/SEC BY
       MOV     DI,100         ;GETTING 10F6 INTO DX+AX
       MUL     DI
       DIV     BX             ;BX=PTS/SEC; RESULT IN DX+AX, BUT
                              :IGNORE DX, SINCE DX=0
       CMP     AX,200         ;DISABLE INTERRUPTS IF >=5000
       JG      FAST2          ;POINTS/SEC
       CLI
FAST2: JMP     GO
;BRANCH TO HERE FOR 1 TO 30 POINTS/SEC--USE 10kHz CLOCK
MED:   MOV     AL,13          ;COUNT AT 10kHz (NOT GATE, RISING
       OUT     DX,AL          ;EDGE OF F3)
       MOV     AX,10000       ;CALCULATE NUMBER OF TICKS OF 10000 Hz
                              CLOCK
       CWD                    ;PER DATA POINT BY DIVIDING
       DIV     BX             ;10000 BY PTS/SEC
;START CLOCK TICKING AT DESIRED RATE
GO:    MOV     DX,ADD8        ;AND LOAD COUNTER 5 WITH TICKS
       DEC     AX             ;(COUNT TO ZERO, DECREMENT AX)
       OUT     DX,AL          ;FOR CORRECT COUNT)
       MOV     AL,AH
       OUT     DX,AL          ;8 BITS AT A TIME
       MOV     DI,[BP]+14     ;GET OVERRUN FLAG ADDRESS
```

Clock Setting Program - Continued

```
        MOV     WORD PTR [DI],0 ;ZERO THE FLAG
        MOV     OVRUN,DI        ;AND STORE THE FLAG ADDRESS
        MOV     DI,[BP]+16      ;GET ADDRESS OF DATA ARRAY
        MOV     DX,ADD9         ;LOAD COUNTER 5 FROM LOAD REGISTER
        MOV     AL,112          ;AND ARM (START COUNTING)
        OUT     DX,AL
        MOV     DX,ADD4         ;ENABLE EXTERNAL START (PINES 3,4 OF
        MOV     AL,132          ;J2 CONNECTOR MUST BE CONNECTED)
        OUT     DX,AL
        PAGE
;BEGIN DATA COLLECTION; COLLECT UPON EXTERNAL START TRIGGER
DONE:   MOV     DX,ADD4         ;CHECK IF DATA READY
        IN      AL,DX
        CMP     AL,128          ;BY CHECKING READY BIT (BIT 7)
        JB      DONE            ;LOOP UNTIL READY
        TEST    AL,64           ;SEE IF DATA OVERRUN FLAG SET
        JNE     ERRMESS         ;IF SO, NOTIFY BASIC PROGRAM AND EXIT
        MOV     DX,ADD5         ;YES, DONE, SO GET LOW BYTE OF DATUM
        IN      AL,DX
        MOV     [DI],AL         ;AND STORE IT
        INC     DI              ;GO TO NEXT LOCATION IN ARRAY (1 BYTE
                                LATER)
        MOV     DX,ADD6         ;GET HIGH BYTE AND STORE IT
        IN      AL,DX
        MOV     [DI],AL
        INC     DI
```

Clock Setting Program - Continued

```
        CMP     PLOT,0          ;DON'T PLOT IF PLOT FLAG=0
        JZ      NOPLOT
;PLOT ROUTINE STARTS HERE
        MOV     TEMP,CX         ;SAVE CX FIRST
        MOV     AH,AL           ;GET HIGH BYTE JUST TAKEN
        MOV     AL,[DI-2]       ;AND LOW BYTE FROM STORAGE SO AX=DATUM
        ADD     AX,2047         ;CALCULATE Y-VALUE TO PLOT =
        CWD                     ;199-((DATUM+2047)/21)
        MOV     BX,21           ;DIVIDE BY 21--QUOTIENT IN AX
        DIV     BX
        MOV     DX,AX           ;RESULT INTO DX
        NEG     DX              ;NEGATE AND ADD TO 199
        ADD     DX,199
        MOV     SI,TEMPSI       ;GET X-VALUE OF LAST POINT ON SCREEN
        INC     SI              ;GO TO NEXT LOCATION ON SCREEN
        CMP     SI,640          ;TEST IF AT RIGHT EDGE OF 640x200
        JL      M1              ;SCREEN
        MOV     SI,0            ;IF SO, GO TO LEFT EDGE TO PLOT
M1:     MOV     CX,SI           ;GET X-VALUE INTO CX
        MOV     TEMPSI,SI       ;SAVE X-VALUE
        MOV     AX,3073         ;AH=12,AL=1 TO WRITE DOT TO SCREEN
        INT     10H             ;PLOT POINT
        MOV     CX,TEMP         ;RESTORE CX
NOPLOT: LOOP    DONE            ;DECREMENT CX AND LOOP IF > 0
;BRANCH TO HERE UPON FINISH OR OVERRUN
```

Clock Setting Program - Continued

```
NOGO:   MOV     DX,ADD4          ;TURN OFF A/D
        MOV     AL,0
        OUT     DX,AL
        STI                      ;RESTORE INTERRUPT SERVICE
        MOV     AX,2
        INT     10H
        POP     BP               ;RESTORE BP
        RET     12               ;6 ARGUMENTS IN CALL X 2=12
ERRMESS: MOV    DI,OVRUN         ;SET OVERRUN FLAG SINCE A/D GOING
        MOV   WORD PTR [DI],CX   ;TOO FAST
        JMP     NOGO
TIMER   ENDP
CSEG    ENDS
        END
```

Appendix A.3 - Integration Program

```
10  LPRINT CHR$(27)"N"CHR$(10)
20  PRINT "Type of integration desired:"
30  PRINT "1) Trapezoidal"
40  PRINT "2) Simpson's"
50  PRINT "3) Both"
60  I$=INPUT$(1)
65  PTR=0
70  FLAG=2: CNT=1
80  IF I$="2" OR I$="S" THEN FLAG=1
90  IF I$="s" THEN FLAG=1
100 IF I$="1" OR I$="T" THEN FLAG=0
110 IF I$="t" THEN FLAG=0
120 CLS
130 INPUT "Data file to be read";D$
140 TAG=0
150 PRINT: PRINT
160 INPUT "Starting point of data to be read";ST#
170 ST=INT(ST#)
180 PRINT: PRINT
190 INPUT "Number of data points to be integrated (odd numbered integer)";N#
200 N=N#
210 CLS
220 IF (2*INT(N#/2))<>N# THEN GOTO 270
230 PRINT "*******"
240 PRINT "THE NUMBER OF DATA POINTS MUST BE AN ODD INTEGER"
250 PRINT "*******"
```

Integration Program - Continued

```
260 PRINT: PRINT: GOTO 190
270 OPEN D$ AS #1 LEN=8
280 FIELD #1, 4 AS X$, 4 AS Y$
290 FIN=ST+N-1
300 GET #1,ST
310 XST=CVS(X$): YST=CVS(Y$)
320 GET #1,FIN
330 XFIN=CVS(X$): YFIN=CVS(Y$)
340 H=(XFIN-XST)/(N-1)
350 TSUM=0: SSUM=0: FL=0
360 FOR I=ST TO FIN
370 GET #1,I
380 X=CVS(X$)
390 Y=CVS(Y$)
400 IF FLAG=1 THEN GOTO 470
410 REM TRAPEZOIDAL INTEGRATION
420 IF I=ST or I=FIN GOTO 430 ELSE GOTO 450
430 TSUM=TSUM+Y*H/2
440 GOTO 460
450 TSUM=TSUM+Y*H
460 IF FLAG=0 THEN 570
470 REM SIMPSON'S INTEGRATION
480 IF I=ST OR I=FIN THEN GOTO 490 ELSE GOTO 510
490 SSUM=SSUM+Y*H/3
500 GOTO 570
```

Integration Program - Continued

```
510 IF FL=1 THEN GOTO 550
520 SSUM=SSUM+4*Y*H/3
530 FL=1
540 GOTO 570
550 SSUM=SSUM+2*Y*H/3
560 FL=0
570 NEXT
580 CLOSE #1
590 TAVG=TSUM/(XFIN-XST): SAVG=SSUM/(XFIN-XST)
595 IF PTR=1 THEN LPRINT: LPRINT: GOTO 640
600 IF TAG=1 THEN LPRINT: GOTO 660
610 LPRINT: LPRINT: LPRINT
620 LPRINT CHR$(14);"INTEGRATED RESULTS"
630 LPRINT: LPRINT: LPRINT
640 LPRINT CHR$(27);"E"
650 LPRINT CHR$(27)"-1" "Data file name:  ";D$" LPRINT CHR$(27)"-0"
660 LPRINT: LPRINT
670 LPRINT CHR$(27)"-1" "CASE";CNT:  LPRINT
680 LPRINT "Points";ST;"through";FIN;"integrated":  LPRINT CHR$(27)"-0"
690 GOTO 700
700 LPRINT:  LPRINT
710 IF FLAG=0 THEN GOTO 750
720 LPRINT "The integral by Simpson's method is";SSUM
730 LPRINT "The average Y value over the interval is";SAVG
740 LPRINT: LPRINT:
```

Integration Program - Continued

```
750 IF FLAG=1 THEN GOTO 780

760 LPRINT "The integral by the Trapezoid method is";TSUM

770 LPRINT "The average Y value over the interval is";TAVG

780 PRINT "Do you want to integrate another set of data from this file?"

790 Y$=INPUT$(1)

800 IF Y$="Y" OR Y$="y" THEN TAG=1:CNT=CNT+1:PRINT:PRINT:LPRINT:LPRINT:
    GOTO 150

820 CLS

830 PRINT "Do you want to integrate data from another file?"

840 ANS$=INPUT$(1)

850 IF ANS$="Y" OR ANS$="y" THEN PTR=1: GOTO 120

855 LPRINT CHR$(27)CHR$(12)

860 STOP

870 END
```

Appendix A.4 - Standard Deviation Program

```
10  LPRINT: LPRINT: LPRINT: LPRINT CHR$(27);"E"

20  N=5801

30  ST=100

40  LPRINT CHR$(14); "VARIANCE RESULTS"

50  LPRINT: LPRINT

60  INPUT "Data file to be read";D$

70  PRINT

80  INPUT "Mean Value";MEAN

90  PRINT: PRINT

100 CLS

110 TOT=1

120 CNT=1

130 OPEN D$ AS #1 LEN=8

140 FIELD #1, 4 AS X$, 4 AS Y$

150 SUM=0

160 FIN=ST+N-1

170 FOR I=ST TO FIN

180 GET #1, I

190 Y+CVS(Y$)

200 DIF=ABS(Y-MEAN)

210 SUM=SUM+DIF 2

220 IF(CNT=100) THEN PRINT (TOT*100) TAB(7) "POINTS ANALYSED": TOT=TOT+1:
    CNT=1

230 CNT=CNT+1

240 NEXT
```

Standard Deviation Program - Continued

```
250 CLOSE #1

260 SDEV=SQR(SUM/(N-1))

270 LPRINT "FILE:" TAB(7) D$ (TAB)15 "MEAN:" TAB(23) MEAN TAB(35)
          "STANDARD DEVIATION:" TAB(47) SDEV

280 CLS

290 INPUT "Next file":D$

300 IF D$="N" OR D$="n" THEN STOP

310 PRINT

320 GOTO 80

330 STOP

340 END
```

Appendix A.5 - Linear Regression Program

```
10  LPRINT: LPRINT: LPRINT: LPRINT CHR$(27);"E"
20  LPRINT CHR$(14); "LINEAR REGRESSION RESULTS"
30  LPRINT: LPRINT
40  LPRINT CHR$(27)"N"CHR$(10)
50  INPUT "Data file to be read";D$
60  LPRINT: LPRINT: LPRINT "FILE:";D$
70  TAG=0!
80  PRINT: PRINT
90  CLS
100 INPUT "Starting point of the data to be read";ST
110 PRINT: PRINT
120 INPUT "Number of data points to be fit";N
130 CLS
140 SUMX=0: SUMY=0: SUMXY=0: SUMX2=0: DIFF=0
150 OPEN D$ AS #1 LEN=8
160 FIELD #1, 4 AS X$, 4 AS Y$
170 FIN=ST+N-1
180 FOR I=ST TO FIN
190 GET #1,I
200 X=CVS(X$)
210 SUMX=SUMX+X
220 SUMX2=SUMX2+X^2
230 Y=CVS(Y$)
240 SUMY=SUMY+Y
250 SUMXY=SUMXY+X*Y
```

Linear Regression Program - Continued

```
260 NEXT
270 K=N*SUMX2-SUMX^2
280 M=(N*SUMXY-SUMX*SUMY)/K
290 B=(SUMY*SUMX2-SUMX*SUMXY)/K
300 FOR I=ST TO FIN
310 GET #1, I
320 X=CVS(X$)
330 YCALC=X*M+B
340 Y=CVS(Y$)
350 DIFF=DIFF+(YCALC-Y)^2
360 NEXT
370 CLOSE #1
380 SDEV=SQR(DIFF/(N-1))
390 TAG=TAG+1
400 LPRINT: LPRINT"CASE";TAG
410 LPRINT  "POINTS";ST;"THROUGH";FIN;"FIT
420 LPRINT  "SLOPE:" TAB(18)M;"VOLTS/SEC"
430 LPRINT  "INTERCEPT:" TAB(18)B;"VOLTS"
440 LPRINT  "STD.DEV.:" TAB(18) SDEV;"VOLTS"
450 CLS
460 PRINT "Do you want to fit another set of data from this file?"
470 ANS$=INPUT$(1)
480 IF ANS$="y" OR ANS$="Y" THEN CLS: GOTO 100
490 CLS
500 PRINT "Do you want to fit data from another file?"
```

Linear Regression Program - Continued

```
510 ANS$=INPUT$(1)

520 IF ANS$="y" OR ANS$="Y" THEN CLS: GOTO 50

530 LPRINT CHR$(27)CHR$(12)

540 STOP

550 END
```

Appendix B

Sieve Analyses and Calculation of the average particle diameters,

Table B.1 - Sieve Analysis

Sieve Interval	Particle Diameter μm	Weight Percent	
		Alumina	Ottawa Sand
710-600	655	-	0.1
600-500	550	-	0.2
500-425	462.5	-	0.3
425-355	390	-	0.7
355-300	327.5	-	1.4
300-250	275	-	0.9
250-212	231	-	12.7
212-180	196	-	11.5
180-150	165	1.1	31.5
150-125	137.5	2.8	22.4
125-106	115.5	5.8	8.9
106-90	98	11.8	4.6
90-75	82.5	24.4	2.9
75-63	69	37.0	1.5
63-53	58	3.6	0.3
53-45	49	4.4	0.1
45-38	41.5	3.3	0.1
38-0	19	5.7	0.1

Calculation of mean particle diameter:

$$\bar{d}p = \frac{1}{\sum_{i=1}^{n} \phi_i/dp_i}$$

$\bar{d}p$ Sauter mean particle diameter

dp_i Average particle diameter of the ith sieve fraction

ϕ_i Weight fraction of particles in the ith sieve fraction

Mean Particle Diameters:

1. Alumina

$$\bar{d}p = \frac{1}{((0.91)/(165+10^{-6}))+....+((0.057)/(19x10^{-6}))}$$

$$= 64x10^{-6} \text{ m}$$

$$= 64 \ \mu m$$

2. Sand

$$\bar{d}p = \frac{1}{((0.001)/(655x10^{-6}))+....+((0.001)/(19x10^{-8}))}$$

$$= 148x10^{-6} \text{ m}$$

$$= 148 \ \mu m$$

Appendix C

Minimum Fluidization, Calculated and Experimental, and Calculation of Archimedes Numbers and Terminal Velocities

Calculated U_{mf}:

1. Alumina

$\rho_p = 3500\ kg/m^3$

$\bar{d}p = 65 \times 10^{-6}\ m$

$g = 9.81\ m/s^2$

Gas properties at 25°C, 1 atm

$\rho_g = 1.1769\ kg/m^3$

$\mu_g = 1.8464 \times 10^{-5}\ kg/ms$

$Ar = \rho_g(\rho_p-\rho_g)g\ \bar{d}p^3/\mu_g^2$

$= 31$

Since $Ar < 10^3$,

$U_{mf} = 0.00075\ (\rho_p-\rho_g)gdp^2/\mu_g$

$= 0.0057\ m/s$

2. Ottawa Sand

$\rho_p = 2650\ kg/m^3$

$\bar{d}p = 148 \times 10^{-6}\ m$

$g = 9.81\ m/s^2$

Gas properties at 25°C, 1 atm

$\rho_g = 1.1769\ kg/m^3$

$\mu_g = 1.8464 \times 10^{-5}\ kg/ms$

$Ar = 290$

Since $Ar < 10^3$

$U_{mf} = 0.023$

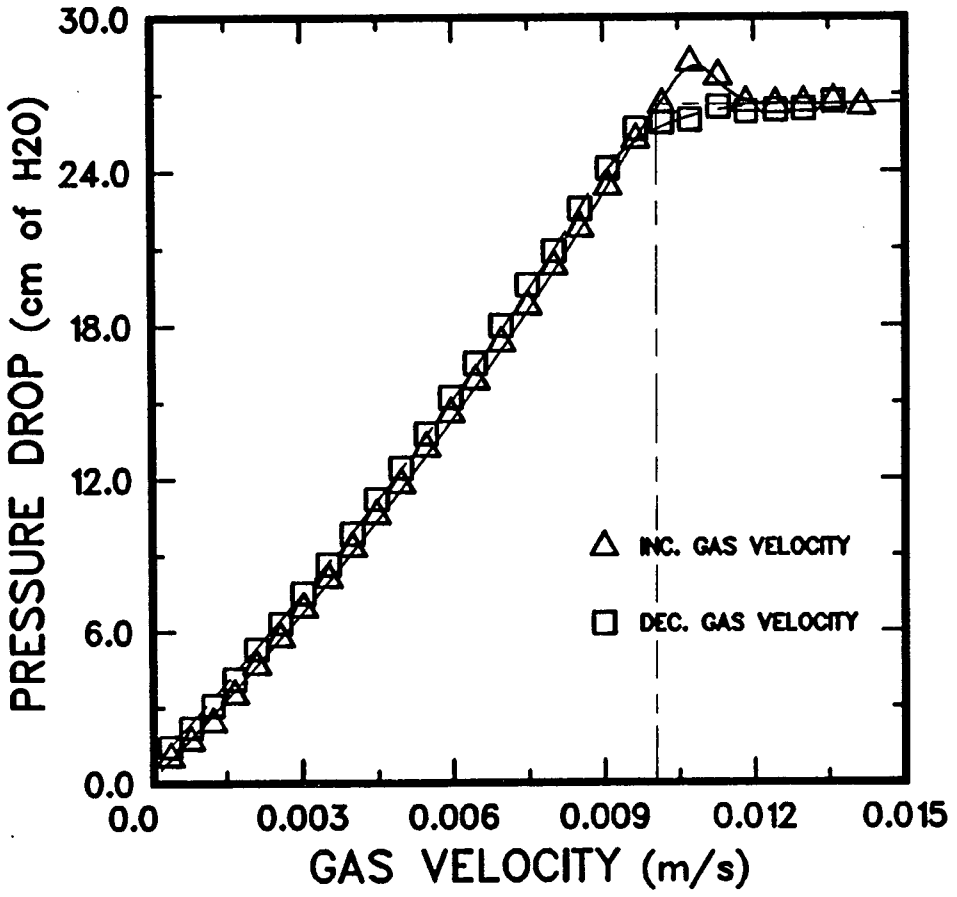

Figure C.1 Minimum fluidization velocity determination for alumina

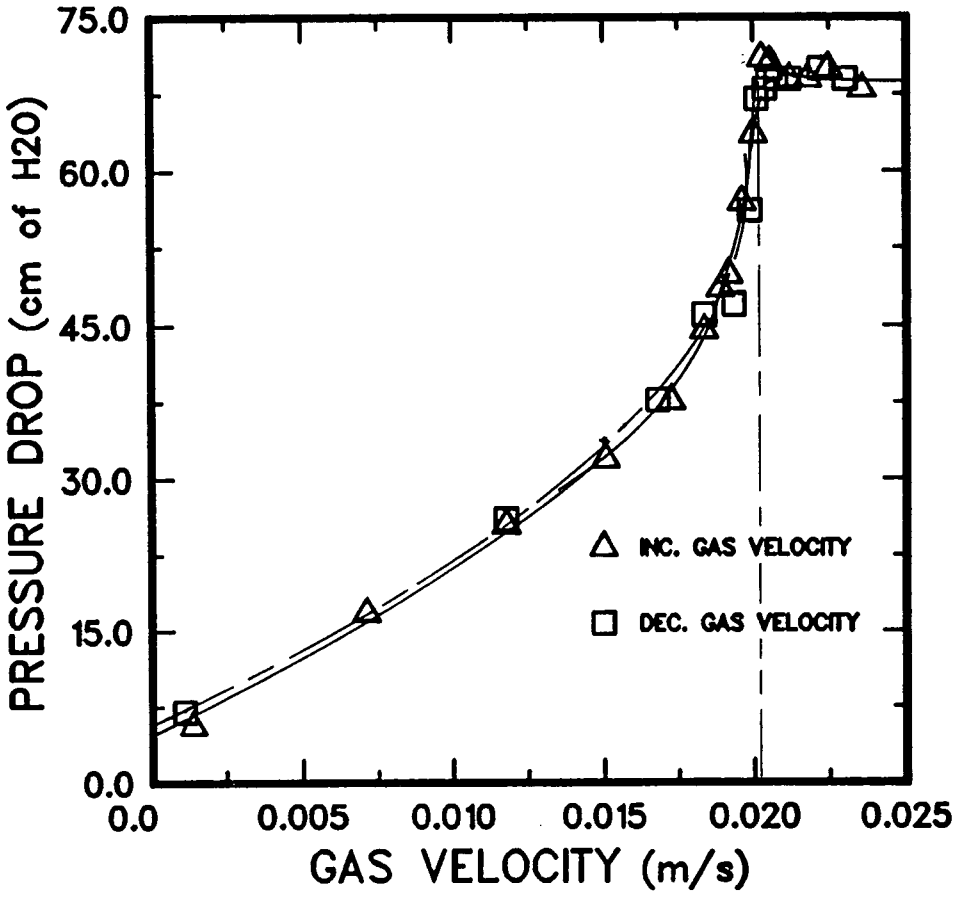

Figure C.2 Minimum fluidization velocity determination for sand.

Terminal Velocity Calculation:

$$\log[N_d^{1/3}] = \log \bar{d}p\left[\frac{4g\rho_g(\rho_p-\rho_g)}{3\mu_g^2}\right]^{1/3}$$

The value of $\log[Nu^{1/3}]$ corresponding to $\log[Nd^{1/3}]$ is found in Appendix A, p. 356-357 of Bubbles, Drops and Particles, Clift and Grace (1979).

$$N_u^{1/3} = 10^{\log[N_u^{1/3}]}$$

$$U_t = \frac{N_u^{1/3}}{\left[\frac{3\rho_g^2}{4(\rho_p-\rho_g)g\mu g}\right]^{1/3}}$$

Gas properties at 25°C, 1 atm

$\rho_g = 1.1769\ kg/m^3$

$\mu_g = 1.8464 \times 10^{-5}\ kg/ms$

1. Alumina

   $N_d^{1/3} = 3.4598$

   $\log[N_d^{1/3}] = 0.5391$

   $\log[N_u^{1/3}] = -0.3740$

   $N_u^{1/3} = 0.4227$

   $U_t = 0.36\ m/s$

2. Sand

   $N_d^{1/3} = 7.2920$

   $\log[N_d^{1/3}] = 0.8628$

   $\log[N_u^{1/3}] = 0.1054$

   $N_u^{1/3} = 1.2747$

   $U_t = 0.99\ m/s$

Appendix D

Dashpot Oil Specifications

Mobil 600 W Cylinder Oil

Enclosed Gear Lubricant

Viscosity SUS at 210°F (99°C) - 137/143 sec

Appendix E

Data Conversion Formulae

1. Circulation Rate

$$G_s = m_{circ} \cdot m_{cal} \cdot \rho_{H_2O} \cdot A_{bb}/A_{fb}$$

G_s	Circulation rate (kg/m^2s)
m_{circ}	Slope of the pressure drop across the butterfly valve versus time data (volts/sec)
m_{cal}	Slope of the pressure transducer calibration curve (m of H_2O/volt)
ρ_{H_2O}	Density of water (kg/m^3)
A_{bb}	Cross-sectional area of the bubbling bed (m^2)
A_{fb}	Cross-sectional area of the fast bed (m^2)

2. Effective Force

$$\bar{F}_{eff} = (\bar{L}-L_o) \cdot m_L \cdot g \cdot X_L/X_{eff}$$

$\bar{F}_{eff}$	Time averaged effective force (N)
$\bar{L}$	Time averaged load beam voltage (volts)
L_o	Load beam voltage at no-flow conditions (volts)
m_L	Slope of the weight versus voltage load beam calibration curve (kg/volts)
X_L	Distance from the load beam contact point to the pivot (m)
X_{eff}	Distance from the lever pivot to the point where the effective force is said to act, taken as 0.23 m
g	Acceleration due to gravity (m/s^2)

3. Standard Deviation

$$\sigma_{eff} = \sigma_L \cdot m_L \cdot g \cdot X_L/X_{eff}$$

σ_{eff} Standard deviation of the time averaged effective force (N)

σ_L Standard deviation of the time averaged load beam voltage (volts)

$m_L, X_L X_{eff}$, g Defined as before

Appendix F

Impact Flowmeter Raw Data

Table F1 - Time averaged load beam signals and signal standard deviations, converted to equivalent forces, for the 30° pan with alumina as the particulate material (circulation rates based on the fast bed cross-sectional area)

Run #	Fast Bed Superficial Gas Velocity, m/s	Test #	Circulation Rate kg/m^2s	Time Averaged Signal, N	Signal Standard Deviation, N
1	3.0	1	11.7	1.64	0.65
		2	11.1	1.78	0.66
		3	9.4	1.63	0.66
		4	9.6	-	-
2	3.0	1	15.0	1.41	0.92
		2	14.8	1.39	0.87
		3	14.6	1.31	0.79
		4	8.9	1.51	0.83
		5	9.4	1.32	1.14
3	3.7	1	19.6	1.73	1.35
		2	16.8	1.63	1.32
		3	18.90	1.70	1.36
		4	12.89	1.63	1.33
		5	19.40	1.61	1.32
4	4.1	1	19.90	1.37	1.12
		2	-	1.21	1.09
		3	-	1.37	1.47
		4	-	1.27	0.92
		5	-	1.32	1.08

...continued

Run #	Fast Bed Superficial Gas Velocity m/s	Test #	Circulation Rate kg/m^2s	Time Averaged Signal, N	Signal Standard Deviation
5	4.1	1	46.2	3.89	1.67
		2	40.3	3.86	1.71
		3	51.9	3.72	1.73
		4	48.4	3.81	1.71
		5	41.1	3.88	1.71
		6	69.2	-	-
6	4.8	1	48.4	5.02	0.92
		2	44.6	5.00	0.97
		3	51.42	4.84	1.01
		4	54.24	4.75	1.23
		5	58.06	-	-
7	5.3	1	61.85	5.04	0.91
		2	-	4.91	1.04
		3	-	-	-
		4	-	-	-
		5	-	-	-
8	4.2	1	12.33	1.43	0.56
		2	-	1.48	0.55
9	3.3	1	11.65	1.72	1.55
		2	-	1.28	1.12
		3	-	1.22	0.42

Table F2 - Time averaged load beam signals and signal standard deviations, converted to equivalent forces, for the 45° pan with alumina as the particulate material (circulation rates based on the fast bed cross-sectional area)

Run #	Fast Bed Superficial Gas Velocity m/s	Test #	Circulation Rate kg/m^2s	Time Averaged Signal, N	Signal Standard Deviation, N
1	3.0	1	18.2	1.74	1.38
		2	17.6	2.06	1.36
		3	17.2	1.91	1.35
		4	-	2.12	1.36
2	3.3	1	34.8	4.44	0.96
		2	-	4.43	0.90
		3	-	4.53	0.90
3	3.8	1	31.5	4.13	1.30
		2	31.3	4.27	1.22
		3	-	4.17	1.34
		4	-	4.16	1.31
4	3.8	1	22.7	3.48	1.68
		2	-	3.90	1.44
		3	-	4.16	1.32
		4	-	3.51	1.65
5	3.5	1	22.0	3.92	1.43
		2	25.5	3.84	1.49
		3	-	3.91	1.41

... continued

Run #	Fast Bed Superficial Gas Velocity m/s	Test #	Circulation Rate kg/m^2s	Time Averaged Signal, N	Signal Standard Deviation, N
6	3.2	1	20.2	4.06	1.16
		2	19.7	3.14	1.03
		3	-	3.80	1.26
7	3.2	1	11.2	1.97	1.09
		2	13.4	1.66	1.27
		3	-	2.03	1.17

Table F3 - Time averaged load beam signals and signal standard deviations, converted to equivalent forces, for the 60° pan with alumina as the particulate material (circulation rates based on the fast bed cross-sectional areas)

Run #	Fast Bed Superficial Gas Velocity, m/s	Test #	Circulation Rate kg/m^2s	Time Averaged Signal, N	Signal Standard Deviation, N
1	4.3	1	21.7	1.22	1.42
		2	29.3	0.84	1.02
		3	23.8	1.17	1.20
		4	17.7	-	-
2	4.4	1	24.0	0.90	1.45
		2	27.8	1.09	1.52
		3	-	1.14	1.62
3	4.4	1	49.3	1.96	1.87
		2	64.5	2.63	1.87
		3	53.7	-	-
4	3.4	1	64.54	2.70	1.81
		2	-	2.65	1.72
		3	-	2.49	1.75
		4	-	1.19	0.94
		5	-	2.14	1.60
5	3.6	1	17.1	1.12	0.98
		2	17.1	1.09	0.99
		3	16.8	0.73	0.80
		4	-	1.20	1.03

... continued

Run #	Fast Bed Gas Velocity, m/s	Test #	Circulation Rate kg/m^2s	Time Averaged Signal, N	Signal Standard Deviation, N
6	3.7	1	38.5	0.56	1.13
		2	37.8	0.52	1.12
		3	-	0.25	0.89
		4	-	0.57	1.19
7	3.0	1	26.3	0.92	1.47
		2	28.6	1.13	1.67
		3	37.4	0.99	1.43
		4	32.1	0.95	1.42
8	2.8	1	35.4	0.50	1.38
		2	37.4	0.57	1.41
		3	39.7	0.59	1.44
		4	40.0	0.56	1.38
		5	38.9	0.43	1.29
9	3.3	1	40.2	0.84	1.52
		2	40.6	0.72	1.51
		3	-	0.77	1.43
		4	-	0.73	1.50
10	3.7	1	48.1	0.77	1.52
		2	44.3	1.45	1.70
		3	49.7	1.10	1.53
		4	50.9	1.33	1.71
		5	45.7	1.26	1.03

Table F4 - Time averaged load beam signals and signal standard deviations, converted to equivalent forces, for 30° angle with sand as the particulate material (circulation rates based on the fast bed cross-sectional area)

Run #	Fast Bed Superficial Gas Velocity, m/s	Test #	Circulation Rate kg/m^2s	Time Averaged Signal, N	Signal Standard Deviation, N
1	4.5	1	9.1	0.75	0.94
		2	12.9	1.00	1.11
		3	10.4	0.53	1.05
2	5.1	1	13.7	2.29	1.37
		2	15.6	2.59	1.38
		3	-	3.87	0.95
3	5.0	1	17.6	4.57	1.07
		2	21.3	4.43	1.13
		3	13.3	4.48	1.07
		4	18.1	-	-
4	4.0	1	35.1	4.98	0.33
		2	36.4	5.01	0.27
		3	37.4	5.03	0.26
5	3.8	1	7.1	3.19	1.50
		2	4.8	3.35	1.45
		3	4.1	3.00	1.52
6	3.5	1	2.6	0.16	0.17
		2	-	0.19	0.15
		3	-	0.22	0.16

Table F5 - Time averaged load beam signals and signal standard deviations, converted to equivalent forces, for 45° pan with sand as the particulate material (circulation rates based on the fast bed cross-sectional area)

Run #	Fast Bed Superficial Gas Velocity, m/s	Test #	Circulation Rate kg/m^2s	Time Averaged Signal, N	Signal Standard Deviation, N
1	3.0	1	6.3	0.32	0.04
		2	-	0.33	0.05
		3	-	0.32	0.03
2	3.0	1	7.2	0.10	0.07
		2	-	-	-
		3	-	-	-
3	4.0	1	14.2	2.89	1.56
		2	17.5	2.66	1.65
		3	13.4	2.89	1.59
4	4.0	1	25.8	3.92	1.47
		2	23.2	3.91	1.48
		3	22.0	3.72	1.56
		4	24.8	-	-
5	6.5	1	11.0	0.08	0.15
		2	10.7	0.06	0.12
		3	10.3	0.17	0.15
6	6.6	1	29.3	4.50	1.05
		2	23.4	4.68	0.82
		3	-	4.65	0.84
7	6.0	1	24.2	2.82	1.87
		2	25.4	2.72	1.91
		3	25.9	2.47	1.89

Table F6 - Time averaged load beam signals and signal standard deviations, converted to equivalent forces, for 60° pan with sand as the particulate material (circulation rates based on the fast bed cross-sectional area)

Run #	Fast Bed Superficial Gas Velocity, m/s	Test #	Circulation Rate kg/m^2s	Time Averaged Signal, N	Signal Standard Deviation, N
1	5.3	1	1.3	0.05	0.01
		2	1.0	0.05	0.01
		3	1.0	0.05	0.01
2	5.2	1	6.3	0.10	0.08
		2	8.3	0.07	0.04
		3	7.5	0.18	0.06
3	5.2	1	2.0	0.13	0.06
		2	5.0	0.20	0.06
		3	2.0	0.08	0.03
4	5.0	1	8.7	0.44	0.36
		2	11.0	0.51	0.51
		3	9.3	-	-
5	5.5	1	12.0	1.88	1.41
		2	11.9	1.96	1.46
		3	16.0	2.18	1.60

... continued

Run #	Fast Bed Superficial Gas Velocity, m/s	Test #	Circulation Rate kg/m^2s	Time Averaged Signal, N	Signal Standard Deviation, N
6	4.8	1	21.7	4.53	1.39
		2	21.4	4.81	1.26
		3	27.2	4.73	1.19
7	4.8	1	39.4	5.21	0.70
		2	37.8	5.13	0.84
		3	37.3	5.07	0.93
8	4.6	1	9.9	1.21	0.95
		2	13.7	1.12	0.82
		3	9.9	0.93	0.74
9	4.7	1	5.1	0.54	0.20
		2	-	0.58	0.22
		3	-	0.56	0.26

Appendix G

Particle Velocity Raw Data

Table G1 - Particle Velocities in the L-valve as a function of Circumferential Position for different alumina circulation rates (circulation rates based on the fast bed cross-sectional area)

Run #	Circulation Rate kg/m^2s	Test #	Particle Velocity, m/s x 10^2 Position #1	Position #2	Position #3	Position #4	Position #5
1	21.2	1	2.14	2.07	2.08	2.07	1.94
		2	2.04	2.00	1.99	1.97	1.98
		3	1.94	2.01	2.00	2.01	1.89
2	60.2	1	5.60	5.96	4.96	5.49	5.29
		2	5.43	5.38	4.91	5.14	6.13
		3	5.58	5.22	6.73	5.95	5.28
3	13.4	1	1.09	1.06	0.93	1.03	1.04
		2	1.03	1.00	1.17	1.06	0.90
		3	1.00	1.17	1.12	1.17	1.15
4	38.8	1	4.58	3.97	4.32	4.30	4.35
		2	3.61	4.42	5.53	5.76	3.18
		3	4.20	5.24	3.47	3.51	4.03
		4	4.83	3.52	3.75	3.77	3.39
5	38.0	1	5.06	3.33	3.10	3.37	3.31
		2	5.01	3.06	3.94	3.10	3.08
		3	5.41	3.02	3.31	5.08	4.33
		4	5.45	3.07	3.35	4.99	2.94

... continued

Run #	Circulation Rate kg/m^2s	Test #	Particle Velocity, m/s x 10^2 Position #1	Position #2	Position #3	Position #4	Position #5
6	35.1	1	3.50	3.22	3.41	3.52	3.30
		2	3.18	3.47	3.39	3.78	3.49
		3	3.41	3.44	3.66	3.60	3.42
7	52.5	1	4.37	4.04	5.57	5.56	5.12
		2	4.99	6.00	5.22	5.23	4.68
		3	4.46	4.46	5.38	4.33	4.83
		4	4.04	5.70	4.70	4.51	4.65
		5	5.28	4.14	4.74	4.88	4.55
8	17.1	1	1.47	-	1.83	-	-
		2	1.45	-	1.48	-	-
		3	1.74	-	1.44	-	-
		4	1.71	-	1.31	-	-
9	21.7	1	2.33	-	2.09	-	-
		2	2.11	-	2.22	-	-
		3	2.32	-	1.82	-	-
10	35.4	1	4.46	-	4.58	-	-
		2	4.69	-	4.39	-	-
		3	4.27	-	4.78	-	-
		4	4.77	-	4.87	-	-
		5	4.64	-	4.58	-	-
11	40.2	1	4.23	-	4.76	-	-
		2	4.12	-	3.27	-	-
		3	5.85	-	3.64	-	-
		4	3.80	-	4.76	-	-
		5	3.08	-	3.15	-	-

...continued

Run #	Circulation Rate kg/m^2s	Test #	Particle Velocity, m/s x 10^2 Position #1	Position #2	Position #3	Position #4	Position #5
12	47.9	1	4.95	-	4.66	-	-
		2	4.53	-	5.34	-	-
		3	4.89	-	4.92	-	-
		4	5.07	-	5.05	-	-
13	49.3	1	6.54	-	6.95	-	-
		2	7.10	-	6.26	-	-
		3	7.22	-	6.83	-	-
		4	6.84	-	6.50	-	-
		5	7.12	-	6.89	-	-
14	11.7	1	0.80	-	0.89	-	-
		2	0.86	-	0.83	-	-
		3	0.97	-	0.86	-	-
15	15.0	1	1.37	-	1.69	-	-
		2	1.31	-	1.41	-	-
		3	1.56	-	1.36	-	-
		4	1.28	-	1.40	-	-
16	19.6	1	1.80	-	1.76	-	-
		2	1.97	-	1.81	-	-
		3	1.98	-	2.10	-	-
		4	1.88	-	2.01	-	-
17	19.9	1	2.48	-	2.10	-	-
		2	2.18	-	2.11	-	-
		3	2.56	-	2.56	-	-
		4	2.41	-	2.47	-	-

... continued

Run #	Circulation Rate kg/m^2s	Test #	Particle Velocity, m/s x 10^2 Position #1	Position #2	Position #3	Position #4	Position #5
18	46.2	1	4.05	-	4.91	-	-
		2	4.84	-	4.40	-	-
		3	4.37	-	4.50	-	-
		4	4.63	-	4.72	-	-
19	48.5	1	6.15	-	6.43	-	-
		2	0.35	-	6.19	-	-
		3	6.01	-	6.78	-	-
		4	5.57	-	7.84	-	-
		5	6.48	-	6.81	-	-

Table G2 - Particle Velocities in the L-valve as a function of Circumferential Position for different sand circulation rates (circulation rates based on the fast bed cross-sectional area)

Run #	Circulation Rate kg/m^2s	Test #	Particle Velocity, m/s x 10^2 Position #1	Position #2	Position #3	Position #4	Position #5
1	14.2	1	1.11	1.14	1.13	1.13	1.25
		2	1.15	1.18	1.21	1.22	1.24
		3	1.25	1.14	1.11	1.10	1.18
2	25.8	1	1.66	1.76	1.70	1.68	1.83
		2	1.74	1.68	1.65	1.80	1.77
		3	1.63	1.64	1.70	1.74	1.83
3	11.0	1	0.92	0.90	1.01	0.92	1.04
		2	0.91	0.95	0.95	0.92	0.87
		3	0.91	0.92	0.93	0.90	1.00
4	29.3	1	2.46	2.42	2.43	2.43	2.48
		2	2.55	2.68	2.55	2.24	2.75
		3	2.31	2.62	2.48	2.43	2.34
5	24.4	1	1.70	1.86	1.72	1.93	1.98
		2	1.59	1.74	1.83	1.68	1.66
		3	1.68	1.73	1.73	1.92	1.85
6	6.3	1	0.39	0.40	0.39	0.39	0.38
		2	0.39	0.37	0.39	0.39	0.38
		3	0.39	0.38	0.40	0.38	0.37

... continued

Run #	Circulation Rate kg/m^2s	Test #	Particle Velocity, m/s x 10^2 Position #1	Position #2	Position #3	Position #4	Position #5
7	7.3	1	0.70	0.71	0.71	0.66	0.70
		2	0.71	0.67	0.69	0.68	0.70
		3	0.68	0.66	0.70	0.70	0.73
8	13.7	1	1.08	1.11	1.12	1.14	1.28
		2	1.10	1.07	1.18	1.10	1.29
		3	1.15	1.02	1.18	1.17	1.25
9	17.6	1	1.64	1.68	1.75	1.76	1.86
		2	1.72	1.80	1.72	1.68	1.70
		3	1.75	1.62	1.69	1.81	1.87
10	35.3	1	2.48	2.35	2.62	2.16	2.58
		2	2.54	2.42	2.20	2.33	2.50
		3	2.39	2.40	2.62	2.42	2.32
11	6.3	1	0.82	0.81	0.81	0.87	0.82
		2	0.83	0.76	0.79	0.81	0.87
		3	0.82	0.84	0.79	0.81	0.81
12	1.8	1	0.64	0.67	0.68	0.62	0.65
		2	0.65	0.67	0.71	0.67	0.68
		3	0.70	0.67	0.67	0.68	0.68
13	2.4	1	0.49	0.51	0.50	0.47	0.48
		2	0.49	0.47	0.49	0.50	0.48
		3	0.50	0.48	0.50	0.50	0.51

... continued

Run #	Circulation Rate kg/m^2s	Test #	Particle Velocity, m/s x 10^2 Position #1	Position #2	Position #3	Position #4	Position #5
14	8.7	1	0.88	0.86	0.95	0.93	0.94
		2	0.88	0.86	0.89	0.91	0.96
		3	0.90	0.94	0.89	0.93	0.88
15	12.0	1	1.30	1.20	1.34	1.29	1.29
		2	1.27	1.23	1.32	1.16	1.32
		3	1.15	1.22	1.25	1.27	1.26
16	21.7	1	2.08	2.00	2.16	2.01	1.97
		2	2.12	2.04	2.02	2.06	1.92
		3	2.12	2.17	2.06	1.97	2.06
17	39.5	1	2.54	2.75	2.40	2.68	2.42
		2	2.39	2.67	2.39	2.82	2.40
		3	2.56	2.53	2.55	2.51	2.67
18	9.9	1	1.01	0.99	0.96	1.01	0.94
		2	0.94	1.03	1.03	0.92	0.94
		3	1.06	1.02	0.96	0.96	1.01
19	5.1	1	0.80	0.77	0.80	0.84	0.79
		2	0.80	0.78	0.80	0.74	0.82
		3	0.74	0.80	0.81	0.82	0.78

Appendix H

Theoretical Model

Force on Pan in Crossflow

Linear Momentum Theorem: Net Force acting on particles and fluid within the control volume = time rate of change of momentum with the control volume plus net rate of outflow of momentum from the control volume, Figure H.1. Since we are interested only in the steady state case, the time rate of change term is zero. Let us ignore the contribution of the gas to the momentum and force since $\rho_g << \rho_p$. The pan and control volume adopted are shown in Figure H.1.

Then:

$$F = \frac{G_s \ell_b w_I}{A_{bb}} (v_e - v_f \cos \theta_f)$$

where: F = force (N)

G_s = total solids mass flow in the slow bed (kg/s)

ℓ_b = bar length (m)

w_I = width of zone where particles are intercept by the bar (m)

A_{bb} = cross-sectional area of the slow bed column (m^2)

v_e = entry velocity of particles, assumed = terminal settling velocity minus gas velocity in the slow bed (m/s)

v_f = average final velocity as particles leave the control surface (m/s)

θ_f = angle between particle trajectory leaving control volume and the vertical downward direction

For the simplest case, assume $w_I = w_b$ = pan width, $v_f = v_e = v_t$ = terminal settling velocity and, $\theta_f = \theta_b$ = angle of pan slope to vertical

Then:

$$F = \frac{G_s \ell_b w_b v_e}{A_{bb}} (1 - \cos \theta_b)$$

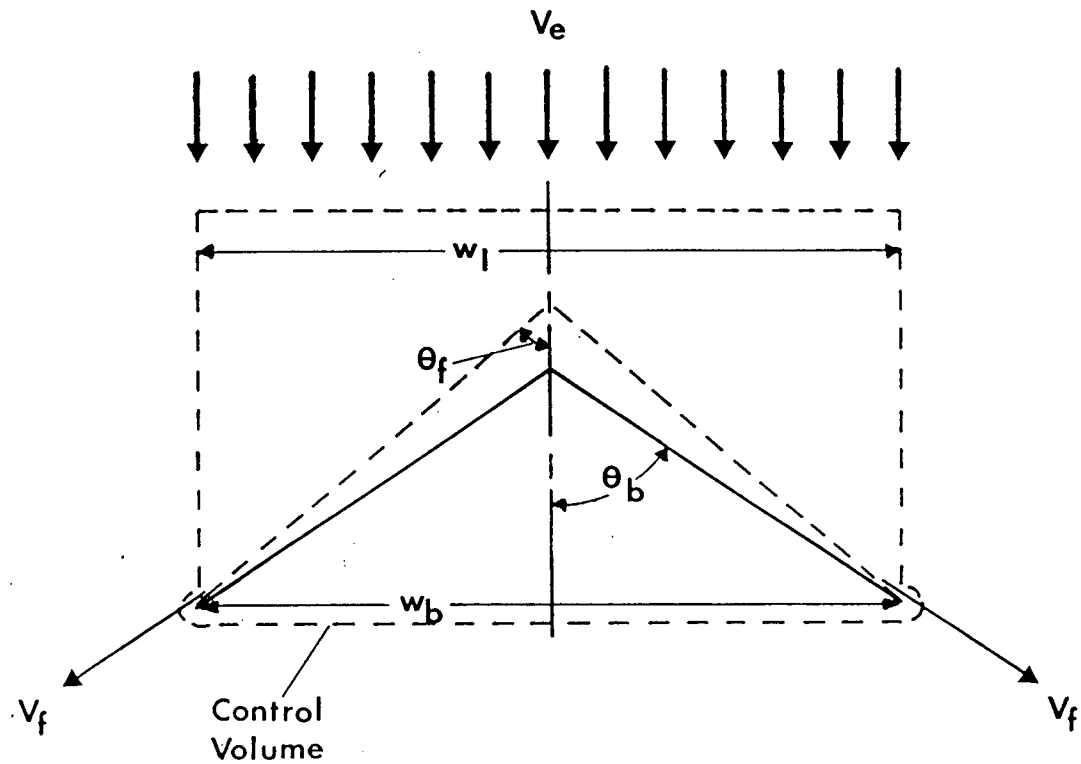

Figure H.1 Schematic of the bar cross-section and control volume

Example: Sand, 45° pan

$$G_s = 50\ kg/m^2\text{-}s \times \frac{\pi}{4} \times (0.15)^2\ m^2 = 0.884\ \frac{kg}{s}$$

$$\ell_b = 14" = 0.356\ m$$

$$w_b = 2" = 0.0508\ m$$

$$v_t = 0.99\ m/s$$

$$A_2 = \frac{\pi}{4} \times (14 \times 0.0254)^2\ m^2 = 0.0993\ m^2$$

$$\theta_b = 45°$$

$$\therefore F = \frac{0.884\ \frac{kg}{s} \times 0.356\ m \times 0.0508\ m}{0.0993\ m^2} \times 0.99\ \frac{m}{s} \times (1-0.707)$$

$$= 0.047\ N$$

In Figure H.2 the experimental results for the 60° pan angle with alumina as the circulating solids are compared with the results predicted by the theoretical model, shown by the solid line. It is evident that the prediction by the theoretical model is poor. The poor prediction by the theoretical model may have resulted from:

- non-uniform distribution of solids in the "slow" bed column.
- particles sticking to and/or sitting on the pan.
- particles bouncing or coming off the pan at angles other than the assumed angle
- the particles not travelling at their terminal velocities when they struck the pan.

The failure to include the first three points in the model would cause underestimation of the actual results. Exclusion of the fourth point would cause the model to overestimate the experimental results.

Clearly, the model underestimates the experimental results. It also fails to predict the three zones apparent in the experimental results. This is because the model does not account for sticking of the equipment at lower circulation rates or peaking of the equipment at higher solids fluxes.

As a result of the simplifying assumptions made in this model, it cannot be used to estimate expected forces.

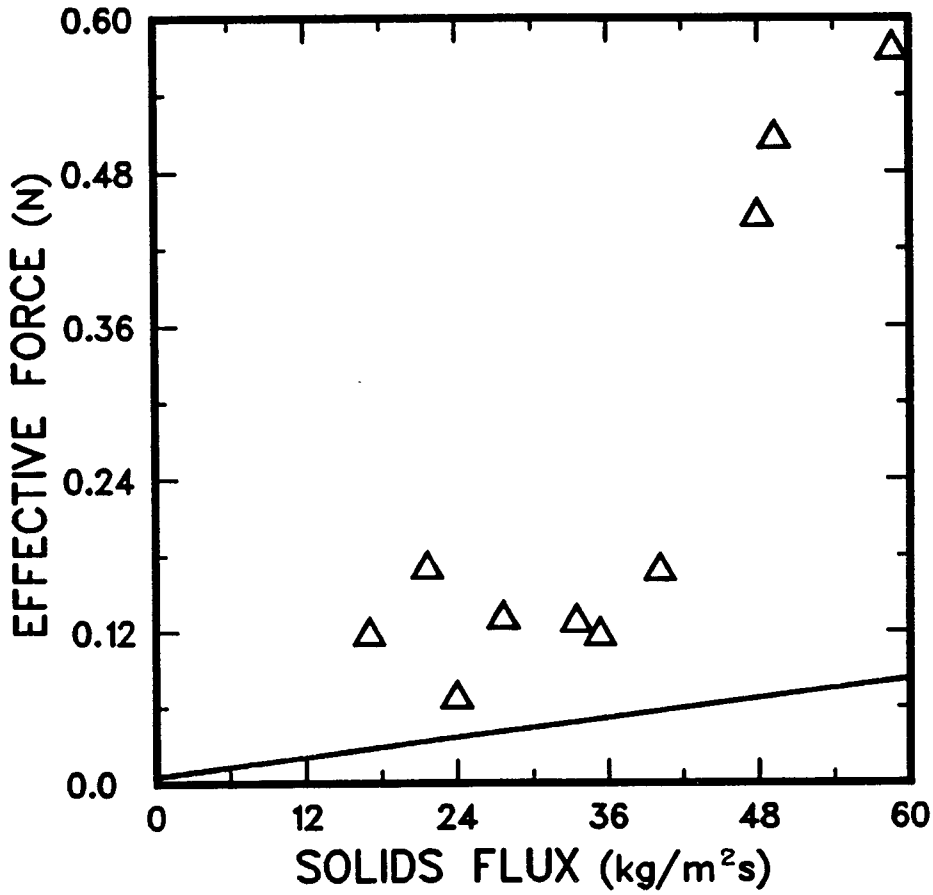

Figure H.2 Comparison of the experimental results for the 60° pan with alumina with the results predicted by the theoretical model.

Appendix I

Operating Instructions

I.1 Electrical Connections

Before working on any of the electrical connections, of all the equipment should be turned off.

I.1.1 Load Beam Connection and Adjustment

1. The five wires of the load beam are colour coded. The wires are connected to the amplifier using the terminal block at the back of the amplifier. Each load beam wire is connected to its appropriate terminal, as indicated by the abbreviation of the wire colour beside the terminal, using the screws in the terminal block, Figure I.1.
2. The output voltage of the amplifier is measured across the terminals marked +0 volts and -0 volts, Figure I.1.
3. The output voltage of the load beam under no-load conditions can be adjusted to zero by the coarse and fine zero adjustment screws on the front panel of the amplifier, Figure I.2.

I.1.2 Load Beam Amplifier Connections

1. When using two or more signal recorders, such as the UV chart chart recorder, the digital voltmeter and/or the Tecmar datalogging board, ensure that all of the ground leads of the equipment are connected to the -0 volts terminal and all of the high potential leads are connected to the +0 volts. If this is not followed, the load beam amplifier will be short circuited.

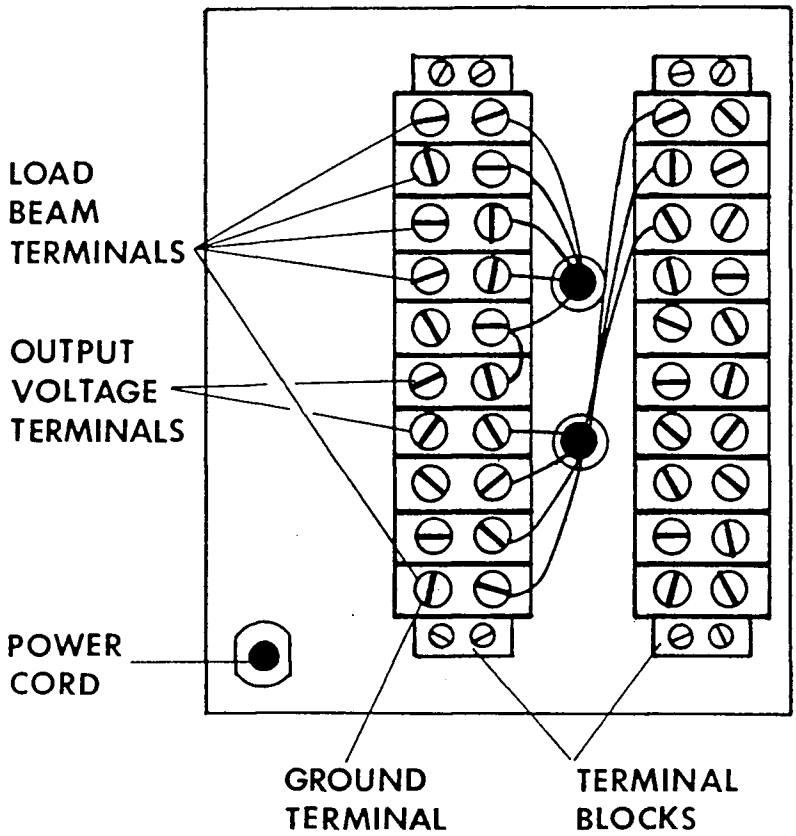

Figure I.1 Load beam amplifier terminal block connections

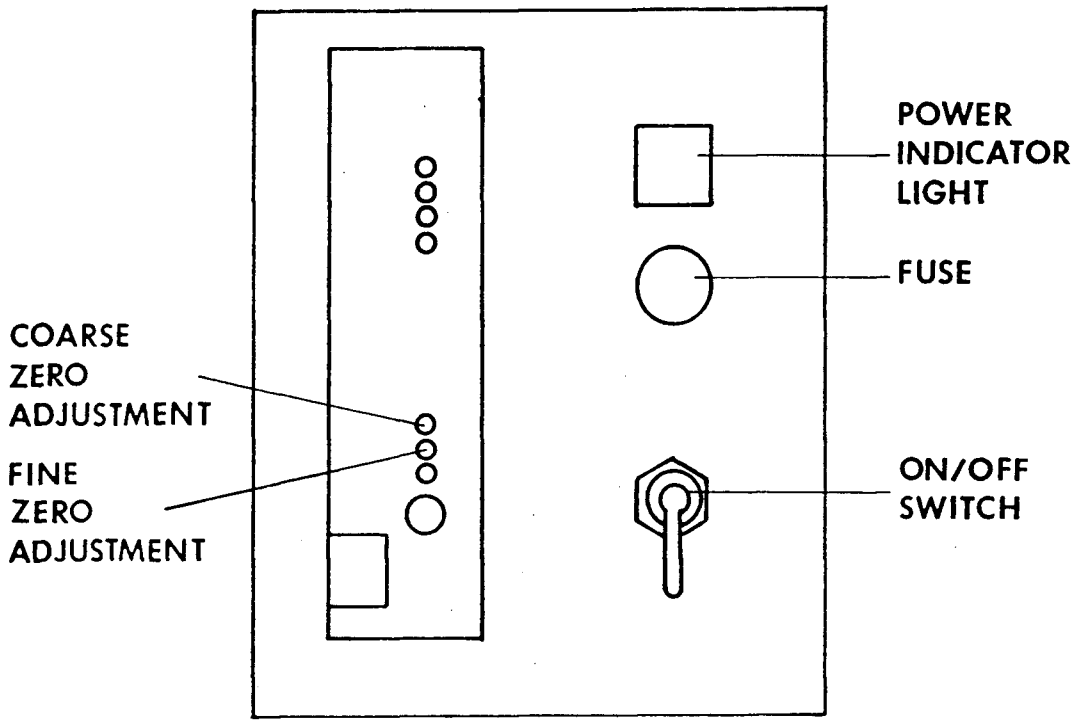

Figure I.2 Load beam amplifier controls

I.1.3 Tecmar Connections

1. All datalogging connections are made using the daughter board ribbon cable, Figure I.3. As designated in the datalogging program, the load beam and pressure transducer are datalogged using Channels 0 and 1 respectively. The ribbon leads corresponding to Channels 0 and 1 are shown in Figure I.3.

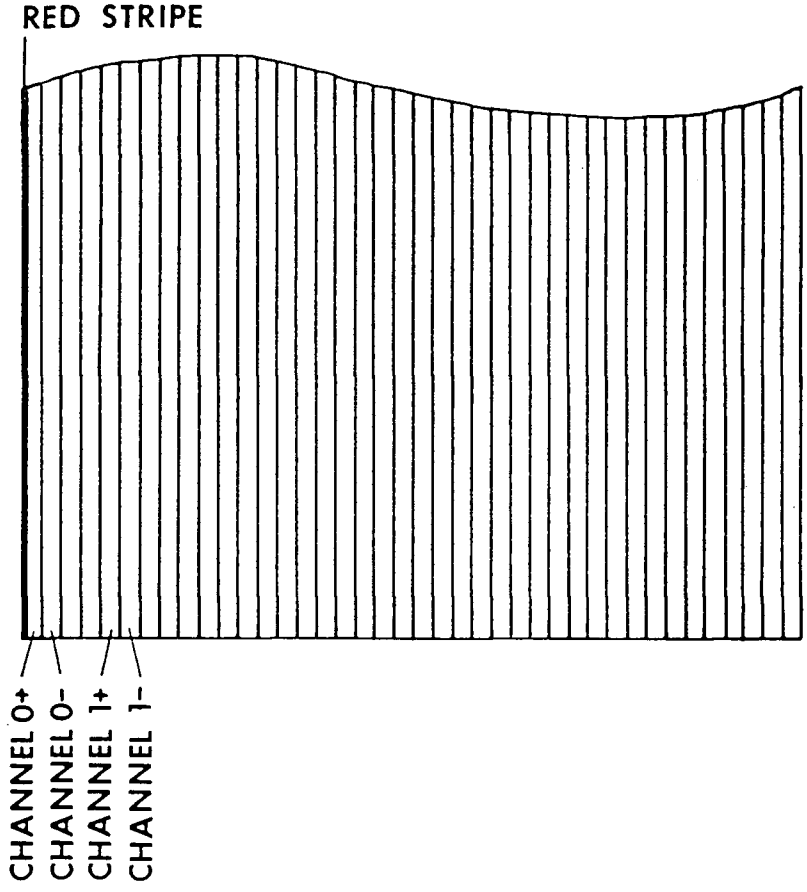

Figure I.3 Tecmar daughter board ribbon cable

I.2 Impact Flowmeter Operation

I.2.1 Impact Flowmeter Column Section Removal

1. Disconnect the load beam from the load beam amplifier by loosening the terminal block screws.
2. Remove the air purge and manometer lines connected to the pressurized box.
3. Remove the screw which holds the grounding wires of the impact flowmeter to the support column.
4. Disconnect the manometer line attached to the impact flowmeter column section.
5. Remove the bolts from the upper and lower flanges of the impact flowmeter column section.
6. Loosen the nuts which fasten the mounting brackets of the sections of return column overlying the impact flowmeter to the support brackets of the column support post.
7. Remove the bolts from the primary cyclone which lie below the support bracket of the primary cyclone.
8. Raise the primary cyclone and attached return column with a lever. Place blocks between the primary cyclone mounting brackets and the support brackets to keep the cyclone and attached column sections elevated.
9. The impact flowmeter column section can now be slipped out of the return column.
10. To install the impact flowmeter column section, reverse the above procedures. Ensure that the rubber gasket and O-rings are positioned properly.

I.2.2 Pressurized Box Removal

1. Carry out steps 1 through 3 of the impact flowmeter column section removal.
2. Remove the Swagelock bolt which seals the port through which the load beam cable enters the pressurized box.
3. Remove the bolts holding the box against the mounting plate.
4. Carefully pull the box away from the mounting plate. Avoid pulling the rubber gasket off the mounting plate.
5. Once the box is free, disconnect the grounding wire leading from the lever arm to the pressurized box by loosening the bolt on the lever arm.
6. The box can now be removed. As the box is pulled away, slip the cable of the load beam through its Swagelock fitting.
7. The box is installed by reversing the above procedures. The surface between the rubber gasket and box should be covered with vacuum grease to seal against leakage when the box is pressurized.

I.2.3 Pan Removal and Replacement

1. Carry out the procedures outlined in Section I.2.2.
2. Remove the load beam from its mounting bracket by undoing the two fastening bolts.
3. Carry out the steps outlined in Section I.2.1.
4. Detach the pan from the lever arm by removing the six mounting screws.
5. If the pan is being exchanged, remove the previous pan's mounting blocks by loosening the screws on the bases of the blocks and sliding the blocks off the end of the lever.
6. The new blocks are installed by reversing procedure 5.
7. Fasten the new pan to the mounting blocks with the six screws which secure the pan to the mounting blocks.
8. Centre the pan in the column and ensure that the pan is level.
9. Tighten the screws holding the mounting blocks to the lever.
10. Reinstall the load beam.
11. For this step the load beam must be connected to the amplifier for the duration of the procedure only. Balance the lever/pan assembly. This is done by adjusting the lever counter-weight. To move the counter-weight, loosen the nuts which secure the weight. Starting with the lever contacting the load beam, move the counter-weight until the load beam amplifier voltage just equals the amplifier voltage at no-load. Reduce the value of the counter-weight by turning the counter-weight locking nuts a quarter turn clockwise. Tighten the lock nuts. Disconnect the load beam amplifier connections.
12. Reverse procedures 1 through 3.

I.2.4 Bearing Adjustment

1. Carry out the steps outlined in Section I.2.2.
2. Loosen the allen screws used to lock the bearing shafts in place. These are located on the fronts of the bearing shaft blocks. It may be necessary to remove the load beam to access them.
3. The bearing shafts may now be adjusted. To remove the pivot, back the bearing shafts into the bearing blocks by turning the shafts counter-clockwise. The pivot can now be removed.
4. To set the bearing, press the bearing shafts into the pivot as far as they will go by turning the knurled knobs of the shafts clockwise. Slowly back the shafts out until the pivot moves freely. Ensure that the sensing screw of the load beam contacts the lever. If it does not, change the position of the lever by rotating one bearing shaft clockwise and the other shaft counter-clockwise.
5. Once the bearing is adjusted and the lever positioned, tighten the bearing shaft locking screws.
6. Reverse step 1.